UNIVERSIDADE ESTADUAL
DE CAMPINAS

Instituto de Matemática, Estatística e
Computação Científica

JEAN RENEL FRANÇOIS

A study of Lagrangian-Eulerian methods for hyperbolic problems and balance laws

Um estudo de métodos Lagrangiano-Euleriano para problemas hiperbólicos e leis de balanço

Campinas
2017

Jean Renel François

A study of Lagrangian-Eulerian methods for hyperbolic problems and balance laws

Um estudo de métodos Lagrangiano-Euleriano para problemas hiperbólicos e leis de balanço

Dissertação apresentada ao Instituto de Matemática, Estatística e Computação Científica da Universidade Estadual de Campinas como parte dos requisitos exigidos para a obtenção do título de Mestre em matemática aplicada.

Dissertation presented to the Institute of Mathematics, Statistics and Scientific Computing of the University of Campinas in partial fulfillment of the requirements for the degree of Master in applied mathematics.

Orientador: Eduardo Cardoso de Abreu

Este exemplar corresponde à versão final da dissertação defendida pelo aluno Jean Renel FRANÇOIS, e orientado pelo Prof. Dr Eduardo Cardoso de Abreu.

Campinas
2017

Agência(s) de fomento e nº(s) de processo(s): CNPq, 132128/2016-0

Ficha catalográfica
Universidade Estadual de Campinas
Biblioteca do Instituto de Matemática, Estatística e Computação Científica
Márcia Pillon D'Aloia - CRB 8/5180

F848s

François, Jean Renel, 1985-
A study of Lagrangian-Eulerian methods for hyperbolic problems and balance laws / Jean Renel François. – Campinas, SP : [s.n.], 2017.

Orientador: Eduardo Cardoso de Abreu.
Dissertação (mestrado) – Universidade Estadual de Campinas, Instituto de Matemática, Estatística e Computação Científica.

1. Leis de conservação (Matemática). 2. Métodos de volumes finitos. 3. Mecânica dos fluidos. 4. Equações diferenciais - Soluções numéricas. I. Abreu, Eduardo Cardoso de,1974-. II. Universidade Estadual de Campinas. Instituto de Matemática, Estatística e Computação Científica. III. Título.

Informações para Biblioteca Digital

Título em outro idioma: Um estudo de métodos Lagrangiano-Euleriano para problemas hiperbólicos e leis de balanço
Palavras-chave em inglês:
Conservation laws (Mathematics)
Finite volume method
Fluid mechanics
Differential equations - Numerical solutions
Área de concentração: Matemática Aplicada
Titulação: Mestre em Matemática Aplicada
Banca examinadora:
Eduardo Cardoso de Abreu [Orientador]
Lucas Catão de Freitas Ferreira
Aparecido Jesuino de Souza
Data de defesa: 19-07-2017
Programa de Pós-Graduação: Matemática Aplicada

Dissertação de Mestrado defendida em 19 de julho de 2017 e aprovada pela banca examinadora composta pelos Profs. Drs.

Prof(a). Dr(a). EDUARDO CARDOSO DE ABREU

Prof(a). Dr(a). LUCAS CATAO DE FREITAS FERREIRA

Prof(a). Dr(a). APARECIDO JESUINO DE SOUZA

As respectivas assinaturas dos membros encontram-se na Ata de defesa nos registros acadêmicos do aluno.

Dedico esse trabalho a minha mãe Lonie Dorlus que é um exemplo de força e de coragem na minha vida.

Dieu est pour nous un refuge et un appui, un secours qui ne manque jamais dans la détresse. C'est pourquoi nous sommes sans crainte quand la terre est boulversée, et que les montagnes chancellent au cœur des mer...

Psaumes 46; La Bible.

Acknowledgements

Jean Renel François thanks the CNPq No. 445758/2014-7 and the graduate Program in Applied Mathematics and Computacional of IMECC / UNICAMP for their institutional scholarship support during my master's degree. I thank my advisor, Eduardo Abreu for the opportunity to study and develop this master's work and for the accompaniment during this time of study. Thanks to my colleagues, especially Jardel viera, Paola Ferraz, Arthur Miranda, and John Sepulveda who were of great help.

Resumo

O foco deste trabalho consiste em estudar e aplicar o esquema Lagrangiano-Euleriano para leis de conservação hiperbólicas escalares e leis de balanço escalares. Portanto, apresentamos ao longo do estudo algumas definições básicas e exemplos de conceitos fundamentais relacionados. O esquema Lagrangiano-Euleriano tem como objetivo não ser dependente de uma estrutura particular do termo de fonte. Um conjunto de experimentos numéricos - escalar e sistemas - para leis de conservação hiperbólica e leis de balanço são apresentados para ilustrar o desempenho do método, como a equação de Burgers, a equação de Buckley-Leverett, Equações de águas rasas e o fluxo trifásico não-miscivel. Enfim, aplicamos a abordagem do esquema Lagrangiano-Euleriano para lei de conservação hiperbólica com fluxo não local e condições iniciais de medida como a Gaussiana e condição inicial oscilatória. Sempre que for possível, os resultados numéricos são comparados com soluções aproximadas ou soluções exatas.

Palavras-chave: Formulação Lagrangiano-Euleriano, Métodos de volumes finitos, Leis de balanço, Problema hiperbólico, Mecânica dos fluidos, Fluxo não local.

Abstract

The focus of this work consists on the study and on the application of the Lagrangian-Eulerian scheme for scalar hyperbolic conservation laws and scalar hyperbolic balance laws. For this purpose, we present some basic definitions and examples of fundamental concepts related throughout the study. The Lagrangian-Eulerian scheme is aimed to be not dependent on a particular structure of the source term. Furthermore, a set of representative numerical experiments - scalar and system - of hyperbolic conservation laws and balance laws are presented to illustrate the performance of the method such as the Burgers' equation, the Buckley-Leverett's equation, Shallow water equations and the Immiscible three-phase flow. For completeness, we apply the Lagrangian-Eulerian framework to hyperbolic conservation laws with nonlocal flux, with measure initial datas such as Guassian initial data and Oscillatory initial data. Whenever possible, we make a comparison between the numerical results and accurate approximate solutions or exact solutions.

Keywords: Lagrangian-Eulerian framework, Finite volume method, Balance laws, Hyperbolic problems, Fluid mechanics, Nonlocal flux.

List of Figures

List of Tables

Contents

1 Introduction

In this work, we study a formal construction of the Lagrangian-Eulerian scheme developed in [35] (see also [1]). A locally conservative and divergence space-time finite control volume in a Lagrangian-Eulerian framework have been explored in several cases such as scalar hyperbolic conservation laws, scalar hyperbolic conservation laws with nonlocal flux and scalar hyperbolic balance laws. The Lagrangian-Eulerian scheme is aspired to be independent on a particular structure of the source term and the flexibility of the Scheme allows its extension to construct approximate solutions of hyperbolic laws systems and balance laws systems. It is worth mention that we follow very closely the works [1, 35], and we take advantage of some matlab codes produced on those cited works as base for our numerical approximations. A simple accurate algorithm to evaluate the Hilbert transform of a real function using interpolations with piecewise–linear functions is developed [11]. The qualitative numerical approximations for our hyperbolic conservation laws with nonlocal flux using the Lagrangian-Eulerian scheme is a novelty in this master dissertation and it is worth emphasizing that a complete and mathematically rigorous understanding of this model constitute an open problem. Indeed, to the best of our knowledge there is no detailed comprehension about such problem.

1.1 Motivation for the research work

Transport models with nonlocal flux appear in various problems in applied and pure sciences, e.g., mechanics and fluid dynamics problems in porous media. Nonlocal flux problems appear in porous media induced by nonlocal effects of diffusion and also with fractional potential pressure (Laplacian) and also in dynamic fracture mechanics. Transport models with nonlocal flux also appear in the granular material flow modeling, which gives origin to an integro-differential conservation law, see [3, 4]. It is also mentioned that related transport models with nonlocal flow are also proposed as a model of dislocation dynamics, where the pertinent primary variable is related to the density of fractures per length in the material under consideration. As another physical motivation of the transport models with the nonlocal flow, we mention real crystals, which in turn show certain defects in the organization of their natural crystalline structure, called dislocations [17]. In [17], the author studies the well-posedness, as well as numerical approximations, of a nonlocal transport equation with a parabolic second order operator. Solutions of the above-mentioned PDEs can exhibit singularities, forming steep gradients and high concentration of quantities. In the present work, we deal with numerical solutions for a similar equation without the second order term with measure initial datas. The

hyperbolic conservation laws problem with nonlocal flux $u_t - (\mathbb{H}(u)u)_x = 0$ studied in this work shows numerical evidence that for a certain class of measure initial data the solution blows up with the conservation of the mass as time evolves for any $R > 0$, and with refined grid cells the solution of the problem $u_t + (\mathbb{H}(u)u)_x = 0$ presents attenuation effect for any $R > 0$, where R represents the mass of the measure initial datum.

A variety of efficient numerical schemes for hyperbolic systems of conservation laws has been developed in the recent past for different problem settings. These schemes evolved following the natural understanding of fundamental concepts from the theory of nonlinear hyperbolic conservation laws concerning the characteristic surfaces properties, existence, uniqueness, and solution of the Riemann problem. In addition, for a scalar balance laws the solution strongly depend on certain properties of the source term [35]. For numerical approximation of the solution of the – scalar and system – hyperbolic conservation laws, balance laws and scalar hyperbolic conservation laws with nonlocal flux, we study the Lagrangian-Eulerian scheme developed in [1, 35] in a cell-centered framework. The Lagrangian-Eulerian scheme consists on one more tentative to deal with the difficult issue of the well-balancing between the computation of the numerical flux function and the source term. The Lagrangian-Eulerian method studied here relates to the (locally conservative) divergence form of the full balance equation. The divergence form allows locally to study the transport and the conservation property, see [1, 35].

1.2 Aims and objectives of the dissertation proposal

This work particularly focuses on the study and on the application of the Lagrangian-Eulerian scheme constructed in [1, 35]. We will first study the Lagrangian-Eulerian framework for classic evolutionary differential models, namely, scalar hyperbolic conservation laws and scalar balance laws problems and its extension for systems of hyperbolic conservation laws and balance laws. Next, we will apply the Lagrangian-Eulerian framework for hyperbolic conservation laws with nonlocal flux. Those are state-of-the-art differential models and there are many numerical works on these subject matter.

The specific objectives of the dissertation are:

- Apply the Lagrangian-Eulerian scheme to scalar hyperbolic conservation laws following closely the lines of [1, 35]. In Section 3.4 we discuss our understanding in the numerical implementation of the Lagrangian-Eulerian scheme for classical hyperbolic problems
- Apply the Lagrangian-Eulerian scheme to scalar hyperbolic conservation laws with nonlocal flux. In Section 3.5 we present and discuss qualitative numerical results for the

scalar hyperbolic conservation laws with nonlocal flux by use of an accurate algorithm to aproximate the Hilbert transform.

- Study the theoretical background of the formal extension of the Lagrangian-Eulerian framework to balance laws (see Chapter 4) and present numerical implementation for classical balance laws problems.

- Extend the Lagrangian-Eulerian scheme for hyperbolic law systems and balance law systems. A finite control volume for each equation is used, which represent the conservation laws or the balance laws in the corresponding case. In this approach, we use the Lagrangian-Eulerian scheme, for balance laws (or conservation laws) in each equation and then we solve each equation explicitly with Δt time step.

1.3 Our findings and numerical studies

The purpose of the presentation and the discussion of our findings and numerical studies is to show our current understanding of the Lagrangian-Eulerian framework that is applied for classical and well-known scalar hyperbolic problems. We perform tests for linear and nonlinear models. On the linear case we study problems with constant and non constant velocities. On the nonlinear case, we approximate the solution of Burgers' equation (convex flux) and Buckley-Leverett's equation (non convex flux). As we will see in Section 3.4, the scheme is able to approximate properly the solution of all presented problems. Based on these first understanding studies and on the numerical experiments reported in Section 3.4, we deal qualitatively with the hyperbolic conservation law problems with nonlocal flux using an accurate method to approximate the Hilbert transform on the real line.

1.4 Organization of the dissertation proposal

The dissertation proposal is organized as follows. In Chapter 2, we present some basics definitions and presentation of some concepts studied throughout the study. In Chapter 3, we present the formal construction of the Lagrangian-Eulerian scheme for scalar hyperbolic conservation laws including the cases of linear and nonlinear hyperbolic in the conservation form. Then we present and discuss numerical experiments for linear and nonlinear scalar conservation laws with convex and non-convex flux functions. Finally, an algorithm for fast Hilbert transform of real functions, qualitative numerical experiments are presented for the hyperbolic conservation laws with nonlocal flux. In Chapter 4, we discuss the Lagrangian-Eulerian scheme for hyperbolic balance laws in the linear and nonlinear case. We perform numerical approximations with grid refinement for scalar balance laws. In chapter 5, we study the extension of the

Lagrangian-Eulerian framework for balance law systems and discuss some numerical experiments for system of hyperbolic conservation laws and balance laws systems. Finally, in Chapter 6, we present our concluding remarks and further perspectives.

2 Definitions and presentation of studied concepts

Many interesting problems in physical, biological, engineering and social sciences can be described by a partial differential equation (PDE). Most real physical processes are governed by partial differential equations. In many cases, simplifying approximations are made to reduce the governing PDEs to ordinary differential equations (ODEs) or even to algebraic equations. However, because of the ever increasing requirement for more accurate modeling of physical processes, engineers and scientists are more and more required to solve the actual PDEs that govern the physical problems. The three classes of PDEs (i.e., elliptic, parabolic, and hyperbolic PDEs) are introduced and many of these partial differential equations are obtained by conservation laws. Therefore, in this Chapter we begin presenting some definitions, properties and examples of fundamental concepts studied by addressing brief definitions of Partial differential equations and examples. We present important concepts of –scalar and system– of hyperbolic Conservation Law and introduce the concepts of two important components in the study of solutions of conservation laws: the shock waves and rarefaction waves.

2.1 Partial differential equations and its classification

A partial differential equation (henceforth abbreviated as PDE) for a function $u(x)$, $x \in \mathbb{R}^n$ is a relation of the form

$$F(x, u, \nabla u, \nabla^2 u, ...) = 0 \tag{2.1.1}$$

where F is a given function of the independent variable $x = (x_1, x_2, x_3, ...x_n)$ and a classical solution function u and of a finite number of its partial derivatives. We call u a solution of (2.1.1) if $u(x)$ is a sufficiently smooth function and after substitution of $u(x)$ and its partial derivatives, (2.1.1) is satisfied identically in $x_1, x_2, ..., x_n$ in some region Ω in the space of these independent variables. Several PDEs involving one or more unknown functions and their derivatives constitute a system.

The order of a PDE or of a system is defined as the order of the highest derivative that occurs in (2.1.1). A PDE is said to be linear if it is linear in the unknown functions and their derivatives, with coefficients depending on the independent variables $x_1, x_2, ..., x_n$. The PDE of order m is called quasilinear if it is linear in the derivatives of order m with coefficients that depend on $x_1, x_2, ..., x_n$ and the derivatives of order $< m$ [22].

Consider a linear second-order differential equation in two independent variables of the form:

$$au_{xx} + bu_{xy} + cu_{yy} + du_x + eu_y + fu = g, \tag{2.1.2}$$

where a, b, c, d, e, f and g depend on (x, y). The classification of (2.1.2) depends on the sign of the discriminant [29],

$$b^2 - 4ac = \begin{cases} < 0, \Longrightarrow \text{Elliptic}, \\ = 0, \Longrightarrow \text{Parabolic}, \\ > 0, \Longrightarrow \text{Hyperbolic}. \end{cases} \tag{2.1.3}$$

In the next sections we will present some classes of classical PDEs.

2.1.1 Classical Examples for Partial differential equations

Partial differential equations occur throughout mathematics. In this section we give some examples of partial differential equations that arise in engineering and science. In many instances one of the independent variables is the time, usually denoted by t, while the others, denoted by $x_1, x_2, \cdots, x_n$ (or by x, y, z when $n \leq 3$) give position in an n-dimensional space.

- Heat equation: $u_t = c^2 u_{xx}$, $c > 0$.
- Heat equation: $u_t = c^2(u_{xx} + u_{yy})$, $c > 0$.
- Wave equation: $u_{tt} = c^2 u_{xx}$, $c > 0$.
- Wave equation: $u_{tt} = c^2(u_{xx} + u_{yy})$, $c > 0$.
- Laplace equation: $u_{xx} + u_{yy} = 0$.

2.2 Conservation laws

The class of conservation laws is a very important class of partial differential equations because as their name indicates, they include those equations that model conservation laws of physics (mass, momentum, energy, etc.) [41, 44].

2.2.1 The scalar conservation laws

In [28, 33], many interesting problems in physical, biological, engineering and social sciences are modeled by a simple paradigm: Consider a domain $\Omega \subset \mathbb{R}^n$ and a quantity of interest u, defined for all points $x \in \Omega$. The quantity of interest u may be the temperature of a rod, the pressure of a fluid, the concentration of a chemical or a group of cells or the density

of a human population. The evolution (in time) of this quantity of interest u can be described by a simple phenomenological observation:

The time rate of change of u in any fixed sub-domain $\omega \subset \Omega$ is equal to the total amount of u produced or destroyed inside ω and the flux of u across the boundary $\partial\omega$.

The above observation says that the change in u is due to two factors: the source or sink, representing the quantity produced or destroyed, and the flux, representing the amount of u that either goes in or comes out of the sub-domain, see Figure 1. This observation is mathematically rendered as

$$\frac{d}{dt}\int_{\omega} u\,dx = -\int_{\partial\omega} F\cdot\nu\,d\sigma(x) + \int_{\omega} S\,dx, \tag{2.2.1}$$

where ν is the unit outward normal, $d\sigma(x)$ is the surface measure, and F and S are the flux and the source or sink respectively. The minus sign in front of the flux term is for convenience. Note that (2.2.1) is an integral equation for the evolution of the total amount of u in ω.

We simplify (2.2.1) by using integration by parts (or the Gauss divergence theorem) on the surface integral to obtain

$$\frac{d}{dt}\int_{\omega} u\,dx + \int_{\omega} \mathrm{div}(F)\,dx = \int_{\omega} S\,dx, \tag{2.2.2}$$

Since (2.2.2) holds for all sub-domains ω of Ω, we can use an infinitesimal ω to obtain the following differential equation:

$$u_t + \mathrm{div}(F) = S, \quad \forall (x,t) \in (\Omega, \mathbb{R}^+). \tag{2.2.3}$$

The differential equation (2.2.3) is often termed as a balance law as it is a statement of the fact that the rate of change in u is a balance of the flux and the source. Frequently, the only change in u is from the fluxes and the source is set to zero. In such cases, (2.2.3) reduces to

$$u_t + \mathrm{div}(F) = 0, \quad \forall \ \ (x,t) \in (\Omega, \mathbb{R}^+). \tag{2.2.4}$$

Equation (2.2.4) is known as a conservation law, as the only change in u comes from the quantity entering or leaving the domain of interest.

The conservation law (2.2.4) (or homogeneous first order hyperbolic equation) and the balance law (2.2.3) are generic to a very large number of models. Explicit forms of the quantity of interest, flux and source depend on the specific model being considered. The modeling of the flux F is the core function of a physicist, biologist, engineer or other domain scientists. We will provides some examples to illustrate conservation laws [28, 33].

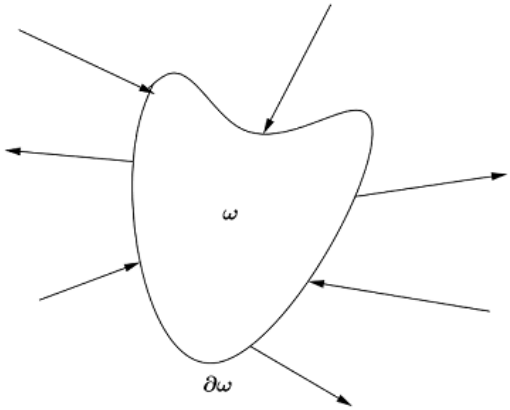

Figure 1 – An illustration of conservation in a domain with the change being determined by the net flux.

2.2.2 Examples for conservation laws

- **Scalar transport equation:**

$$u_t + \operatorname{div}(a(x,t)u) = 0, \qquad \forall \ \ (x,t) \in \mathbb{R} \times \mathbb{R}^+, \tag{2.2.5}$$

with initial condition $u(x,0) = u_0(x), \qquad \forall \ \ x \in \mathbb{R}.$

This equation is linear, the flux in this case is $F = au$. In the simple case of one space dimension and a constant velocity field $a(x,t) \equiv$ a, (2.2.5) reduces to

$$u_t + au_x = 0. \tag{2.2.6}$$

The scalar one-dimensional equation (2.2.6) is often referred to an advection equation [28, 33].

- **The heat equation:**

$$u_t - \operatorname{div}(k\nabla u) = 0, \tag{2.2.7}$$

here $F(u) = -k\nabla u$, and k is the conductivity tensor for the medium. If the conductivity is assumed to be unity and the material is one-dimensional (like a rod), (2.2.7) reduces to the well-known one-dimensional heat equation (2.2.8)

$$u_t - u_{xx} = 0. \tag{2.2.8}$$

The scalar transport equation (2.2.5) and the heat equation (2.2.7) are both linear equations and deal with the evolution of a single scalar quantity.

- **Scalar inviscid Burgers' equation**

$$u_t + \left(\frac{u^2}{2}\right)_x = 0, \qquad x \in \mathbb{R}, \quad t > 0. \tag{2.2.9}$$

along with discontinuous initial data $u(x,0) = u_0(0)$.

- **Buckley-Leverett equation:**

$$u_t + (F(u))_x = 0, \qquad x \in \mathbb{R}, \quad t > 0, \tag{2.2.10}$$

where the flux function is

$$F(u) = \frac{u^2}{u^2 + \mu(1-u)^2}$$

with initial condition $u(x,0) = u_0(0)$ and μ constant.

The flux F in (2.2.4) is often a function of u and its derivatives,

$$F = F(u, \nabla u, \nabla^2 u, ...).$$

For simplicity of our analysis, we neglect the role of the higher than first-order derivatives. Hence, the flux is of the form:

$$F = F(u, \nabla u) \tag{2.2.11}$$

If (2.2.11) is of the form $F = F(u)$, then the conservation law (2.2.4) is a first-order PDE. It is usually classified as hyperbolic. The scalar transport equation (2.2.5) is an example for hyperbolic equations.

If we have $F = F(\nabla u)$, then the conservation law (2.2.4) is a second-order PDE and is often classified as parabolic. The heat equation (2.2.7) is an example of a parabolic equation. When the flux F depends on both the function u and its first derivative, the conservation law (2.2.4) is termed as a convection-diffusion equation [28, 33].

2.3 Theory of scalar conservation laws

Definition: Consider the initial-value problem of the form:

$$\begin{cases} u_t + f(u(x,t))_x = 0, & x \in \mathbb{R} \quad t > 0. \\ u(x,0) = u_0(x), & x \in \mathbb{R}, \end{cases} \tag{2.3.1}$$

where $f \in C^2(\mathbb{R})$ with convex flux ($f''(u) > 0$) and $u_0(x) \in C^2(\mathbb{R})$.

We say u is a strong or classical solution of (2.3.1) if :

- u is continuous for all $x \in \mathbb{R}$ and $t > 0$;
- u_x and u_t exist and are continuous for all $x \in \mathbb{R}$ and $t > 0$;
- u satisfies (2.3.1) for all $x \in \mathbb{R}$ and $t > 0$.

It is well known that the Cauchy problem (2.3.1) does not have, in general, a smooth solution beyond some finite time interval, even when u_0 is sufficiently smooth. For this reason, we study the weak solutions containing the discontinuities; these weak solutions are, in general, not unique and one needs an admissibility criterion to select physically relevant solutions. Here, we study the one-dimensional scalar case to highlight some of these fundamental issues in the theory of hyperbolic equations of conservation laws [28, 33, 39, 44].

2.3.1 Shock Formation

We next rewrite equation (2.3.1) in the nonconservative form

$$u_t + f'(u)u_x = 0, \qquad x \in \mathbb{R} \quad t > 0. \tag{2.3.2}$$

We define the **characteristic curve** of equation (2.3.1) (or equation (2.3.2)) to be the solution to the differential equation

$$\frac{d}{dt}x(t) = f'(u(x,t)). \tag{2.3.3}$$

If we consider a solution of partial differential equation (2.3.2), $u = u(x,t)$, then along any characteristic curve (a curve $x = x(t)$ on which (2.3.3) is satisfied), and since u is a solution to partial differential equation (2.3.2), we have

$$\begin{aligned} \frac{d}{dt}u(x(t),t) &= u_x(x(t),t)\frac{d}{dt}x(t) + u_t(x(t),t) \\ &= u_x(x(t),t)f'(u(x(t),t)) + u_t(x(t),t) \\ &= 0, \end{aligned} \tag{2.3.4}$$

That means that along any characteristic curve defined by equation (2.3.3), the solution to partial differential equation (2.3.2) (or to (2.3.1)) is constant and the characteristic curves are straight lines $x(t) = f'(u)t + c$, where c is constant [41, 44].

If u is a sufficiently smooth solution to the initial-value problem defined by conservation law (2.3.1) for $x \in \mathbb{R}$, $t > 0$ or (2.3.2) along with initial condition $u(x,0) = u_0(x)$, $x \in \mathbb{R}$, then u will satisfy

$$u(x,t) = u_0(x - f'(u(x,t))\,t), \qquad \forall x \in \mathbb{R}, t > 0. \tag{2.3.5}$$

Using the chain rule in (2.3.5) we have

$$\begin{cases} u_t = \dfrac{-f'(u)u_0'(x - tf')}{1 + f''(u)u_0't}, \\[2ex] u_x = \dfrac{u_0'(x - tf')}{1 + f''(u)u_0't}. \end{cases} \tag{2.3.6}$$

We consider the case where $1 + f''(u)u_0't = 0$, then $f''(u)u_0' = \dfrac{-1}{t}$, as $f'' > 0$ we have $u_0' < 0$. Then at $t^* = \dfrac{-1}{\min(f''u_0')}$ (or $1 + f''(u)u_0't^* = 0$), u_t and u_x show a **blow-up** which means that u can not be defined for $t \geq t^*$, or we have a shock at time $t = t^*$.

Let $\phi = \phi(x,t)$ be any function, we say that ϕ has compact support, if it is identically zero outside of some bounded region of the $x-t$ plane. Now we say that a function $u(x,t) \in L^1(\mathbb{R}\times\mathbb{R}^+)$ is a **weak solution** of (2.3.1) if

$$\int_0^\infty \int_{-\infty}^\infty [u\phi_t + f(u)\phi_x]\, dx\, dt + \int_{-\infty}^\infty u_0(x)\phi(x,0)dx = 0, \tag{2.3.7}$$

for all smooth functions $\phi \in C_0^1\left(\mathbb{R}\times\mathbb{R}^+\right)$ with compact support [28, 33, 41, 44].

2.3.2 Rankine-Hugoniot condition

The notion of weak solution allows for solutions u which need not even be continuous. However, weak solutions u have some restrictions on types of discontinuities, etc. For example, suppose u is a weak solution of (2.3.1) such that u is discontinuous across some curve $x = \xi(t)$, but u is smooth on either side of the curve. Let $u^-(x,t)$ be the limit of u approaching (x,t) from the left of the curve $x = \xi(t)$ and let $u^+(x,t)$ be the limit of u approaching (x,t) from the right $x = \xi(t)$. We claim that the curve $x = \xi(t)$ cannot be arbitrary, but rather there is a relation between $x = \xi(t)$, u^- and u^+.

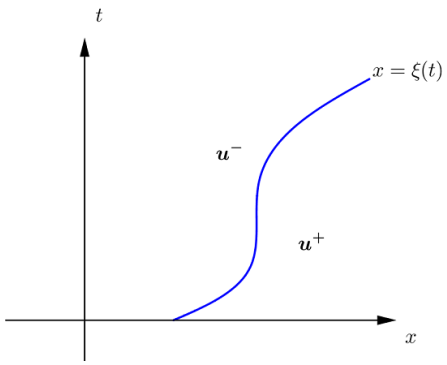

Figure 2 – Illustration of the speed of propagation of the discontinuity.

Theorem: If u is a weak solution of (2.3.1) such that u is discontinuous across the curve $x = \xi(t)$ but u is smooth on either side of $x = \xi(t)$, then u must satisfy the condition

$$\frac{f(u^-) - f(u^+)}{u^- - u^+} = \xi'(t), \tag{2.3.8}$$

across the curve of discontinuity, where $u^-(x,t)$ is the limit of u approaching (x,t) from the left and $u^+(x,t)$ is the limit of u approaching (x,t) from the right $x = \xi(t)$.

For shorthand notation, we define

$$\begin{cases} [u] = u^- - u^+, \\ [f(u)] = f(u^-) - f(u^+), \\ \sigma = \xi'(t). \end{cases}$$

We call $[u]$ and $[f(u)]$ the jumps of u and $f(u)$ across the discontinuity curve and σ the speed of propagation of the discontinuity. Therefore, if u is a weak solution with discontinuity along a curve $x = \xi(t)$, the solution must satisfy

$$[f(u)] = \sigma[u]. \tag{2.3.9}$$

where $\sigma = \xi'(t)$. This is called the **Rankine-Hugoniot jump condition** [28, 41, 44]

2.3.3 Examples

Consider the scalar inviscid Burger's equation [28, 41, 44],

$$\begin{cases} u_t + \left(\dfrac{u^2}{2}\right)_x = 0, & x \in \mathbb{R}, \quad t > 0 \\ u(x,0) = u_0(x), & x \in \mathbb{R}, \end{cases} \tag{2.3.10}$$

where

$$u(x,0) = \begin{cases} 1, & \text{for } \ x < 0, \\ 0, & \text{for } \ x > 0. \end{cases} \tag{2.3.11}$$

Using the method of characteristics to solve this equation we have that u is constant along the projected characteristic curves given by $x = u_0(r)t + r$. If $r < 0$ then $u_0(r) = 1$, which implies that the projected characteristic curves are $x(t) = t + r$ for $r < 0$ and the solution u should be equal to 1 along those curves. Also for $r > 0$, $u_0(r) = 0$ which means the projected characteristic curves are given by $x(t) = r$ for $r > 0$ and the solution u should be equal to 0 along these curves. We have crossing of characteristics curves (see, Figure 3). Clearly, this is a contradiction and we can't hope to find any continuous solution which solves this problem. Then, we look for a weak solution, by looking for a piecewise continuously differentiable function which satisfies the Rankine Hugoniot jump condition [28, 41, 44].

For the Rankine-Hugoniot condition we have $\xi'(t) = \dfrac{1}{2}$, where $u^- = 1$ and $u^+ = 0$. Thus, the weak solution of (2.3.10) satisfying (2.3.11) is given by

$$u(x,t) = \begin{cases} 1, & \text{for } \ x < \dfrac{t}{2}, \\ 0, & \text{for } \ x > \dfrac{t}{2}. \end{cases} \tag{2.3.12}$$

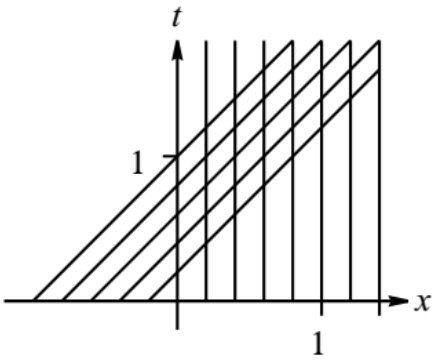

Figure 3 – Characteristic curves for (2.3.10)-(2.3.11).

Besides the intersection of the characteristics curves, another particularity of the non-linear

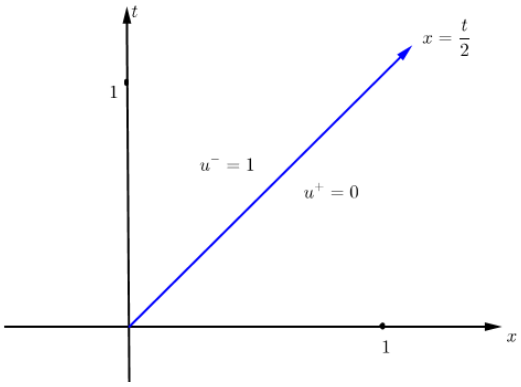

Figure 4 – Shock curve.

equations is the possibility of existence regions of the plane $x - t$ where these curves are not defined. We will modify the feature of the characteristic method in these regions so that we can get solutions of the problem across the $x - t$ plane. This modification generates what is called **rarefaction waves** [28, 41, 44].

Consider the inviscid Burgers' equation (2.3.10) with initial condition

$$u(x,0) = \begin{cases} 0, & \text{for } x < 0, \\ 1, & \text{for } x > 0. \end{cases} \tag{2.3.13}$$

By the characteristics methods [28, 41, 44], we see that u should be constant along the projected characteristic curves, $x(t) = u_0(r)t + r$. Here, if $r < 0$, then $u_0(r) = 0$ and therefore, $x(t) = r$. If $r > 0$, then $u_0(r) = 1$ and therefore, $x(t) = t + r$. Consequently, we have no crossing of characteristics curves. However, we still have a problem. In fact, we have a region on which we don't have enough information (see, Figure 5)!

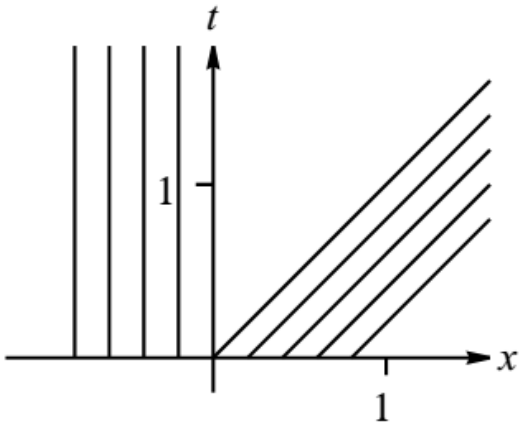

Figure 5 – Characteristic curves for (2.3.13)-(2.3.14) .

In this case, a weak solution of (2.3.10) satisfying (2.3.13) is given by

$$u(x,t) = \begin{cases} 0, & \text{for } x \leq \dfrac{t}{2}, \\ \dfrac{x}{t}, & \text{for } 0 \leq x \leq t, \\ 1, & \text{for } x \geq \dfrac{t}{2}. \end{cases} \tag{2.3.14}$$

This type of solution which "fans" the wedge $0 < x < t$ is called a rarefaction wave.

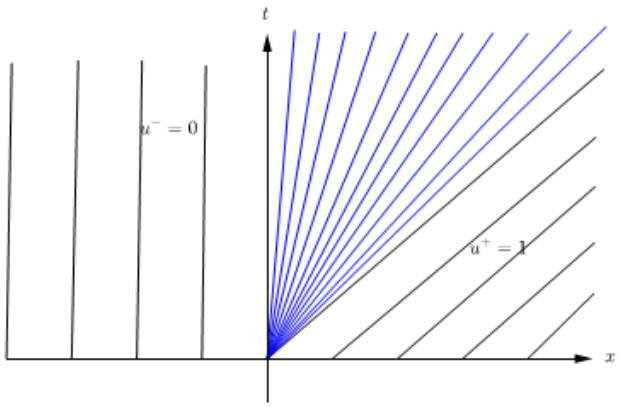

Figure 6 – Rarefaction fan.

2.3.4 The Entropy Condition

As we have seen in the last section, weak solutions to conservation laws may contain discontinuities that are due to a discontinuity in the initial condition or to characteristics that cross each other, or may occur reasonably randomly as long as the jump conditions are satisfied

across the discontinuities. In addition, we saw that the weak solutions to conservation laws need not be unique.

If we write the inviscid Burgers' equation

$$u_t + (\frac{u^2}{2})_x = 0, \tag{2.3.15}$$

in the quasilinear form $u_t + uu_x = 0$ and multiply by $2u$, we obtain $2uu_t + 2u^2u_x = 0$, which can be rewritten as

$$(u^2)_t + (\frac{2}{3}u^3)_x = 0. \tag{2.3.16}$$

This is again a conservation law, now for u^2 rather than u itself, with flux function $f(u^2) = \frac{2}{3}\left(u^2\right)^{3/2}$

The differential equations (2.3.15) and (2.3.16) have precisely the same smooth solutions. However, they have different weak solutions, as we can see by considering the Riemann problem with $u^- > u^+$. A weak solution of (2.3.15) is a shock traveling at speed

$$\sigma_1 = \frac{\left[\frac{1}{2}u^2\right]}{[u]} = \frac{1}{2}\left(u^- + u^+\right), \tag{2.3.17}$$

whereas a weak solution to (2.3.16) is a shock traveling at speed

$$\sigma_2 = \frac{\left[\frac{2}{3}u^3\right]}{[u^2]} = \frac{2}{3}\left(\frac{(u^-)^3 - (u^+)^3}{(u^-)^2 - (u^+)^2}\right). \tag{2.3.18}$$

We have then

$\sigma_2 - \sigma_1 = \frac{1}{6}\frac{(u^- - u^+)^2}{u^- + u^+}$, and so $\sigma_2 \neq \sigma_1$ when $u^- \neq u^+$, and the two equations have different weak solutions [28].

Entropy Condition (Lax): For a convex scalar conservation law, a discontinuity propagating with speed σ given by (2.3.8) satisfies the Lax entropy condition if

$$f'(u^-) > \sigma > f'(u^+). \tag{2.3.19}$$

Note that $f'(u)$ is the characteristic speed.

We say that a curve of discontinuity is a **shock curve** for a solution u if the curve satisfies the Rankine-Hugoniot jump condition and the entropy condition for that solution u. We say that u is a weak, admissible solution of (2.3.1) only if u is a weak solution such that any curve of discontinuity for u is a shock curve.

A function f is uniformly convex if there exists a constant $\theta > 0$ such that $f'' > \theta > 0$. In particular, this means f' is strictly increasing.

For convex or concave function, the Rankine-Hugoniot speed σ from (2.3.8) must lie between $f'(u^-)$ and $f'(u^+)$, so (2.3.19) reduces to simply the requirement that $f'(u^-) > f'(u^+)$. If $u^- > u^+$ then the correct solution would be a shock curve for a uniformly convex flux function and if $u^- < u^+$, the correct solution would be a rarefaction wave for a uniformly convex flux function. For Burgers' equation with $f(u) = u^2/2$, the Lax Entropy Condition requires $u^- > u^+$ for an admissible shock, since $f''(u)$ is everywhere positive rather than negative.

For the case when f is uniformly convex, requiring that curves of discontinuity satisfy the entropy condition (2.3.19) guarantees uniqueness of (2.3.1). In the case, when f is not uniformly convex, condition (2.3.19) is not enough to guarantee uniqueness of solutions. In order to guarantee uniqueness of solutions, we introduce the Oleinik entropy condition [28, 41, 44].

Entropy condition (Oleinik): The condition that

$$\frac{f(u^-) - f(u)}{u^- - u} \geq \frac{f(u^-) - f(u^+)}{u^- - u^+}, \tag{2.3.20}$$

for all u between u^- and u^+ is known as the Oleinik entropy condition [28, 41, 44].

2.4 Hyperbolic systems of conservation laws in one space dimension

Hyperbolic systems of partial differential equations can be used to model a wide variety of phenomena that involve wave motion or the advective transport of substances.

In one space dimension, a homogeneous first-order $n \times n$ system of conservation laws equations in x and t has the form

$$u_t(x,t) + f(u(x,t))_x = 0, \quad t \in \mathbb{R}^+, x \in \mathbb{R}, \tag{2.4.1}$$

or

$$\begin{cases} \dfrac{\partial}{\partial t}u^1 + \dfrac{\partial}{\partial x}\left[f^1\left(u^1, u^2, ..., u^n\right)\right] = 0, \\ \quad ..... \\ \dfrac{\partial}{\partial t}u^n + \dfrac{\partial}{\partial x}\left[f^n\left(u^1, u^2, ..., u^n\right)\right] = 0, \end{cases} \tag{2.4.2}$$

where $u : \mathbb{R} \times \mathbb{R} \longrightarrow \mathbb{R}^n$ is a vector with n components representing the unknown functions (pressure, velocity, etc.,) i.e, $u = [u^1, u^2, ..., u^n]^T$ and $f = [f^1, f^2, ..., f^n]^T$ is the flux vector.

Calling

$$A(u) = Df(u) = \begin{pmatrix} \frac{\partial f^1}{\partial u^1} & \cdots & \frac{\partial f^1}{\partial u^n} \\ & \cdots & \\ \frac{\partial f^n}{\partial u^1} & \cdots & \frac{\partial f^n}{\partial u^n} \end{pmatrix}, \tag{2.4.3}$$

the $n \times n$ Jacobian matrix of the map f at the point u, the system (2.4.2) can be written in the quasilinear form

$$u_t + A(u)u_x = 0. \tag{2.4.4}$$

In the linear case,

$$u_t + Au_x = 0, \tag{2.4.5}$$

we have $f(u) = Au$ where $A \in \mathbb{R}^{n\times n}$ is a constant matrix (in both space and time) entries, with $u(x, 0) = u_0(x)$ as initial condition (see [28, 29, 33, 44]).

2.4.1 Hyperbolicity and well-balancing

Definition: (strictly hyperbolic system). The system of conservation laws (2.4.2) is strictly hyperbolic if, for every u, the Jacobian matrix $A(u) = Df(u)$ has n real, distinct eigenvalues (diagonalizable): $\lambda_1(u) < ... < \lambda_n(u)$.

Thus, the concept of hyperbolicity for a system is tied to the eigenstructure of the underlying matrix. A matrix A is diagonalizable if it has a complete set of eigenvectors, i.e, there exists n linearly independent vectors $r_1(u), ..., r_n(u) \in \mathbb{R}^n$ and corresponding eigenvalues $\lambda_1(u) < ... < \lambda_n(u) \in \mathbb{R}$ such that $A(u)r_i(u) = \lambda_i(u)r_i(u), \quad i = 1, ..., n$ [28, 29, 33, 44].

The n-th field of conservation law (2.4.1) is **genuinely nonlinear** if $(\text{grad}\lambda_n(u)).r_n(u) \neq 0$ (where grad is the gradient with respect to the components of the u vector) for all $u \in \mathbb{R}^n$. If $(\text{grad}\lambda_n(u)).r_n(u) = 0$ for all $u \in \mathbb{R}^n$, we say that the n-th field of conservation law (2.4.1) is **linearly degenerate** [44].

2.4.2 Linear case and nonlinear cases

Consider the linear systems (2.4.5), where A is a diagonalizable constant matrix. Then we can perform the transformation

$$R^{-1}u_t + R^{-1}ARR^{-1}u_x = 0, \tag{2.4.6}$$

where R is the matrix of eigenvectors of A. Introducing the characteristic variable

$$w(x, t) = R^{-1}u(x, t),$$

we obtain the decoupled system

$$w_t + \Lambda w_x = 0, \tag{2.4.7}$$

where $\Lambda = R^{-1}AR$ is the diagonal matrix consisting of the eigenvalues λ_p of A, $p = 1, 2, ..., n$. We thus have a set of n independent advection equations for components w_p of w:

$$(w_p)_t + \lambda_p (w_p)_x = 0, \qquad \text{for } \; p = 1, 2, \cdots, n. \tag{2.4.8}$$

with solution $w_p(x,t) = (w_p)_0(x - \lambda_p t)$, where $(w_p)_0(x) \equiv R^{-1}u_0(x)$ is the initial data.

We use the decoupling of the linear system to solve the problem

$$u_t + Au_x = 0 \tag{2.4.9}$$

with

$$u(x,0) = \begin{cases} u^-, & x < 0, \\ u^+, & x > 0, \end{cases} \tag{2.4.10}$$

where u^- and u^+ are two constant states. A hyperbolic partial differential equation with the initial data consisting of two constant states is called a *Riemann problem*. The solution of (2.4.9)-(2.4.10) can be written

$$u(x,t) = \sum_{p=1}^{n} (w_p)_0(x - \lambda_p t) r_p, \tag{2.4.11}$$

where all the functions $(w_p)_0(x)$ are step functions with a jump at $x = 0$. Let denote

$$(w_p)_0(x) = \begin{cases} w_p^-, & x < 0, \\ w_p^+, & x > 0. \end{cases} \tag{2.4.12}$$

The solution is thus piecewise constant, with changes when $x - \lambda_p t$ changes sign for some p. From this observation the solution is

$$u(x,t) = \sum_{p:\lambda_p < x/t} w_p^+ r_p + \sum_{p:\lambda_p > x/t} w_p^- r_p. \tag{2.4.13}$$

The solution is thus constant on wedges in the $x - t$ plane as seen in Figure 7.

The derivation of (2.3.9) is valid for systems of conservation laws as well as for scalar equations. However, for a system of n equations, $u^- - u^+$, and $f(u^-) - f(u^+)$ will both be n-vectors and we will not be able to simply divide as in (2.3.8) to obtain the shock speed. In fact, for arbitrary states u^- and u^+, there will be no scalar value σ for which (2.3.9) is satisfied. Special relations must exist between the two states in order for them to be connected by a shock: the vector $f(u^-) - f(u^+)$ must be a scalar multiple of the vector $u^- - u^+$. We have already seen this condition in the case of a linear system, where $f(u) = Au$. In this case the

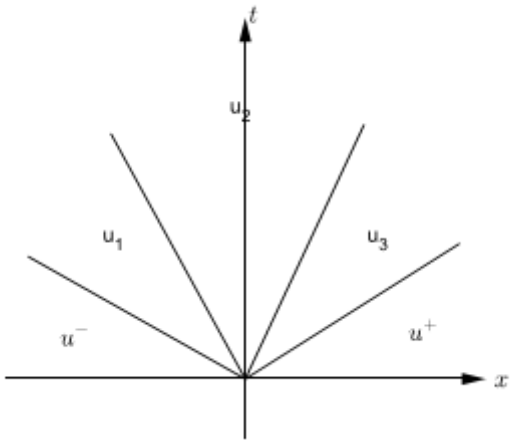

Figure 7 – Solution of the linear Riemann problem in the $x-t$ plane, $n=4$.

Rankine–Hugoniot condition (2.3.9) becomes $A[u] = \sigma[u]$, which means that $u^- - u^+$ must be an eigenvector of the matrix A. The propagation speed σ of the discontinuity is then the corresponding eigenvalue λ.

If the coefficient matrix is diagonalizable, a linear system can be decoupled into a number of independent scalar problems. This is however not true for a non-linear system where the diagonalizing transformation R is now a function of $u(x,t)$.

Let k be a genuinely nonlinear field. A k-shock is a discontinuity satisfying (2.3.9) and for which it holds (see, [28, 29, 33, 44]),

$$\lambda_k(u^-) > \sigma > \lambda_k(u^+),$$
$$\lambda_{k-1}(u^-) < \sigma < \lambda_{k+1}(u^+).$$

2.4.3 Nonstrictly Hyperbolic System of Conservation Laws

Consider the first-order $n \times n$ system of conservation laws in one dimensional space (2.4.1). We suppose that this system is hyperbolic: for every $u \in \mathbb{R}^{\ltimes}$ the eigenvalues $\lambda_i(u)$, $i = 1, 2 \cdots, n$ are real. The system (2.4.1) is nonstrictly hyperbolic if $\lambda_i(u) = \lambda_j(u)$ for some states u and for $i \neq j$, then waves pertaining to different characteristic families may not separate as time evolves. When this happens, nonlinear interactions of these waves may alter the asymptotic state.

In particular, if we consider a 2×2 system in one dimensional space we have $\lambda_1(u) = \lambda_2(u)$ then u is called an *umbilic point*. The strict hyperbolicity fails precisely at the umbilic points of a certain surface. For hyperbolic equations, umbilic points are typically isolated and at an isolated umbilic point, A is typically diagonalizable. Moreover, such umbilic points persist under perturbations of the function f, providing that the hyperbolicity of (2.4.1) is maintained.

The difficulty for non-strictly hyperbolic conservation laws is that there is no well-defined ordering of the eigenvalues in the domain of the problem. [25, 30, 37, 31].

2.4.4 Examples of hyperbolic systems

- **The wave equation:** The simplest example of (2.4.5) is given by the one-dimensional second-order wave equation,

$$u_{tt} - c^2 u_{xx} = 0. \tag{2.4.14}$$

This equation is also known as the string equation (see [28, 29, 33, 41, 44]), as it models vibrations in media like strings and rods. The wave equation can be written as a first-order system by defining auxiliary variables $v = cu_x$ and $w = -u_t$. With this change of variables, we show that (2.4.14) transforms to

$$\begin{cases} v_t + cw_x = 0, \\ w_t + cv_x = 0. \end{cases} \tag{2.4.15}$$

Hence, the wave equation (2.4.15) is an example of the strictly hyperbolic linear system (2.4.5) with

$$u = \begin{bmatrix} v \\ w \end{bmatrix}, \qquad A = \begin{bmatrix} 0 & c \\ c & 0 \end{bmatrix}. \tag{2.4.16}$$

- **Shallow water equations:** To derive the one-dimensional shallow water equations, we consider fluid in a channel of unitary width and assume that the vertical velocity of the fluid is negligible and the horizontal velocity $v(x,t)$ is roughly constant throughout any cross section of the channel, $h(x,t)$ is the height. The quantity hv is often called the discharge in shallow water theory, since it measures the flow rate of water past a point [28], We have

$$\begin{bmatrix} h \\ hv \end{bmatrix}_t + \begin{bmatrix} hv \\ v^2 h + \frac{1}{2} g h^2 \end{bmatrix}_x = \begin{bmatrix} 0 \\ 0 \end{bmatrix}. \tag{2.4.17}$$

If we define

$$u = \begin{bmatrix} h \\ hv \end{bmatrix}, \qquad f(u) = \begin{bmatrix} hv \\ v^2 h + \frac{1}{2} g h^2 \end{bmatrix}, \tag{2.4.18}$$

the nonlinear equations can be written in the form of (2.4.2). And the Jacobian matrix is

$$A = \begin{bmatrix} 0 & 1 \\ -v^2 + gh & 2v \end{bmatrix}. \tag{2.4.19}$$

The eigenvalues are $\lambda_1 = v - c$, $\lambda_2 = v + c$ and the right eigenvectors are $r_1 = (1, v-c)^T$, $r_2 = (1, v+c)^T$,

where $c = \sqrt{gh}$. However, this nonlinear system is **strictly hyperbolic** [28]. If we assume that h and v are smooth the system (2.4.17, becomes

$$\begin{bmatrix} v \\ \varphi \end{bmatrix}_t + \begin{bmatrix} \frac{v^2}{2} + \varphi \\ v\varphi \end{bmatrix}_x = 0, \tag{2.4.20}$$

where $\varphi = gh$. Notice that if $h = 0$, the eigenvalues coincide. In that case the system is no longer hyperbolic and this induces difficulties at both theoretical and numerical levels. If $|v| < \sqrt{gh}$ the characteristic velocities have opposite signs and information propagates upward as well as downward the flow, what is called subcritical or fluvial. On the other hand, when $|v| > \sqrt{gh}$, the flow is supercritical, or torrential and all information go downwards. A transcritical regime exists when some parts of a flow are subcritical, other supercritical . A subcritical flow is therefore determined by one upstream and one downstream value, whereas a supercritical flow is completely determined by the two upstream values. Two quantities are useful in this context. The first one is a dimensionless parameter called the Froude number $Fr = \frac{|v|}{\sqrt{gh}}$. It is the analogue of the Mach number in gas dynamics, and the flow is subcritical (resp. supercritical) if $Fr < 1$ (resp. $Fr > 1$). The other important quantity is the so-called critical height hc which writes $hc = (\frac{M}{\sqrt{g}})^{\frac{2}{3}}$, for M a given discharge hv. It is a very readable criterion for criticality: the flow is subcritical (resp. supercritical) if $h > hc$ (resp. $h < hc$) [16, 28].

- **Isentropic gas dynamics:** Consider this coupled system of two nonlinear conservation laws

$$\begin{cases} \rho_t + (\rho v)_x = 0, \\ (\rho v)_t + (\rho v^2 + P(\rho))_x = 0. \end{cases} \tag{2.4.21}$$

Here ρ is the mass density, v is the velocity and P the pressure. $P(\rho)$ is a given function specifying the pressure in terms of density which satisfies $P'(\rho) > 0$ for all $\rho > 0$. If we define

$$u = \begin{bmatrix} \rho \\ \rho v \end{bmatrix} = \begin{bmatrix} u^1 \\ u^2 \end{bmatrix}, \qquad f(u) = \begin{bmatrix} \rho v \\ \rho v^2 + P(\rho) \end{bmatrix} = \begin{bmatrix} u^2 \\ (u^2)^2/u^1 + P(u^1) \end{bmatrix}. \tag{2.4.22}$$

the nonlinear equations (2.4.21) of isentropic gas dynamics can be written in the form of (2.4.2). And the Jacobian matrix is

$$A = \begin{bmatrix} 0 & 1 \\ -v^2 + P'(\rho) & 2v \end{bmatrix}. \tag{2.4.23}$$

The eigenvalues are $\lambda_1 = v - c$, $\lambda_2 = v + c$ and the right eigenvectors are $r_1 = (1, v - c)^T$, $r_2 = (1, v + c)^T$, where the velocity v may now vary from point to point, as does the

sound speed $c = \sqrt{P'(\rho)}$. However, since $P'(\rho) > 0$ at all points in the gas, this nonlinear system is **strictly hyperbolic** [28].

- **Gas dynamics:** The Euler equations describing the evolution of a non viscous gas take the form

$$\begin{cases} \rho_t + (\rho v)_x = 0, & \text{(conservation of mass)}, \\ (\rho v)_t + (\rho v^2 + p)_x = 0, & \text{(conservation of momentum)}, \\ (\rho E)_t + (\rho E v + p v)_x = 0, & \text{(conservation of energy)}. \end{cases} \tag{2.4.24}$$

Here ρ is the mass density, v is the velocity while $E = (p/\rho)(\gamma - 1)^{-1} + (v^2/2)$ is the total specific energy, $\gamma > 1$. The system is closed by a constitutive relation of the form $p = p(\rho, e)$, giving the pressure as a function of the density and the internal energy e. The particular form of p depends on the gas under consideration [28, 29, 33, 44].

We know that for smooth flows, the system (2.4.24) can be equivalently written in a nonconservative form , namely

$$\begin{cases} \rho_t + v\rho_x + \rho v_x = 0, \\ v_t + v v_x + (1/\rho)\rho_x = 0, \\ p_t + \gamma p v_x + v p_x = 0. \end{cases} \tag{2.4.25}$$

The Jacobian of the system (2.4.25) has distinct eigenvalues. $\lambda_1 = v - c < \lambda_2 = v < \lambda_3 = v + c$,

where $c = \sqrt{\dfrac{\gamma p}{\rho}}$ is the speed of sound; the associated eigenvectors can be taken as

$r_1 = (\rho, -c, \rho c^2)^T, r_2 = (1, 0, 0)^T, r_3 = (\rho, c, \rho c^2)^T$.

Thus, we have grad $(\lambda_1, r_1) = -(1 + \gamma)c/2$, grad $(\lambda_2, r_2) = 0$, grad $(\lambda_3, r_3) = (1 + \gamma)c/2$, implying thereby that the first and third characteristic fields are genuinely nonlinear, while the second one is linearly degenerate. This nonlinear system is **strictly hyperbolic** [28].

- **Immiscible three-phase flow:** Three-phase flow is described by a pressure equation, expressing Darcy's law of force, coupled with two saturation equations, which generalize the classical Buckley-Leverett equation and express the conservation of mass of water, oil, and gas. The pressure equation implies that the total fluid velocity is independent of position, so we take it to be constant. After nondimensionalizing the time and space variables, fluid viscosities, and capillary pressures in the standard way [31], one obtains the following system of partial differential equations

$$\frac{\partial s_w}{\partial t} + \frac{\partial}{\partial x} f_w(s_w, s_g) = D_w, \tag{2.4.26}$$

$$\frac{\partial s_g}{\partial t} + \frac{\partial}{\partial x} f_g(s_w, s_g) = D_g. \tag{2.4.27}$$

Here s_w and s_g denote the water and gas saturations, and the oil saturation is $s_o = 1 - s_w - s_g$. The state of the fluid is defined by the saturation pair, denoted $S = (s_w, s_g)$. The fractional flow functions f_w and f_g are given in terms of the relative permeability functions k_w , k_g, and k_o and the fluid viscosities μ_w, μ_g , and μ_o by

$$f_w = \frac{k_w/\mu_w}{k_w/\mu_w + k_g/\mu_g + k_o/\mu_o}, \tag{2.4.28}$$

and

$$f_g = \frac{k_g/\mu_g}{k_w/\mu_w + k_g/\mu_g + k_o/\mu_o}, \tag{2.4.29}$$

The diffusion terms

$$D_w = \frac{\partial}{\partial x}\left(B_{ww}\frac{\partial s_w}{\partial x}\right) + \frac{\partial}{\partial x}\left(B_{wg}\frac{\partial s_g}{\partial x}\right), \tag{2.4.30}$$

and

$$D_g = \frac{\partial}{\partial x}\left(B_{gw}\frac{\partial s_w}{\partial x}\right) + \frac{\partial}{\partial x}\left(B_{gg}\frac{\partial s_g}{\partial x}\right), \tag{2.4.31}$$

represent the effect of capillary pressure differences among fluids; here B_{ww}, B_{wg} , B_{gw}, and B_{gg} are the components of the diffusion matrix B given by

$$B = \begin{pmatrix} \frac{k_w}{\mu_w}(1 - f_w) & -\frac{k_w}{\mu_w} f_g \\ -\frac{k_g}{\mu_g} f_w & \frac{k_g}{\mu_g}(1 - f_g) \end{pmatrix} \begin{pmatrix} \frac{\partial p_{wo}}{\partial s_w} & \frac{\partial p_{wo}}{\partial s_g} \\ \frac{\partial p_{go}}{\partial s_w} & \frac{\partial p_{go}}{\partial s_g} \end{pmatrix}. \tag{2.4.32}$$

For simplicity, we assume that each of the relative permeability functions depends solely on its corresponding fluid saturation. We also adopt the assumption of Leverett about the capillary pressure differences, namely that p_{wo} depends solely on s_w and p_{go} depends solely on s_g. The partial differential equations (2.4.26) and (2.4.27) have solutions that propagate as waves. The propagation speeds of continuous waves are the eigenvalues of the Jacobian derivative matrix $\frac{\partial(f_w, f_g)}{\partial(s_w, s_g)}$, provided that these eigenvalues are real. There are two eigenvalues corresponding to each pair of saturations; the smaller is called the slow characteristic speed and the larger is called the fast characteristic speed. Both are nonnegative in the saturation triangle $\{(s_w, s_g) : 0 \le s_w \le 1, 0 \le s_g \le 1, s_w + s_g \le 1\}$. A model of Corey-Pope type has the peculiarity that for a particular state in the interior of the saturation triangle, $S^u = (s_w^u, s_g^u)$, the characteristic speeds coincide, or resonate. Such a state is called an **umbilic point**. For fixed relative permeability functions, the viscosities of the fluids determine the location of the umbilic point [31].

- **Elastic string problem:**

  The following two conservation laws are derives from a model of elastic strings,(see, [25, 30, 37])

$$\begin{cases} u_t + (\phi u)_x = 0, & x \in \mathbb{R}, \quad t > 0, \\ v_t + (\phi v)_x = 0, & x \in \mathbb{R}, \quad t > 0, \end{cases} \tag{2.4.33}$$

  where $\phi = \phi(u, v)$. This system models the propagation of forward longitudinal and transverse waves in a stretched elastic string which moves in a plane.

  The feature of interest in system (2.4.33) is that the equations are non-strictly hyperbolic in the following sense. Introducing vector notation $U = (u, v)$, $F = (\phi u, \phi v)$, then for the differentiable solutions the system (2.4.33) can be written as

$$U_t + AU_x = 0, \tag{2.4.34}$$

  where $A = A(U) = \dfrac{\partial F}{\partial U}$. Let (r, θ) be the polar coordinates, $r^2 = u^2 + v^2$, $\mathrm{tg}\theta = v/u$ and write $\phi = \phi(r, \theta)$, then we find from the differentiated form of (5.2.11) with

$$A = \begin{pmatrix} \phi + u\phi_u & u\phi_v \\ \\ v\phi_u & \phi + v\phi_v \end{pmatrix}, \tag{2.4.35}$$

  the eigenvalues of A (characteristic speeds of the system) are

$$\begin{cases} \lambda_1 = \phi, \\ \lambda_2 = \dfrac{\partial}{\partial r}(r\phi) = \phi + r\dfrac{\partial \phi}{\partial r}. \end{cases}$$

  In the elastic string problem, solutions with $r = 0$ are physically inadmissible, and we shall look in general at solutions of (2.4.33) in the punctured plane $\mathbb{R}^2 - \{0\}$. Thus (2.4.33) is not strictly hyperbolic on $\Sigma \equiv \{(r, \theta) : \partial\phi/\partial r = 0\} = \{(r, \theta) : \lambda_1 = \lambda_2\}$.

  The eigenvector w_1 corresponding to λ_1 is parallel to $(-\phi_v, \phi_u)$, so that $w_1.\nabla\lambda_1 = 0$ and hence every shock of this family is a contact discontinuity. The eigenvector w_2 corresponding to λ_2 is parallel to (u, v), and $w_2.\nabla\lambda_2 = r(r\phi)_{rr}$ and so this family is genuinely nonlinear if $(r\phi)_{rr} = 2\phi_r + r\phi_{rr} \neq 0$ [25, 30, 37].

3 Lagrangian-Eulerian scheme for scalar hyperbolic conservation laws

For the construction of the Lagrangian-Eulerian scheme and the study of an equivalent finite difference scheme to the Lagrangian-Eulerian approach based on locally conservative finite volume method we follow very closely the works [1, 35]. We address the usefulness of identifying modified equations which models the qualitative behavior of the difference scheme in connection to the original equation taking into account the regularity of the initial data. Computational results for linear and nonlinear scalar conservation laws with convex and non-convex flux functions – Linear hyperbolic conservation law with constant and variable velocity, inviscid Burgers' equations and Bucklet-Leverett's equations– are presented and discussed to show our current understanding of the Lagrangian-Eulerian framework. Finally, by means of an accurate algorithm developed in [11] for approximating the Hilbert transform, we present and discuss qualitative numerical experiments for hyperbolic conservation laws with nonlocal flux, showing evidence of attenuation and blow up of concentration type by means of some initial measure data such as square pulse initial data, Gaussian initial data and Oscillatory initial data.

3.1 The Lagragian-Eulerian formulation

Consider the initial value problem for single conservation laws as follows:

$$\frac{\partial u}{\partial t} + \frac{\partial H(u)}{\partial x} = 0, \qquad t > 0, \qquad x \in \mathbb{R}, \tag{3.1.1}$$

$$u(x,0) = \eta(x), \qquad x \in \mathbb{R}, \tag{3.1.2}$$

where $H(u)$ is a smooth function of $u = u(x,t)$. For the construction of the Lagrangian-Eulerian procedure, we first consider the equation (3.1.1) written in locally conservative space-time generalized divergence form, along with $u(x,0) = \eta(x)$,

$$\nabla_{t,x} \begin{bmatrix} u \\ H(u) \end{bmatrix} = 0, \quad t > 0, \quad x \in \mathbb{R}. \tag{3.1.3}$$

In order to set the finite dimensional function spaces relying on solving the approximate problem by the Lagrangian-Eulerian method for (3.1.1)-(3.1.2), we now introduce some notation. The plane region $\mathbb{R}\times\overline{\mathbb{R}} = \{(x,t);\ -\infty < x < \infty;\ t \geq 0\}$ will be replaced by the lattice $\mathbb{N} \times \mathbb{Z} = \{(j,n);\ j = 0, \pm 1, \pm 2, \ldots;\ n = 0, 1, 2, \cdots\}$, and instead of functions $u(\cdot,t) \in L^p(\mathbb{R})$

for $t \geq 0$, we will consider the sequences $U^n = (U^n)_j$, $j \in \mathbb{Z}$ for $n = 0, 1, 2, \cdots$, for a given mesh $h > 0$ and a time level

$$t^n = \sum_{i=0}^{i=n-1} \Delta t^i, \tag{3.1.4}$$

with $t^0 = 0$, for non-constant time step Δt^i. In the time level t^n, we have $x_j^n = jh$, $x_{j+\frac{1}{2}}^n = jh + \frac{h}{2}$ on the uniform local grid or original grid, here $h_j^n = \Delta x^n = x_{j+\frac{1}{2}}^n - x_{j-\frac{1}{2}}^n = h$, $j \in \mathbb{Z}$, where $x_{j\pm\frac{1}{2}}^n$ are endpoint of the cell. For the non-uniform grid we have $h_j^{n+1} = \overline{\Delta x}^{n+1} = \overline{x}_{j+\frac{1}{2}}^{n+1} - \overline{x}_{j-\frac{1}{2}}^{n+1}$, in the time level t^{n+1}. Here x_j^n and $\overline{x}_j^{n+1}$ are the centers of the cells respectively. The numerical solution of u in the cells $[x_{j-\frac{1}{2}}^n, x_{j+\frac{1}{2}}^n]$ and $[\overline{x}_{j-\frac{1}{2}}^{n+1}, \overline{x}_{j+\frac{1}{2}}^{n+1}]$ are defined by,

$$U(x_j, t^n) = U_j^n = \frac{1}{h} \int_{x_{j-\frac{1}{2}}^n}^{x_{j+\frac{1}{2}}^n} u(x, t^n) dx, \quad \text{and} \quad \overline{U}_j^{n+1} = \frac{1}{h_j^{n+1}} \int_{\overline{x}_{j-\frac{1}{2}}^{n+1}}^{\overline{x}_{j+\frac{1}{2}}^{n+1}} u(x, t^{n+1}) dx \quad j \in \mathbb{Z}, \tag{3.1.5}$$

respectively, and the initial condition is $U(x_j^0, t^0) = U_j^0$ in the cells $[x_{j-\frac{1}{2}}^0, x_{j+\frac{1}{2}}^0]$, $j \in \mathbb{Z}$. Notice, in the equations (3.1.5), the quantity $u(x, t)$ is a solution of (3.1.1). The discrete counterpart of the space $L^p(\mathbb{R})$ is l_h^p, the space of sequences $U = (U_j)$, with $j \in \mathbb{Z}$, such that $\|U\|_{l_h^p} = \left(h \sum_{j \in \mathbb{Z}} |U_j|^p \right)^{\frac{1}{p}}$, $1 \leq p < \infty$ or $\|U\|_{l_h^\infty} = \sup_{j \in \mathbb{Z}} |U_j|$ where U is defined in the appropriate l_p-space.

3.1.1 The local Lagrangian-Eulerian conservation relation

As in [1, 35], we consider cell-centered finite-volume cell in a Lagrangian framework (see left picture in Figure 8) and it reads:

$$D_j^n = \{(t, x) \ / \ t^n \leq t \leq t^{n+1}, \ \sigma_j^n(t) \leq x \leq \sigma_{j+1}^n(t)\}, \tag{3.1.6}$$

where $\sigma_j^n(t)$ is a parameterized curve to be defined in the following $\sigma_j^n(t^n) = x_j^n$; i.e., define the space-time local control volume D_j^n (see top picture in Figure 8) to be the set contained between $[x_j^n, x_{j+1}^n]$ (bottom) and $[\overline{x}_{j-\frac{1}{2}}^{n+1}, \overline{x}_{j+\frac{1}{2}}^{n+1}]$ (top), and two integral curves given by $\sigma_j^n(t)$ (left) and $\sigma_{j+1}^n(t)$, $t, \in [t^n, t^{n+1}]$ (right). From the basic calculus we know the divergence theorem states that the outward flux of a vector field through a closed surface is equal to the volume integral of the divergence over the region inside the surface. Thus, from the conservation law (3.1.3) we get:

$$\iint_{D_j^n} \nabla_{t,x} \begin{bmatrix} u \\ H(u) \end{bmatrix} dV = 0 \qquad \Leftrightarrow \qquad \oint_{\partial D_j^n} \begin{bmatrix} u \\ H(u) \end{bmatrix} \cdot \vec{n} ds = 0. \tag{3.1.7}$$

This means that by enforcing discrete local conservation over space-time control volumes D_j^n which "fill-up" the space-time domain, this method satisfies global conservation in space-time.

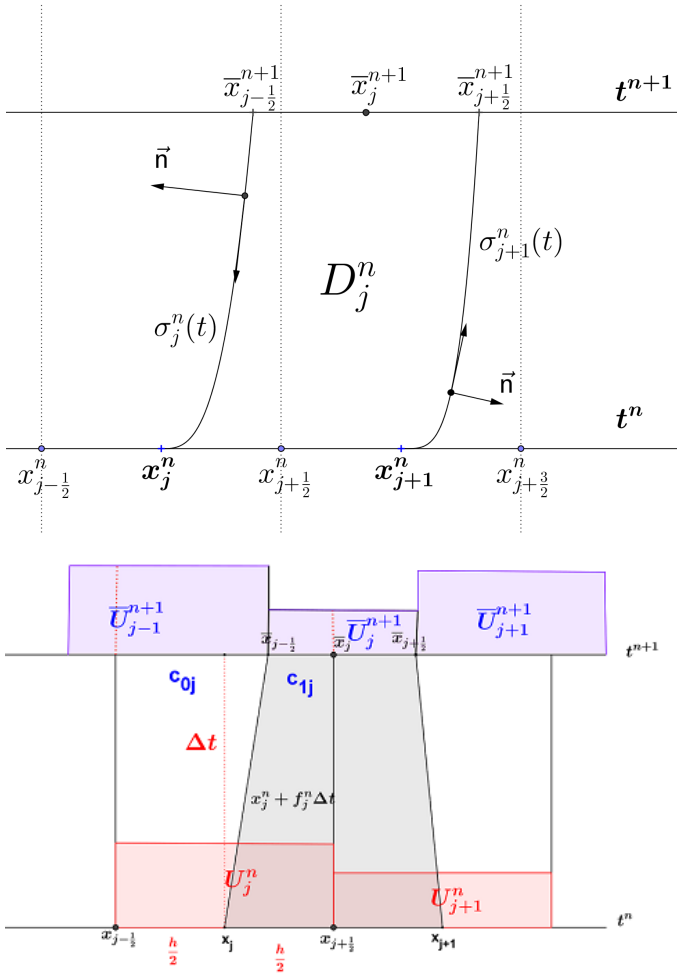

Figure 8 – The local space-time control-volume D_j^n (top) and the geometrical interpretation of the Lagrangian-Eulerian Method scheme (bottom).

Equations (3.1.7) implies that parameterized curves $\sigma_j^n(t)$ and $\sigma_{j+1}^n(t)$ are naturally impervious zero-flux boundaries. From this fact region D_j^n will be called "Integral tube" and for $t^n \leq t \leq t^{n+1}$ we get $\dfrac{d\sigma_j^n(t)}{dt} \perp \vec{n}$ and $\dfrac{d\sigma_{j+1}^n(t)}{dt} \perp \vec{n}$ since the slope $\dfrac{d\sigma_j^n(t)}{dt}$ is equal to the slope of the vector $[u, H(u)]^T$ over curves $\sigma_j^n(t)$ and $\sigma_{j+1}^n(t)$, for $j \in \mathbb{Z}$. Therefore, $\sigma_j^n(t)$ are the solutions of the following system of ordinary differential equations:

$$\frac{d\sigma_j^n(t)}{dt} = \frac{H(u)}{u}, \qquad \sigma_j^n(t^n) = x_j^n, \qquad t^n < t \leq t^{n+1}, \tag{3.1.8}$$

where $u \neq 0$ (this assumption can easily be suppressed by introducing some extra notation in the analysis to define the endpoints $[\overline{x}_{j-\frac{1}{2}}^{n+1}, \overline{x}_{j+\frac{1}{2}}^{n+1}]$ by analytical straight lines). Thus, as a natural consequence of (3.1.7)-(3.1.8), the integrals over curves $\sigma_j^n(t)$ vanish and then the line integral over the boundary of the region ∂D_j^n in (3.1.7) leads to the (natural) local conservation,

$$\int_{\overline{x}_{j-\frac{1}{2}}^{n+1}}^{\overline{x}_{j+\frac{1}{2}}^{n+1}} u(x, t^{n+1})dx = \int_{x_j^n}^{x_{j+1}^n} u(x, t^n)dx, \tag{3.1.9}$$

where we define $\overline{x}_{j-\frac{1}{2}}^{n+1} = \sigma_j^n(t^{n+1})$ and $\overline{x}_{j+\frac{1}{2}}^{n+1} = \sigma_{j+1}^n(t^{n+1})$. Next, we use (3.1.5) with the conservation law (3.1.9) to get:

$$\begin{aligned}
\overline{U}_j^{n+1} &= \frac{1}{h_j^{n+1}} \int_{\overline{x}_{j-\frac{1}{2}}^{n+1}}^{\overline{x}_{j+\frac{1}{2}}^{n+1}} u(x, t^{n+1})\, dx \\
&= \frac{1}{h_j^{n+1}} \int_{x_j^n}^{x_{j+1}^n} u(x, t^n)\, dx \\
&= \frac{h}{h_j^{n+1}} \left[\frac{1}{h} \int_{x_j^n}^{x_{j+\frac{1}{2}}^n} u(x,t^n)dx + \frac{1}{h} \int_{x_{j+\frac{1}{2}}^n}^{x_{j+1}^n} u(x,t^n)dx \right], \\
&= \frac{1}{h_j^{n+1}} \frac{1}{2} h \left[U_j^n + U_{j+1}^n \right] \\
&= \frac{h}{h_j^{n+1}} \left[\frac{1}{2} U_j^n + \frac{1}{2} U_{j+1}^n \right].
\end{aligned} \tag{3.1.10}$$

The resulting local approximations $\overline{U}_j^{n+1}$, $j \in \mathbb{Z}$, are defined over the original grid, given by:

$$U_j^{n+1} = \frac{1}{h} \left[c_{0j} \overline{U}_{j-1}^{n+1} + c_{1j} \overline{U}_j^{n+1} \right]. \tag{3.1.11}$$

Here $c_{0j} = (\frac{h}{2} + f_j^n k^n)$, $c_{1j} = h - c_{0j} = (\frac{h}{2} - f_j^n k^n)$ and we use the approximation $f_j^n = \frac{H(U_j^n)}{U_j^n} \approx \frac{H(u)}{u}$ and notice that now the curve $\sigma_j^n(t)$ is a straight line for f_j^n along with $k^n = \Delta t^n = t^{n+1} - t^n$ (see bottom picture in Figure 8).

Notice that the nonlinear quantity $H(u)/u$ is related to the unknown solution u, and so one cannot find the exact tracelines of the fluid particles. Although simple at first glance, is not well understood how to define a good, robust and efficient approximations to $H(u)/u$ by means of nonlinear reconstructions. Here we use a quite simple explict approximation $f_j^n \approx \frac{H(u)}{u}$ (but with quite good results), for both hyperbolic and balance laws, which is advantageous to the numerical analysis. Indeed, all machinery developed for implicit strategies for source terms in the case of balance laws can be used for the family of problems involving ODEs in (3.1.8). Finally, the combination of equations (3.1.8) and (3.1.11) form the basic building block of the Lagrangian-Eulerian scheme of approximate solutions to hyperbolic conservation laws and balance laws.

3.2 The Lagrangian-Eulerian scheme for scalar linear hyperbolic conservation laws

Now we will define an equivalent finite difference method of a Lagrangian-Eulerian approach based on locally conservative finite volume method and to the hyperbolic linear constant-coefficient case and leave the proof of its consistency, stability and convergence in the sense of classical Lax stalibity in [1, 35].

Consider the linear flux function $H(u) = a\,u,\ a \in \mathbb{R}$ to the conservation law (3.1.3), with the Lagrangian-Eulerian approach (3.1.8)-(3.1.11), whose exact well-known solution is $u(x,t) = \eta(x - at)$. Therefore, we set $f_j^n = a$ and then $h_j^{n+1} = h$, $j \in \mathbb{Z}$. Thus, the solutions of the family of initial value problem:

$$\frac{d\sigma_j^n(t)}{dt} = a, \qquad \sigma_j^n(t^n) = x_j^n, \tag{3.2.1}$$

is precisely $\sigma_j^n(t) = a(t - t^n) + x_j^n$ and, in connection with the definitions above, also reads that $\overline{x}_{j-\frac{1}{2}}^{n+1} = \sigma_j^n(t^{n+1}) = ak^n + x_j^n$. Moreover, using a simple mathematical reasoning the above construction can be viewed as an analogue of finite difference scheme for scalar linear hyperbolic conservation laws. The procedure for balance laws is quite straightforward. Then, we notice from equation (3.1.10) that:

$$\begin{aligned}
\overline{U}_j^{n+1} &= \frac{1}{h_j^{n+1}} \int_{\overline{x}_{j-\frac{1}{2}}^n}^{\overline{x}_{j+\frac{1}{2}}^n} u(x, t^{n+1})\, dx \\
&= \frac{1}{h_j^{n+1}} \int_{x_j^n}^{x_{j+1}^n} u(x, t^n)\, dx \\
&= \frac{1}{h_j^{n+1}} \frac{1}{2} h \left[U_j^n + U_{j+1}^n \right] \\
&= \frac{1}{2} \left[U_j^n + U_{j+1}^n \right].
\end{aligned} \tag{3.2.2}$$

By replacing (3.2.2) in the equation (3.1.11), it reads (the one-step or *the two-level* finite difference scheme):

$$U_j^{n+1} = \frac{1}{4} \left[U_{j-1}^n + 2U_j^n + U_{j+1}^n \right] - \frac{ak^n}{2h} \left[U_{j+1}^n - U_{j-1}^n \right], \tag{3.2.3}$$

then, with fixed $k = k^n$, we get the equivalent difference finite scheme to the scalar linear conservation laws:

$$U_j^{n+1} = \frac{1}{4} \left[U_{j-1}^n + 2U_j^n + U_{j+1}^n \right] - \frac{ak}{2h} \left[U_{j+1}^n - U_{j-1}^n \right]. \tag{3.2.4}$$

The linear Lagrangian-Eulerian scheme (3.2.4) is designed to a straightforward application of Lax equivalence theory.

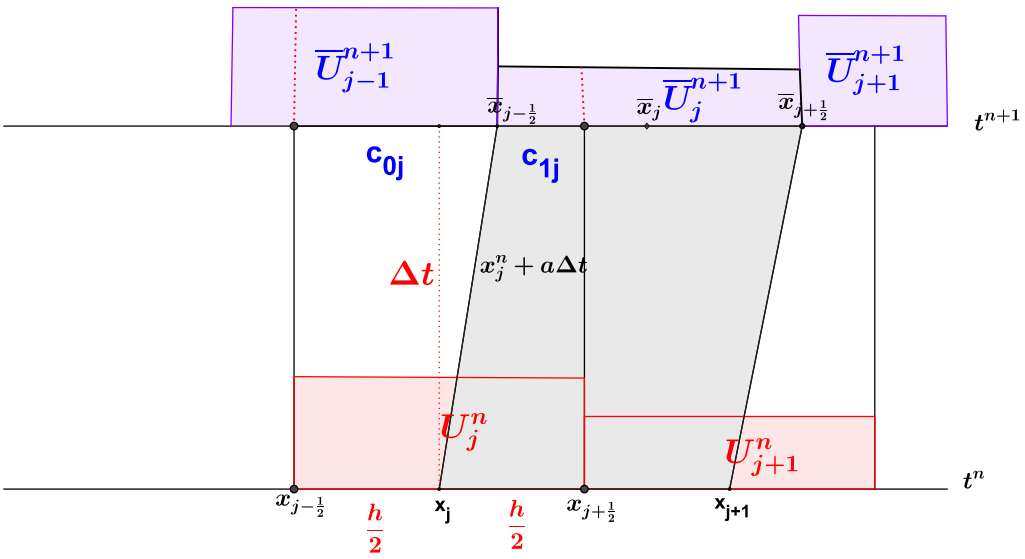

Figure 9 – The geometrical interpretation of the Lagrangian-Eulerian Method scheme for linear case with $a > 0$.

3.2.1 The modified equation for the linear Lagrangian-Eulerian scheme

Here we will use modified equations for the Lagrangian-Eulerian scheme with the aim of understanding the qualitative behaviour of numerical solutions (related to the two-level Lagrangian-Eulerian scheme (3.2.4). Let $\phi(x,t)$ in C^∞, this is supposed to be a function that agrees exactly with U_j^n at the grid points and so, unlike $u\,(x,t)$, the function $\phi(x,t)$ satisfies (3.2.4) exactly:

$$\phi\,(x,t+k) = \frac{1}{4}\left[\phi(x-h,t) + 2\phi(x,t) + \phi(x+h,t)\right] - \frac{ak}{2h}\left[\phi(x+h,t) - \phi(x-h,t)\right].$$

Expanding these terms in Taylor series about (x,t) and simplifying gives :

$$\phi_t + a\phi_x = -\frac{1}{2}k\phi_{tt} - \frac{1}{6}k^2\phi_{ttt} + \frac{h^2}{4k}\phi_{xx} - \frac{ah^2}{6}\phi_{xxx} + O(k^3).$$

We can rewrite this as

$$\phi_t + a\phi_x = \frac{h^2}{2k}\left(\frac{1}{2} - \frac{a^2k^2}{h^2}\right)\phi_{xx} - \frac{ah^2}{6}\left(1 - \frac{a^2k^2}{h^2}\right)\phi_{xxx} + O(k^3), \tag{3.2.5}$$

or in a more convenient form (keep in mind $v = \dfrac{a\,k}{h}$ with ratio k/h fixed),

$$\phi_t + a\phi_x = \frac{a\,h}{2\,v}\left(\frac{1}{2} - v^2\right)\phi_{xx} - \frac{ah^2}{6}\left(1 - v^2\right)\phi_{xxx} + O(k^3). \tag{3.2.6}$$

Equations of the form (3.2.6) arise in fluid dynamics when both diffusion (viscosity term ϕ_{xx}) and dispersion (capillarity term ϕ_{xxx}) play a role. The diffusion smoothes out the discontinuous solutions of (3.1.1) while the dispersion causes high-frequency oscillations. The dispersion process is an example of combined convection and diffusion. Thus, from equation (3.2.6) one might expect numerical solutions by scheme (3.2.4) for the purely linear hyperbolic PDE be contaminated by both spurious dispersion and diffusion effects. Thus, let's consider the numerical experiments related to a linear hyperbolic conservation laws to the Lagrangian-Eulerian scheme (3.2.4), which in turn will be the building block to the anologue Lagrangian-Eulerian scheme [1, 35].

3.3 Lagrangian-Eulerian scheme for scalar nonlinear hyperbolic conservation laws and its conservative form

We essentially mimic the procedure in the linear case, but now notice that the curves $\sigma_j^n(t)$ are not straight lines in general but rather solutions of the system of ordinary differential equations (3.1.8), we write here again for clarity of presentation:

$$\frac{d\sigma_j^n(t)}{dt} = \frac{H(u)}{u}, \qquad t^n < t \leq t^{n+1},$$

with the initial condition $\sigma_j^n(t^n) = x_j^n$, related to the diffential problem:

$$\frac{\partial u}{\partial t} + \frac{\partial H(u)}{\partial x} = 0, \quad u(x,0) = \eta(x). \tag{3.3.1}$$

The idea here is to use the linear Lagrangian-Eulerian scheme as building block to construct *local* approximations with the natural first choice to develop a fully explicit scheme $f_j^n = \dfrac{H(U_j^n)}{U_j^n} \approx \dfrac{H(u)}{u}$ with the initial condition $\sigma_j^n(t^n) = x_j^n$ (see Figure 10). Now, the solutions $\sigma_j^n(t)$ of the differential equations (3.1.8) system are (local) straight lines, but they are not parallel as in the linear case.

In order to start the procedure let us first revisit the coefficients in the linear case,

$$\begin{cases} c_{0j} = \dfrac{h}{2} + f_j^n k^n \quad \text{and} \quad c_{1j} = \dfrac{h}{2} - f_j^n k^n, \\ \\ \text{with} \quad \max\limits_j \left| \dfrac{f_j \Delta t^n}{h} \right| < \dfrac{\sqrt{2}}{2} \quad \text{and} \quad k^n = \min\limits_n \Delta t^n, \end{cases} \tag{3.3.2}$$

where the stability CFL condition in (3.3.2) is given by the construction of the scheme. Thus, we use equations (3.1.9)-(3.1.10) to write:

$$\overline{U}_j^{n+1} = \frac{1}{h_j^{n+1}} \frac{1}{2} h \left[U_j^n + U_{j+1}^n \right], \tag{3.3.3}$$

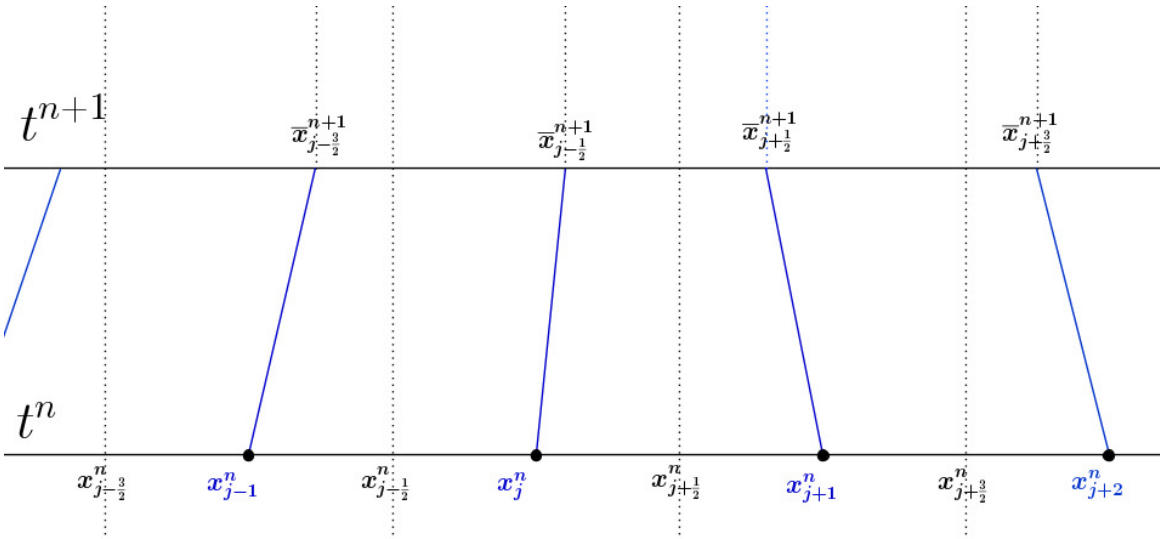

Figure 10 – Lagrangian-Eulerian scheme nonlinear case

and plugging this into (3.1.11) reads,

$$\begin{aligned} U_j^{n+1} &= \frac{1}{h}\left[c_{0j}\frac{1}{h_{j-1}^{n+1}}\frac{h}{2}(U_{j-1}^n+U_j^n)+c_{1j}\frac{1}{h_j^{n+1}}\frac{h}{2}(U_j^n+U_{j+1}^n)\right] \\ &= \frac{c_{0j}}{2}\frac{1}{h_{j-1}^{n+1}}(U_{j-1}^n+U_j^n)+\frac{c_{1j}}{2}\frac{1}{h_j^{n+1}}(U_j^n+U_{j+1}^n). \end{aligned} \tag{3.3.4}$$

Now, notice that for each $j\in\mathbb{Z}$,

$$h_j^{n+1}=\overline{x}_{j+\frac{1}{2}}^{n+1}-\overline{x}_{j-\frac{1}{2}}^{n+1}=x_{j+1}^n+f_{j+1}^nk^n-(x_j^n+f_j^nk^n)=h+(f_{j+1}^n-f_j^n)k^n, \tag{3.3.5}$$

and, also that:

$$h_j^{n+1}=h+(f_{j+1}^n-f_j^n)k^n=(\frac{h}{2}+f_{j+1}^nk^n)+(\frac{h}{2}-f_j^nk^n)=c_{0j+1}+c_{1j}. \tag{3.3.6}$$

On the other hand we have,

$$c_{0j}=h_{j-1}^{n+1}-c_{1j-1}\quad\text{and}\quad c_{1j}=h_j^{n+1}-c_{0j+1}, \tag{3.3.7}$$

along with,

$$\begin{cases} c_{1j-1}=\dfrac{h}{2}-f_{j-1}^nk^n=\dfrac{1}{2}(h_{j-1}^{n+1}-f_{j-1}^nk^n-f_j^nk^n), \\ \\ c_{0j+1}=\dfrac{h}{2}+f_{j+1}^nk^n=\dfrac{1}{2}(h_{j+1}^{n+1}+f_{j+1}^nk^n+f_j^nk^n). \end{cases} \tag{3.3.8}$$

Finally, plugging (3.3.7) into (3.3.4) we get, along with $\mathbb{W}(U_j^n,U_{j+1}^n)\equiv\frac{f_j^n+f_{j+1}^n}{h_j^{n+1}}(U_j^n+U_{j+1}^n)$,

$$U_j^{n+1}=\frac{1}{4}[U_{j-1}^n+2U_j^n+U_{j+1}^n]-\frac{k^n}{4}\left(\mathbb{W}(U_{j+1}^n,U_j^n)-\mathbb{W}(U_{j-1}^n,U_j^n)\right). \tag{3.3.9}$$

The finite difference scheme (3.3.9) is the *Lagrangian-Eulerian scheme* for the nonlinear scalar problem (3.3.1). Hereafter this numerical scheme will called LEH1 (Lagrangian Eulerian Hyperbolic scheme 1).

Notice, if we set $f_j^n = a$ and plug it into (3.3.9) we recover the linear Lagrangian-Eulerian scheme (3.2.4). Moreover, the scheme (3.3.9) can also be written in conservative form,

$$U_j^{n+1} = U_j^n - \frac{k^n}{h}\left[F(U_j, U_{j+1}^n) - F(U_{j-1}^n, U_j^n)\right], \tag{3.3.10}$$

where the *Lagrangian-Eulerian numerical flux function* is defined by,

$$F(U_j^n, U_{j+1}^n) = \frac{1}{4}\left[\frac{h}{k^n}\left(U_j^n - U_{j+1}^n\right) + h\,\mathbb{W}(U_j, U_{j+1})\right]. \tag{3.3.11}$$

A numerical formulation of the type Lagrangian-Eulerian scheme for nonlinear case, which we present as one generalization of the Lagrangian-Eulerian scheme (3.3.9), it called in this work as LEH2 (Lagragian Eulerian Finite Difference scheme) as the follow scheme,

$$U_j^{n+1} = \frac{1}{4}(U_{j-1}^n + 2U_j^n + U_{j+1}^n) - \frac{k}{2h}(H(U_{j+1}^n) - H(U_{j-1}^n)), \tag{3.3.12}$$

where $k = k^n$ and with CFL condition

$$\max_j \left| H'(U_j^n)\frac{k}{h}\right| \leq \frac{\sqrt{2}}{2}. \tag{3.3.13}$$

This method results to be conservative, i.e., the scheme (3.3.12) can be writed in the form conservative

$$U_j^{n+1} = U_j^n - \frac{k}{h}(\overline{F}(U_j^n, U_{j+1}^n) - \overline{F}(U_{j-1}^n, U_j^n)), \tag{3.3.14}$$

where

$$\overline{F}(U_j^n, U_{j+1}^n) = \frac{1}{4}\left[\frac{h}{k}(U_j^n - U_{j+1}^n) + 2(H(U_{j+1}^n) + H(U_j^n))\right]. \tag{3.3.15}$$

3.4 Our findings and numerical studies

Here we show our current understanding of the Lagrangian-Eulerian framework that is applied for classical and well-known hyperbolic problems. We present and discuss computational results for linear and nonlinear scalar conservation laws with convex and non-convex flux functions. The numerical results are compared with accurate approximate solutions or exact solutions whenever possible.

3.4.1 Linear case

It is shown numerical solutions for initial value problem for scalar linear conservation laws,

$$\begin{cases} u_t + (a(x,t)\,u)_x = 0, & x \in \mathbb{R}, \quad t > 0 \\ u(x,0) = u_0(x), & x \in \mathbb{R}, \end{cases} \tag{3.4.1}$$

with scheme (3.2.4) along with various $a(x,t)$ functions.

Example 3.4.1. Scalar linear hyperbolic conservation law with Shu's linear test [20, 21].

Consider the initial value problem

$$\begin{cases} u_t + \left(\frac{1}{2}u\right)_x = 0, & x \in \mathbb{R}, \quad t > 0, \\ u(x,0) = u_0(x), & x \in \mathbb{R}, \end{cases} \tag{3.4.2}$$

where $a(x,t) = a = \dfrac{1}{2}$, and

$$u_0(x) = \begin{cases} \frac{1}{6}\left(G(x,\beta,z-\delta) + G(x,\beta,z+\delta) + 4G(x,\beta,z)\right), & -0.8 \le x \le -0.6, \\ 1, & -0.4 \le x \le -0.2, \\ 1 - |10\,(x-0.1)|\,, & 0 \le x \le 0.2, \\ \frac{1}{6}\left(F(x,\alpha,a-\delta) + F(x,\alpha,a+\delta) + 4F(x,\alpha,a)\right), & 0.4 \le x \le 0.6, \\ 0, & otherwise, \end{cases} \tag{3.4.3}$$

$$G\,(x,\beta,z) = e^{-\beta(x-z)^2},$$
$$F\,(x,\alpha,a) = \sqrt{max\left(1-\alpha^2\,(x-a)^2\,,0\right)}.$$

The constants are taken $z = -0.7, \quad \delta = 0.005, \quad \alpha = 10, \quad \beta = \dfrac{log2}{36\delta^2}$. The solution contains a smooth but narrow combination of Gaussians, a square wave, a sharp triangle wave and a half ellipse as we can see in the Figure 11 .

In Figure 12 we show and discuss numerical aproximations for the scalar linear hyperbolic conservation laws with a standard test case called Shu's linear test with 128, 256 and 512 cells respectively and with the Lagrangian-Eulerian scheme (3.2.4). As it is known in [1, 35] for the range of CFL condition bigger than 0.5 (left pictures), the modified equation shows that the dispersive terms are dominant and the wave group travel with velocity less than a. Analogously in right pictures of Figure 12 is shown the case which the diffusive term is dominant in modified equation, when the CFL-range is less than 0.5, and the effect is captured by the method.

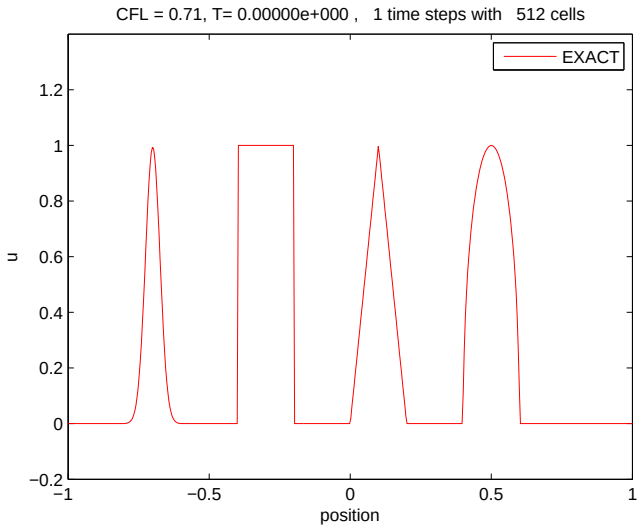

Figure 11 – Exact solution with 512 grid cells.

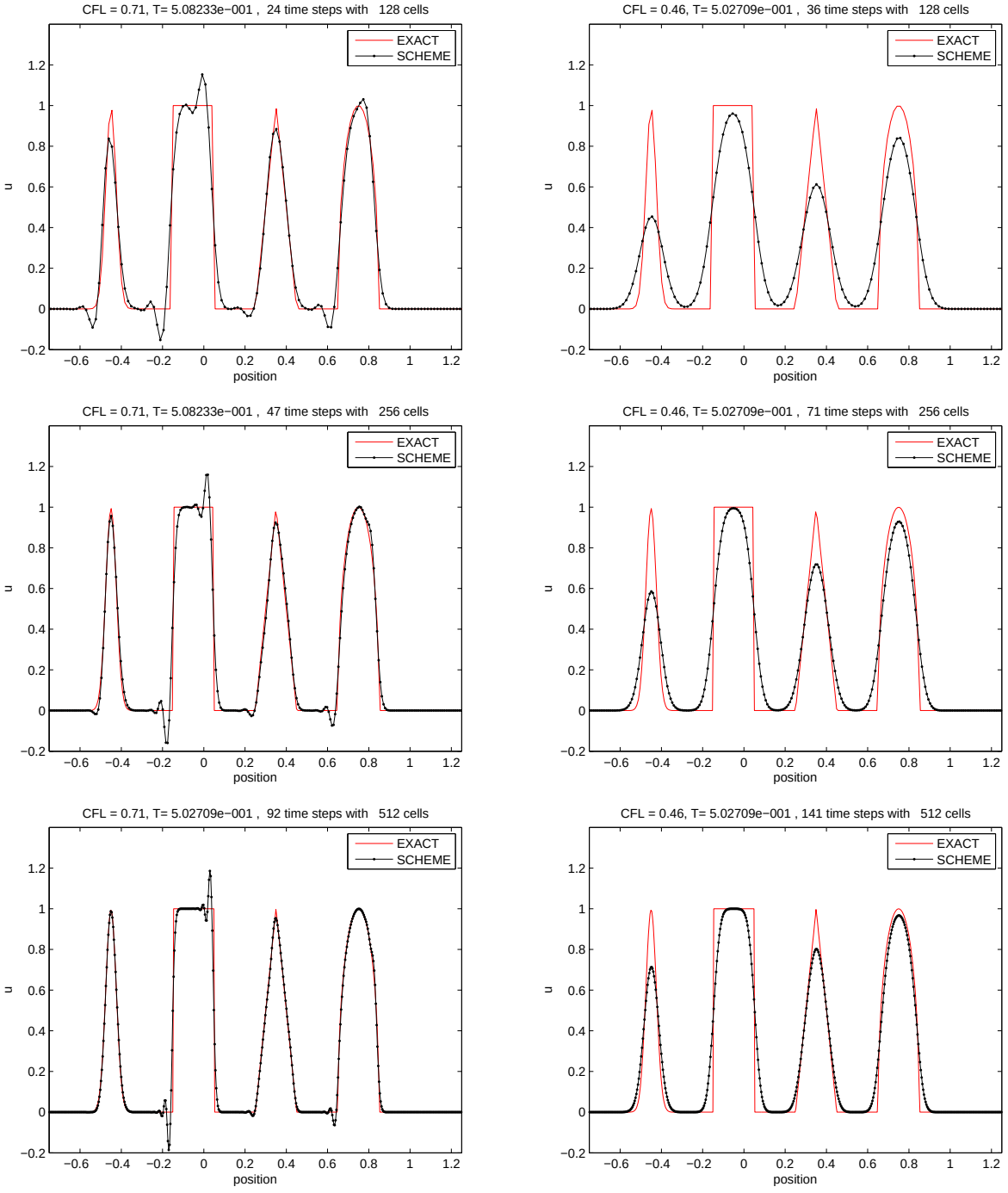

Figure 12 – Numerical solution for scalar linear hyperbolic conservation laws with Shu's linear test. The solution is shown with time $T = 0.5$ and with 128, 256, 512 cells. CFL-condition bigger than 0.5 (left) and CFL-condition less than 0.5 (right).

Example 3.4.2. Scalar linear hyperbolic conservation laws with velocity depending on t.

In this example we take the velocity only depending on t. Following [20], we test this case with $a(x,t) = \text{sen}(t)$ for $x \in [0,2]$ by means of the Lagrangia-Eulerian scheme (3.3.12). For this example exact solution is $u(x,t) = u_0(x + 1 + cos(t))$ where $u_0(x) = 0.75 + 0.25\text{sen}(\pi\, x)$. Figure 13 shows the initial value (time $T = 0$) and the numerical solutions at times $T = 0.5\,,\ 1$ with 128 cells.

Example 3.4.3. Scalar linear hyperbolic conservation laws with velocity depending on x.

Let $a(x,t) = \text{sen}(x)$ over $[0, 2\pi]$. The exact solution, see [20], with initial condition $u(x,0) = 1$ is given by

$$u(x,t) = \frac{\text{sen}(2\ \arctan(e^{-t}\,\text{tg}(x/2)))}{\text{sen}(x)}.$$

Pictures in Figure 14 show the initial condition (top) and the solution at times $T = 0.5$ and $T = 1$ (middle and bottom) with 128 cells by means of the Lagrangian-Eulerian scheme (3.1.11).

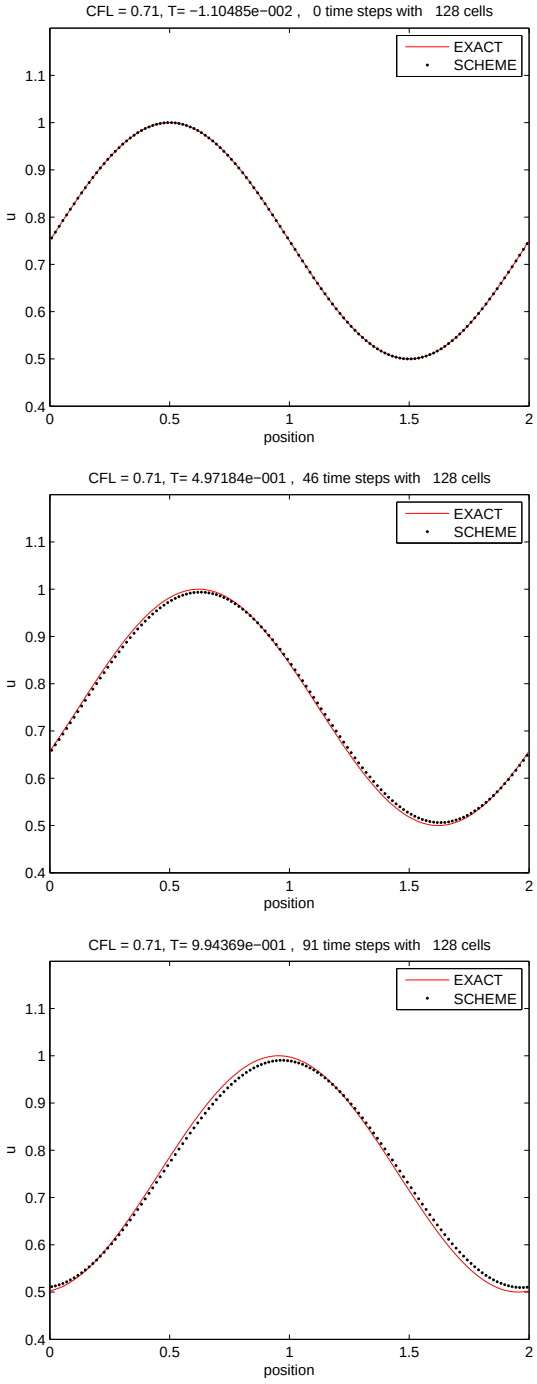

Figure 13 – Numerical solution for the scalar linear hyperbolic conservation laws with velocity depends on t. The solution is shown at time T=0, 0.5, 1 respectively with 128 cells. The velocity is variable in time, test case with $a(x,t) = \text{sen}(t)$.

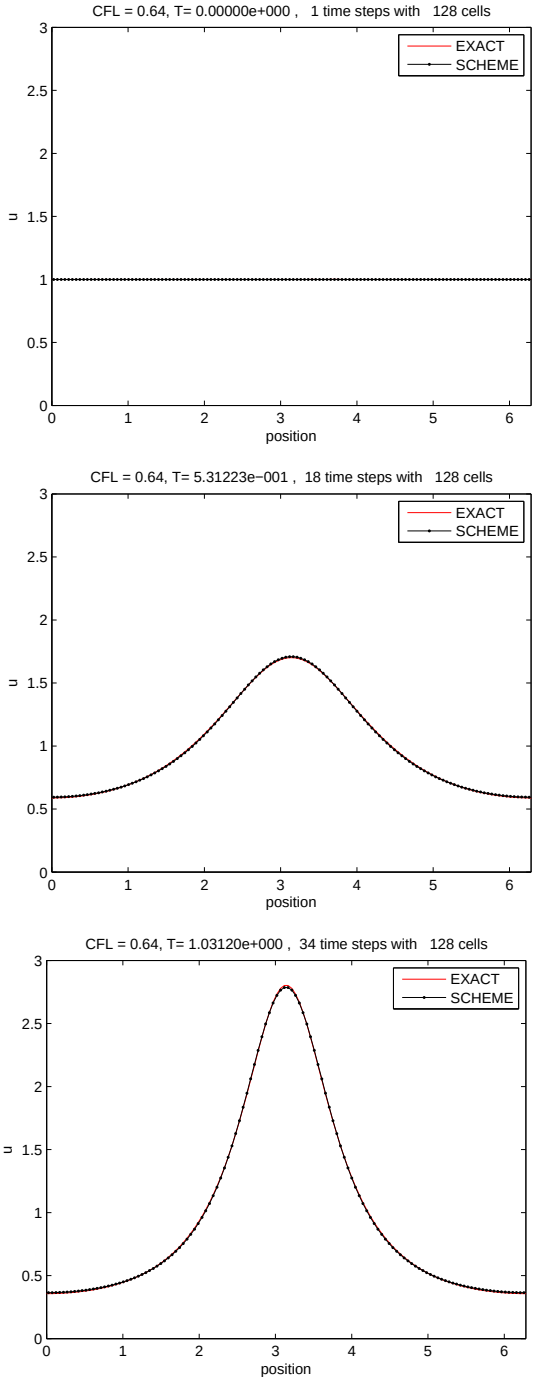

Figure 14 – Numerical test with 128 cells at time T=0, 0.5, 1, with variable velocity in space. In this test $a(x,t) = \text{sen}(x)$.

3.4.2 Nonlinear case

Example 3.4.4. Inviscid Burgers' equation with discontinuous initial data.

Left of Figure 15, we present the solutions of the problem with Burgers' equation,

$$u_t + \left(\frac{u^2}{2}\right)_x = 0, \qquad x \in \mathbb{R}, \quad t > 0. \tag{3.4.4}$$

along the discontinuous initial data (left picture),

$$u(x,0) = \begin{cases} 1, & x < 0, \\ 0, & x > 0, \end{cases} \tag{3.4.5}$$

at time $T = 1$ with 128, 256 and 512 cells (top to bottom).

Right of Figure 15, it is shown the numerical solutions for (3.4.4) with another discontinuous initial data,

$$u(x,0) = \begin{cases} -1, & x < 0, \\ 1, & x > 0, \end{cases} \tag{3.4.6}$$

which the exact solution is a transonic rarefaction wave. We use meshes with 128, 256 and 512 cells (top to bottom).

On these frames are shown snapshot graphs with waves moving from left to right. We get a very nice looking numerical approximate solution with scheme (3.3.9), which in turn seems to be propagating at entirely entropy-correct Rankine-Hugoniot speed and similar good results are shown to the rarefaction case as well. Here, as the rarefaction wave is crossed, there is a sign change in the characteristic speed u and thus there is one point at which $u = 0$, the sonic point. However, our numerical scheme shows no spurious anomalies around $u = 0$.

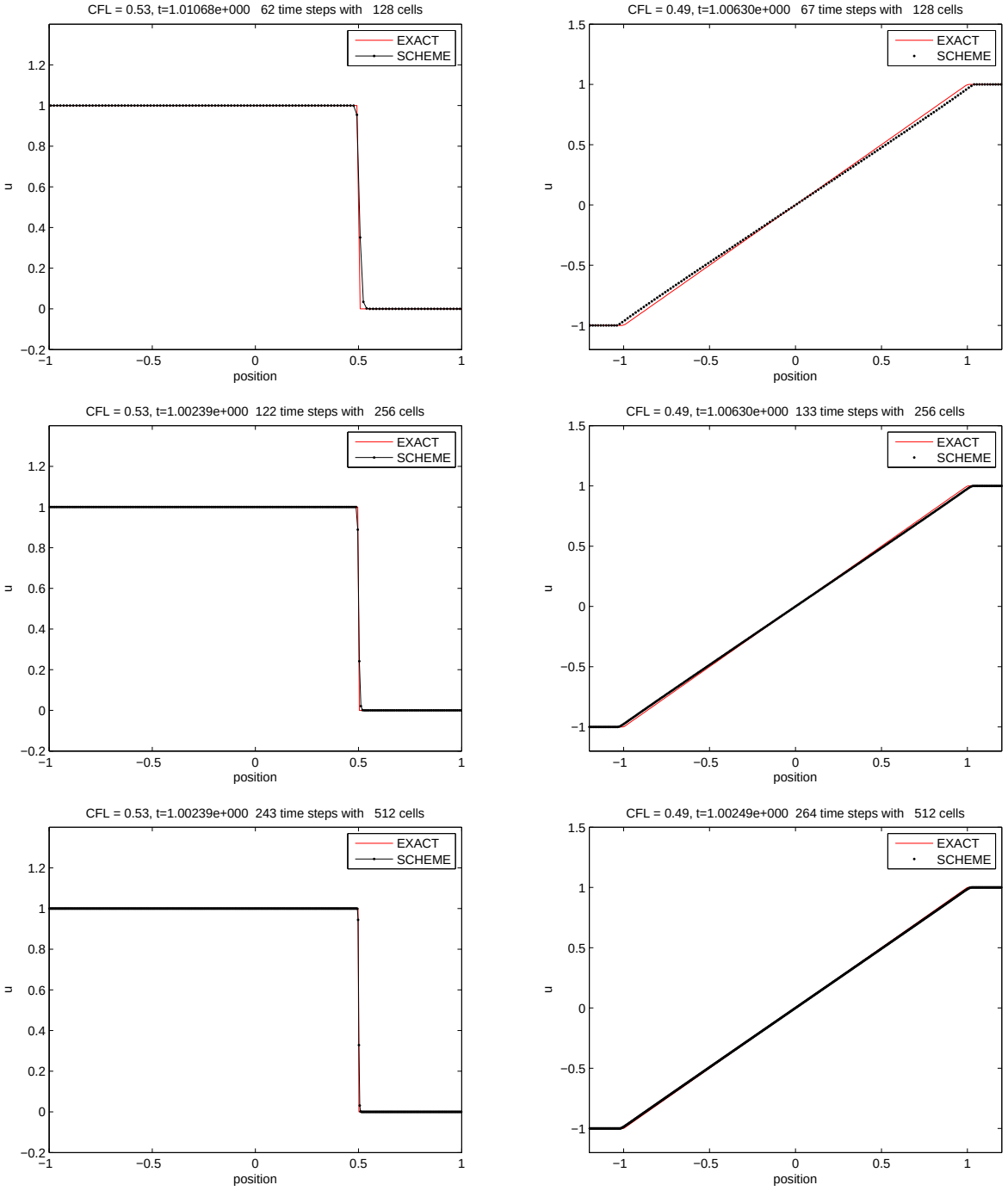

Figure 15 – Burgers' flux function, shock wave solution with initial condition $u(x,0) = 1, x < 0$ and $u(x,0) = 0, x > 0$, at time $t = 1.0$ (left). Rarefaction wave with initial condition $u(x,0) = -1, x < 0$ and $u(x,0) = 1, x > 0$, end time $t = 1.0$ (right).

Example 3.4.5. Buckley-Leverett's equation

In Figure 16 we present the solution of the problem with nonlinear one-dimensional Buckley-Leverett's equation,

$$u_t + (H(u))_x = 0, \qquad x \in \mathbb{R}, \quad t > 0, \tag{3.4.7}$$

where

$$H(u) = \frac{u^2}{u^2 + 0.5(1-u)^2},$$

with initial condition

$$u(x,0) = \begin{cases} 1, & x < 0, \\ 0, & x > 0, \end{cases} \tag{3.4.8}$$

at time $t = 1$ with 128, 256 and 512 (top to bottom).

Another example with the Buckley-Leverett flux function is seen on Figure 17, where we set a square wave as initial condition

$$u(x,0) = \begin{cases} 1, & -1 < x < 0, \\ 0, & \text{otherwise.} \end{cases} \tag{3.4.9}$$

The solution profile starts as a rarefaction wave followed by a shock on the left side and a rarefaction wave followed by a shock on the right side for small times (middle picture). When the left shock meets the right rarefaction (see middle and bottom pictures in Figure 17), we observe the expected decaying pattern [34]; see also [18], Section 3. These test cases here are simulated with 256 cells at time t=0, 0.5, 1.

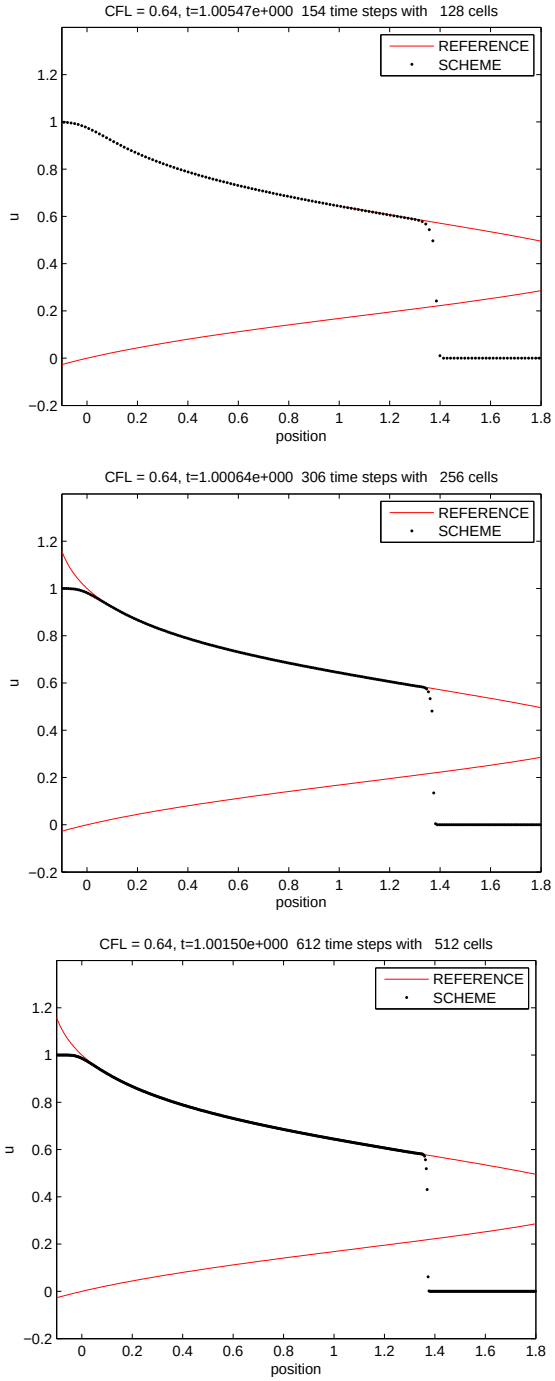

Figure 16 – Buckley-Leverett flux function ($H(u) = u^2/(u^2+0.5(1-u)^2)$) with initial condition $u(x,0) = 1, x < 0$ and $u(x,0) = 0, x > 0$.

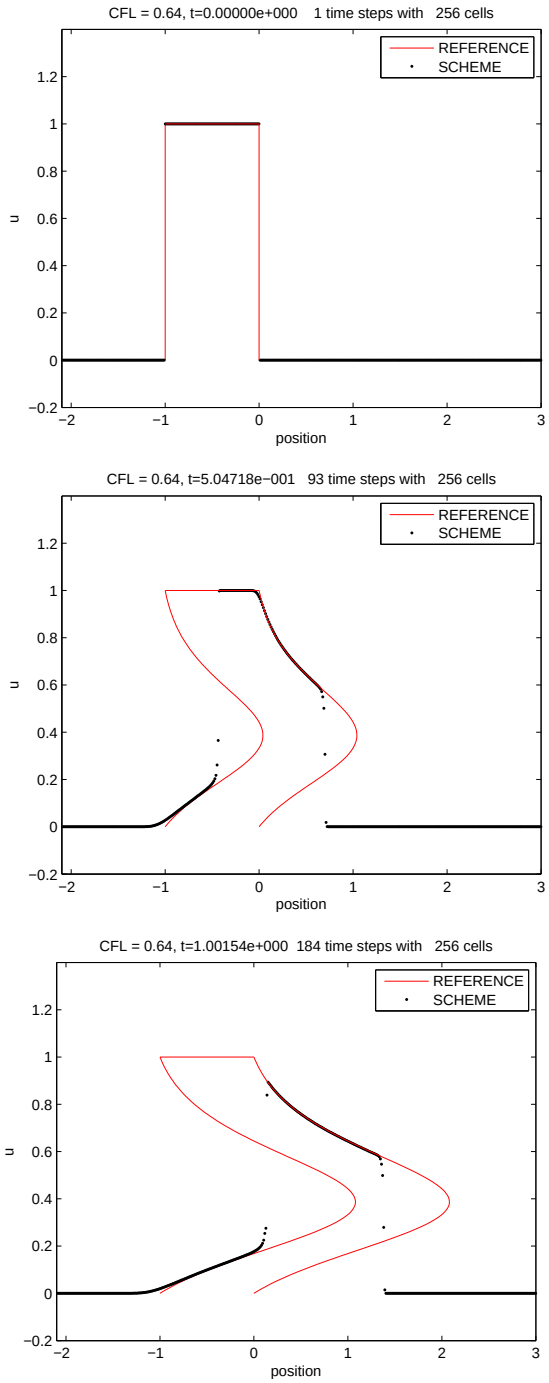

Figure 17 – Buckley-Leverett flux function with initial condition $u(x,0) = 1, -1 < x < 0$ and $u(x,0) = 0$, otherwise. Snapshots at $t = 0$, $t = 0.5$ and $t = 1$, respectively.

3.5 Scalar hyperbolic conservation laws with nonlocal flux

In this Section, numerical approximations of the scalar hyperbolic conservation law with nonlocal flux are shown. By the use of the Lagrangian-Eulerian scheme and a simple accurate algorithm to evaluate the Hilbert transform of a real function using interpolations with piecewise–linear functions, we compute qualitatively correct approximations by showing evidence of attenuation and blow-up of concentration type with mass-preserving with measure initial data [11, 17].

3.5.1 Approximation of the Hilbert transform

The Hilbert transform is an important mathematical tool for many engineering problems. Computation of the Hilbert transform has attracted much attention in the literature. Existing numerical methods for this computation fall into two major categories: fast Fourier transform (FFT) related methods and non-FFT methods. The existing FFT method comes with fast algorithms but it suffers from low order of approximation accuracy. Some non-FFT methods have higher order of approximation accuracy but require high computational cost [11, 17, 32]. Therefore it is important to develop reliable methods to compute the Hilbert transform.

Here, we describe an algorithm for approximate the Hilbert transform on the real line. The computational complexity of this algorithm is $O(N\log N)$, with N being the dimension of the core matrix, and it has an optimal numerical accuracy [11]. Consider the nonlinear transport equation with nonlocal flux, in particular the equation:

$$u_t = \nu u_{xx} + (\mathbb{H}(u)u)_x, \qquad t > 0, \quad x \in \mathbb{R}, \tag{3.5.1}$$

$$u(x,0) = f(x), \qquad x \in \mathbb{R}, \tag{3.5.2}$$

where $\mathbb{H}(u)$ is the Hilbert transform of the variable $u = u(x,t)$, namely

$$\mathbb{H}(u(x,t)) = \frac{1}{\pi} PV\left(\frac{1}{x} * u\right)(x,t) = \frac{1}{\pi} PV \int_{-\infty}^{\infty} \frac{u(x,t)}{x-y}\, dy = \frac{1}{\pi} \lim_{\varepsilon \to 0} \int_{|x-y|>\varepsilon} \frac{u(y,t)}{x-y}\, dy, \tag{3.5.3}$$

and the unknown function $u = u(x,t)$ associated with the nonlocal transport model problem (3.5.1)-(3.5.2) denotes the flow of velocity while the positive ν stands for the viscosity of the fluid (see [9, 17]). Moreover, for numerically approximate the hyperbolic conservation law problems with nonlocal flux, we present a simple accurate algorithm for approximating the Hilbert transform on the real line [9, 11, 17, 32].

For $h > 0$, let $\tau = \{x_n = x_0 + nh\}_{n=0}^{N}$ be a grid of equally spaced $N+1$ points, determining the closed interval $I_\tau = [x_0, x_N]$. The grid τ should be such that the function $u(x,t)$ can be approximated by zero outside I_τ. Then, for every interior point $x_k \in \tau$ with

$k = 1, \ldots, N-1$, we have

$$\begin{aligned}\mathbb{H}u(x_k,t) &\backsimeq \frac{1}{\pi}\lim_{\varepsilon\to 0^+}\sum_{n=0}^{N-1}\int_{|y-x_k|>\varepsilon, x_n\le y\le x_{n+1}}\frac{u(y,t)}{x_k-y}\,dy,\\ &= \frac{1}{\pi}\lim_{\varepsilon\to 0^+}\left[\int_{x_{k-1}}^{x_k-\varepsilon}+\int_{x_k+\varepsilon}^{x_{k+1}}\right]\frac{u(y,t)}{x_k-y}\,dy\\ &+\frac{1}{\pi}\sum_{n=0}^{k-2}\int_{x_n}^{x_{n+1}}\frac{u(y,t)}{x_k-y}\,dy+\frac{1}{\pi}\sum_{n=k+1}^{N-1}\int_{x_n}^{x_{n+1}}\frac{u(y,t)}{x_k-y}\,dy.\end{aligned} \tag{3.5.4}$$

If the nodal values $u(x_k,t)$ of the considered function are known, on each interval $[x_n, x_{n+1}]$ the function $u(y,t)$ is approximated by linear interpolation. Although this is the simplest interpolation formula, it is suitable for our problem, since u is at least second order differentiable,

$$u\,(y,t) \simeq u\,(x_n,t) + \frac{u\,(x_{n+1,t}) - u\,(x_n,t)}{h}\,(y-x_n)\,. \tag{3.5.5}$$

Each contribution can now be evaluated analytically and the approximated Hilbert transform (3.5.4) becomes

$$\begin{aligned}\mathbb{H}u(x_k,t) \backsimeq -\frac{1}{\pi}\{&u(x_{k+1},t)-u(x_k,t)\\ &+\sum_{n=1}^{N-1-k}\left[-\left(1-(n+1)b_n\right)u(x_{k+n},t)+\left(1-nb_n\right)u(x_{k+n+1},t)\right]\\ &+\sum_{n=1}^{N-1-k}\left[-\left(1-(n+1)b_n\right)u(x_{k-n},t)+\left(1-nb_n\right)u(x_{k-n-1},t)\right]\},\end{aligned} \tag{3.5.6}$$

where $b_n = \log\left(\dfrac{n+1}{n}\right)$. The right-hand side of (3.5.6) defines a linear operator which maps the vector of sample values $U = (u(x_0,t), u(x_1,t)\ldots, u(x_N,t))$ into the approximate values of the Hilbert transform on interior grid points. Such an operator is the proposed discrete Hilbert transform $\mathbb{H}_\tau$, with the subscript denoting explicitly the dependence on the grid τ. In matrix form it reads,

$$\mathbb{H}_\tau U = AU_{int} + CU_{bnd}, \tag{3.5.7}$$

where the vector U has been split into its projection on internal nodes $U_{int} = (u(x_1,t), \ldots, u(x_{N-1},t))$ and boundary points $U_{bnd} = (u(x_0,t), u(x_N,t))$ whereas A is a $(N-1)\times(N-1)$ antisymmetric Toeplitz matrix,

$$A = \begin{pmatrix} a_0 & a_1 & \ldots & a_{N-3} & a_{N-2}\\ -a_1 & a_0 & \ldots & a_{N-4} & a_{N-3}\\ \vdots & \vdots & \vdots & \vdots & \vdots\\ -a_{N-2} & -a_{N-3} & \ldots & -a_1 & a_0\end{pmatrix}, \tag{3.5.8}$$

along with the matrix entries,

$$a_k = -\frac{1}{\pi}. \begin{cases} 0, & \text{for } k = 0, \\ 2b_1, & \text{for } k = 1, \\ (k+1)b_k - (k-1)b_{k-1}, & \text{for } k > 1, \end{cases} \tag{3.5.9}$$

where

$$b_k = \log\left(\frac{k+1}{k}\right), \tag{3.5.10}$$

and C is a rectangular $(N-1) \times 2$ matrix

$$C = \begin{pmatrix} 0 & c_N - 1 \\ -c_1 & -c_{N-2} \\ \vdots & \vdots \\ -c_{N-1} & 0 \end{pmatrix}, \tag{3.5.11}$$

$c_k = -\frac{1}{\pi}(1 - kb_k)$. An antisymmetric Toeplitz matrix is completely defined by its first row. Thus the evaluation of the $N-1$ elements $(a_0, \dots, a_{N-2})$ is enough to determine A, and that requires only $N-2$ calculations of the algorithm.

3.5.2 Numerical experiments for scalar hyperbolic conservation laws with nonlocal flux

For our numerical experiments convenience, we rewrite the one-dimensional nonlinear transport equation with nonlocal flux given in the computational domain $[a, b]$, as follows

$$\begin{cases} u_t \pm (\mathbb{H}(u)u)_x = 0, & (x,t) \in \overline{\Omega} \times (0,T], \\ u(a,t) = 0, \quad u(b,t) = 0, & t \in [0,T], \\ u(x,0) = f(x), & x \in \Omega, \end{cases} \tag{3.5.12}$$

where

$$\mathbb{H}(u(x,t)) = \frac{1}{\pi} PV\left(\frac{1}{x} * u\right)(x,t) = \frac{1}{\pi} PV \int_a^b \frac{u(x,t)}{x-y}\, dy = \frac{1}{\pi} \lim_{\varepsilon \to 0} \int_{|x-y|>\varepsilon} \frac{u(y,t)}{x-y}\, dy, \tag{3.5.13}$$

is the Hilbert transform and the quantity $\int_{\mathbb{R}} f(x)\, dx$ is the mass of the initial datum with a physical significance for attenuation or blow-up of concentration type.

Example 3.5.1. Square pulse measure.

In this example, we consider the nonlocal transport model problems (3.5.12) with initial condition

$$f(x) = \begin{cases} \dfrac{R}{h}, & \text{if } |x - 0.5| \le \dfrac{h}{2}, \\ 0, & \text{otherwise}, \end{cases} \tag{3.5.14}$$

with $h = 1$ and for three distinct values of the mass R (R=1, 20, 40). Analyzing the Figures 18 - 20, it seems that the problem can be better interpreted for $u_t = -(\mathbb{H}(u)u)_x$. In this case, the term $-(\mathbb{H}(u)u)$ is decreased with a large gradient and the solution is faster as the height of the initial condition decreases. Otherwise it happens when analyzing $u_t = (\mathbb{H}(u)u)_x$ the term $(\mathbb{H}(u)u)$ is increased with a large gradient. For the case $u_t + (\mathbb{H}(u)u)_x = 0$, the numerical results show that the solution is an attenuation and as the mass of the initial condition increases, the solution increases in height.

In Figures 18 - 19 we have a mass-preserving diffusion mechanism with mesh grid refinement. The numerical experiments show that even with thick mesh grid the Lagrangian-Eulerian scheme seems to solve numerically well the problem and the numerical diffusion effect is not very significant.

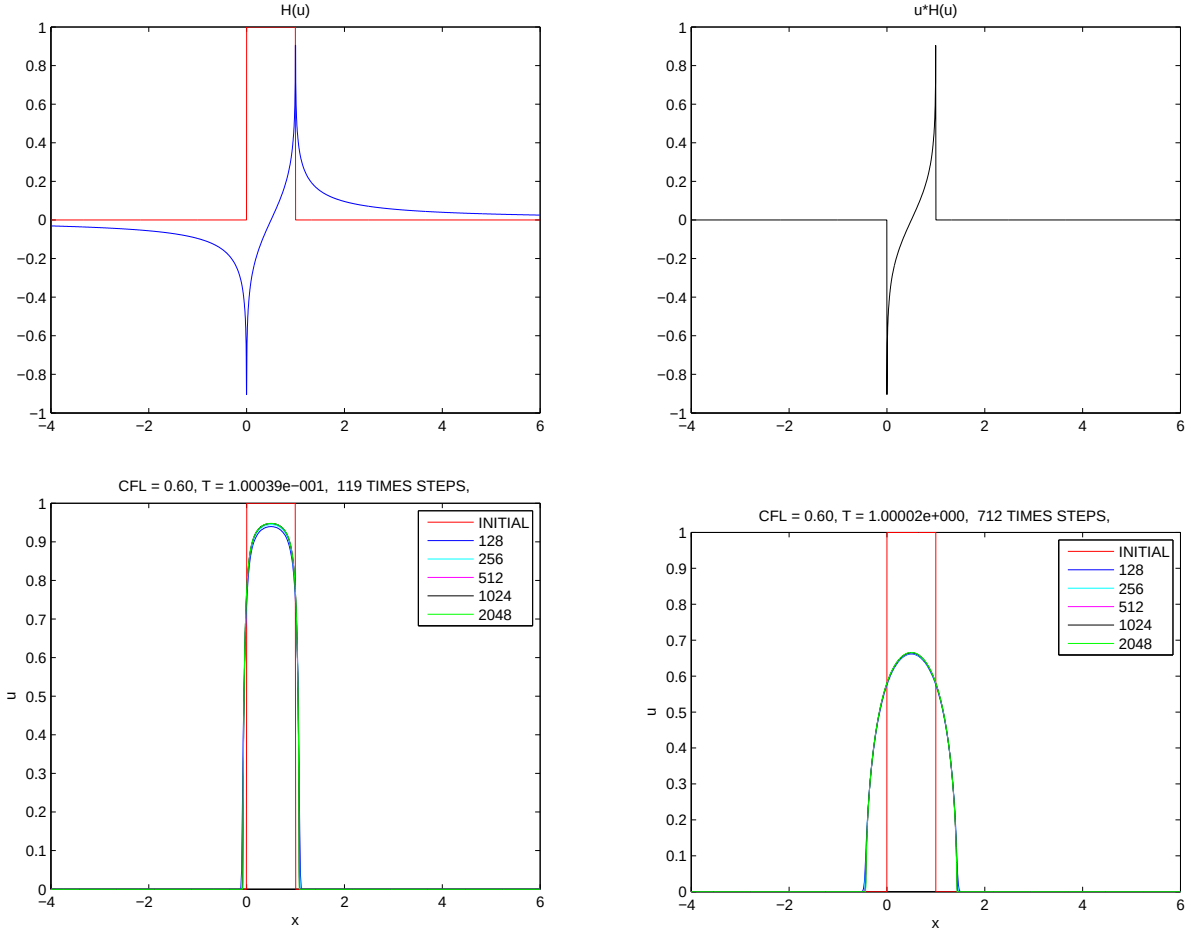

Figure 18 – Numerical solution for $u_t + (\mathbb{H}(u)u)_x = 0$ with f given in (3.5.14) with mass $R = 1$. We show numerical approximations for the Hilbert transform and the Hilbert transform versus $u(x,t)$ with 512 grid cells at time T=0.1 (top). The solution is shown at times $T = 0.1$ (left), $T = 1$ (right) and with 128, 256, 512, 1024, 2048 cells. The computational time is 40 seconds.

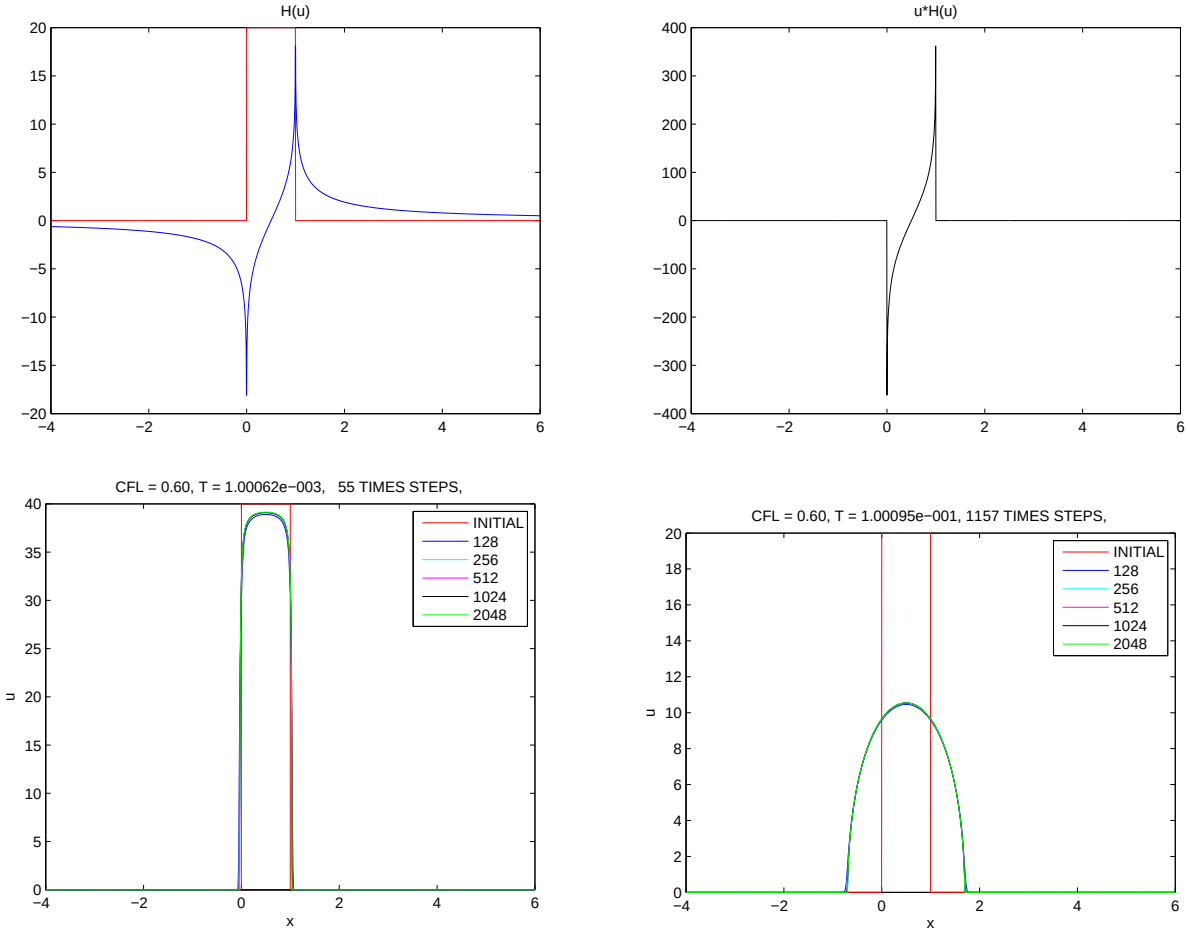

Figure 19 – Numerical solution for $u_t + (\mathbb{H}(u)u)_x = 0$ with f given in (3.5.14) with mass R=40 (bottom left), 20 (bottom right). We show numerical approximations for the Hilbert transform and the Hilbert transform versus $u(x,t)$ with 512 grid cells at time $T = 0.1$ (top) with mass R=20. The solution is shown at times T=0.04 (left), T=0.1 (right) and with 128, 256, 512, 1024, 2048 cells. The computational time is 40 seconds.

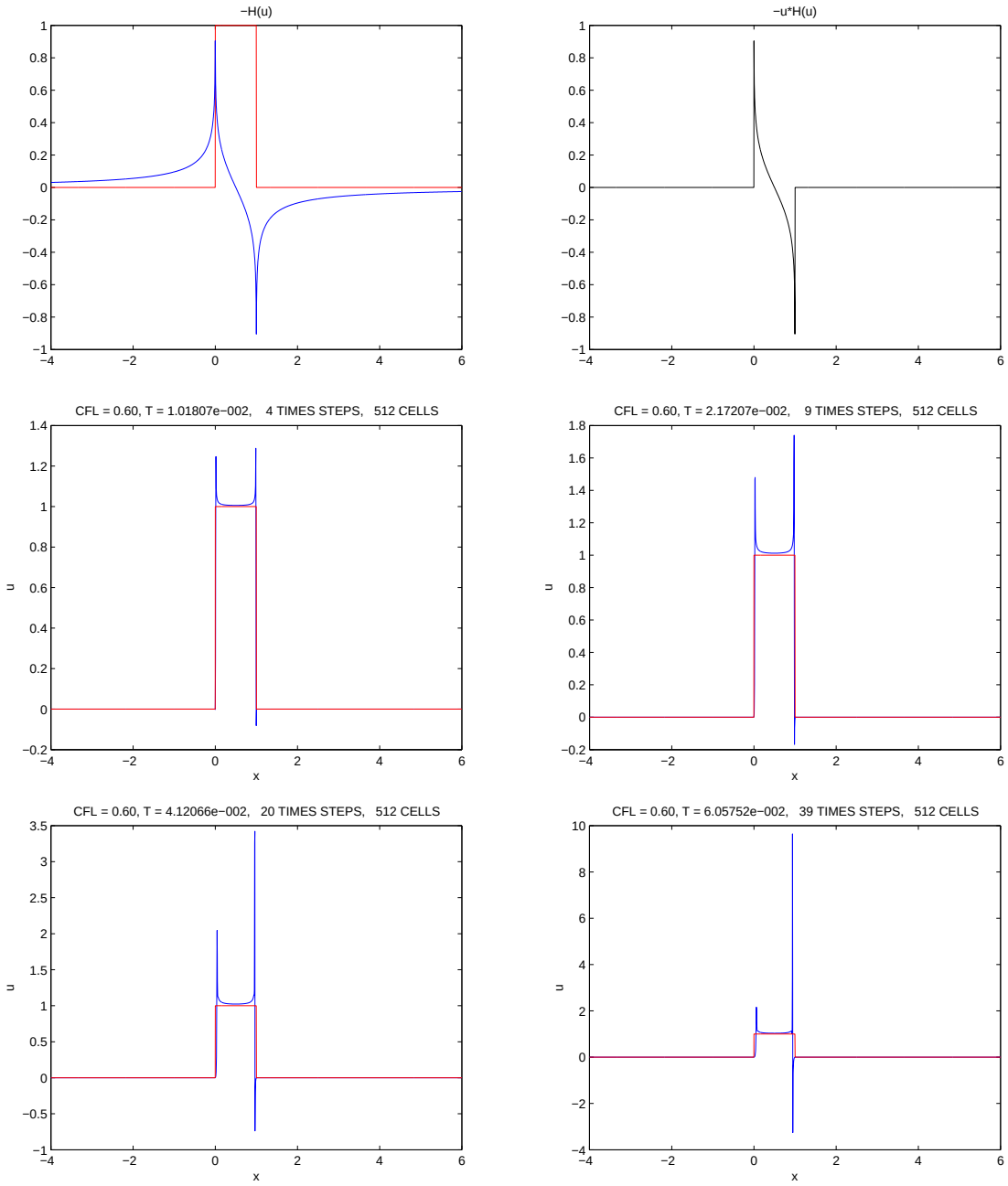

Figure 20 – Numerical solution for $u_t - (\mathbb{H}(u)u)_x = 0$ with f given in (3.5.14) with mass $R = 1$. We show the approximation for the Hilbert transform and the Hilbert transform versus $u(x,t)$ with 512 grid cells at time T=0.1 (top). The solution of the model is shown at several times with 512 grid cells and 0.60 as the CFL condition. The computational time is 40 seconds.

Example 3.5.2. Gaussian data .

In this example, we consider the nonlocal transport model problems (3.5.12) with initial condition

$$f(x) = R\exp\left[-(x-0.5)^2/\pi\right], \tag{3.5.15}$$

for several values of the mass R (R=0.04, 0.5, 1, 20, 35).

Analyzing the Figures 21 , 22 it seems that the problem $u_t + (\mathbb{H}(u)u)_x = 0$ better captures the effect of attenuation and the problem $u_t - (\mathbb{H}(u)u)_x = 0$ captures better the effect of blow-up of concentration type. In Figure 21 we have a mass-preserving diffusion mechanism with mesh grid refinement. Numerical experiments show that even with thick mesh grid the Lagrangian-Eulerian scheme seems to solve well the problem and the numerical diffusion effect is not very significant. In Figure 22, we have a blow-up of concentration type with 512, 1024 grid cells at distinct times of simulation.

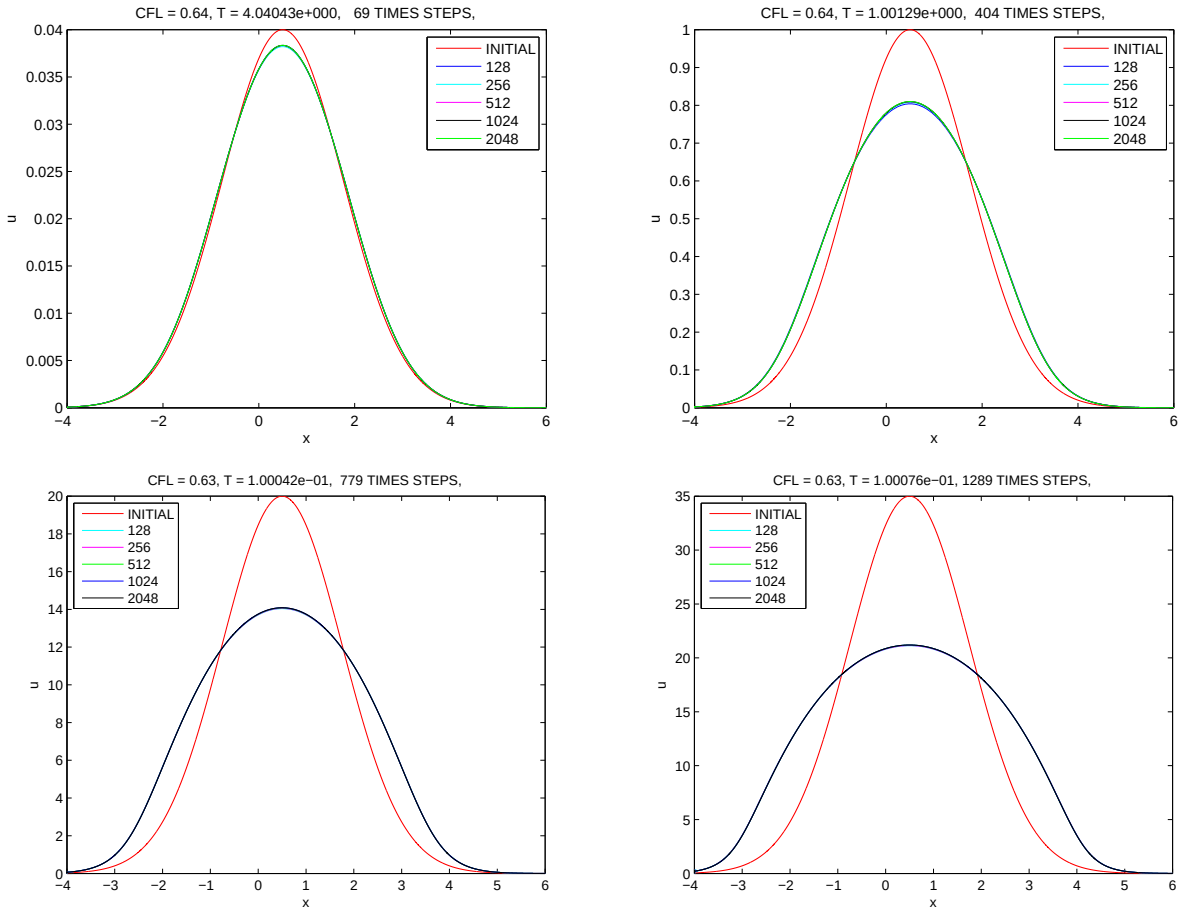

Figure 21 – Numerical solution for $u_t+(\mathbb{H}(u)u)_x = 0$ with f given in (3.5.15) with mass R=0.04, 1 (top) and R=20, 35 (bottom). The solution is shown at several times and with 128, 256, 512, 1024, 2048 cells. The computational time is 1 minute.

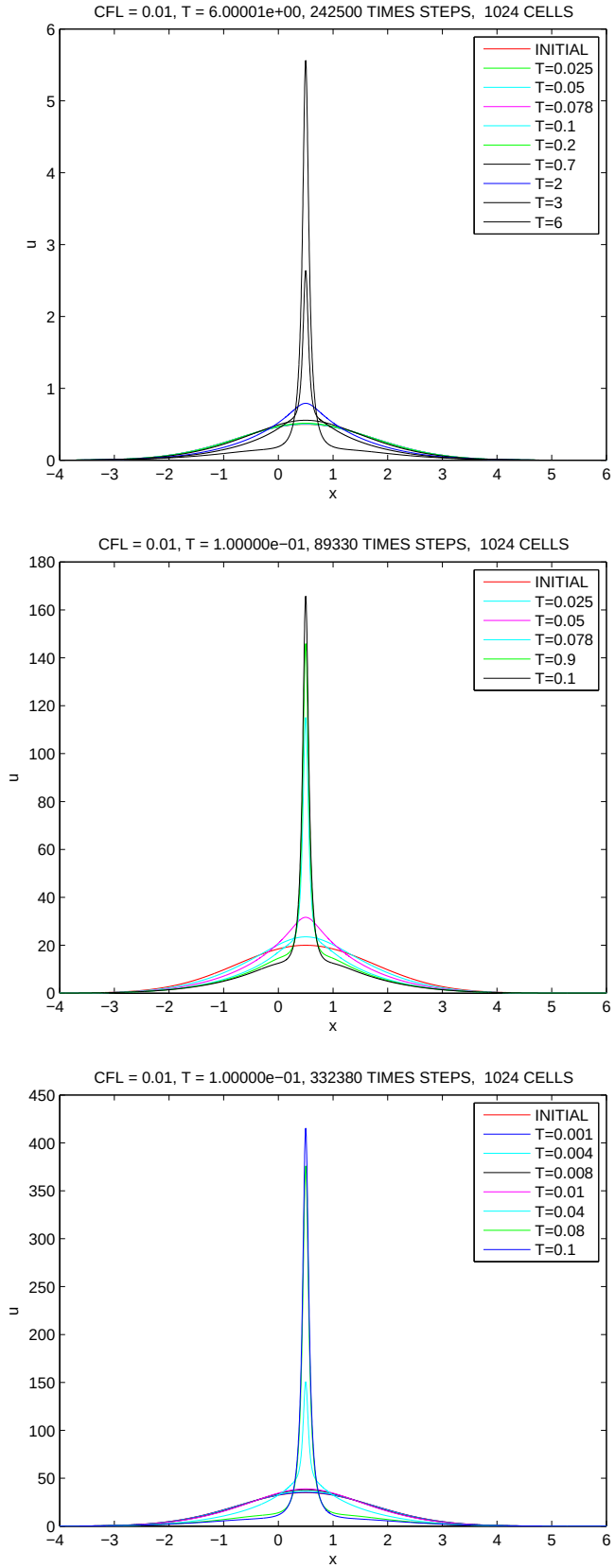

Figure 22 – Numerical solution for $u_t - (\mathbb{H}(u)u)_x = 0$ with f given in (3.5.15). The solution is shown at several times of simulation with mass R=0.5 (top), 20 (middle), 35 (bottom) with 1024 grid cells. The computational time is 3 days.

True value given by the norms $\|u\|_{L1}$= 62.8320 and $\|u\|_{L1}$= 109.9561 for the Figure 22.

πR	T=0.01	T=0.025	T=0.05	T=0.078	T=0.1
N	$\|u\|_{L1}$	$\|u\|_{L1}$	$\|u\|_{L1}$	$\|u\|_{L1}$	$\|u\|_{L1}$
128	62.8110	62.8002	62.7805	62.7681	62.7272
256	62.8152	62.8118	62.8027	62.7986	62.7834
512	62,8175	62.8158	62.8118	62.8100	62.8014
1024	62.8188	62.8175	62.8161	62.8145	62.8081

Table 1 – Numerical computation of $\|u\|_{L1}$-norm corresponding to the numerical experiments reported in Figure 22 linked to nonlocal transport equation (3.5.12) at several simulation times with $\pi R = 62.832$ and R=20.

πR	T=0.001	T=0.008	T=0.01	T=0.08	T=0.1
N	$\|u\|_{L1}$	$\|u\|_{L1}$	$\|u\|_{L1}$	$\|u\|_{L1}$	$\|u\|_{L1}$
128	109.9309	109.9173	109.9100	109.6654	109.5451
256	109.9331	109.9257	109.9221	109.8180	109.7515
512	109.9344	109.9302	109.9283	109.8651	109.8172
1024	109.9353	109.9331	109.9317	109.9216	109.9202

Table 2 – Numerical computation of $\|u\|_{L1}$-norm corresponding to the numerical experiments reported in Figure 22 linked to nonlocal transport equation (3.5.12) at several simulation times with $\pi R = 109.9561$ and R=35.

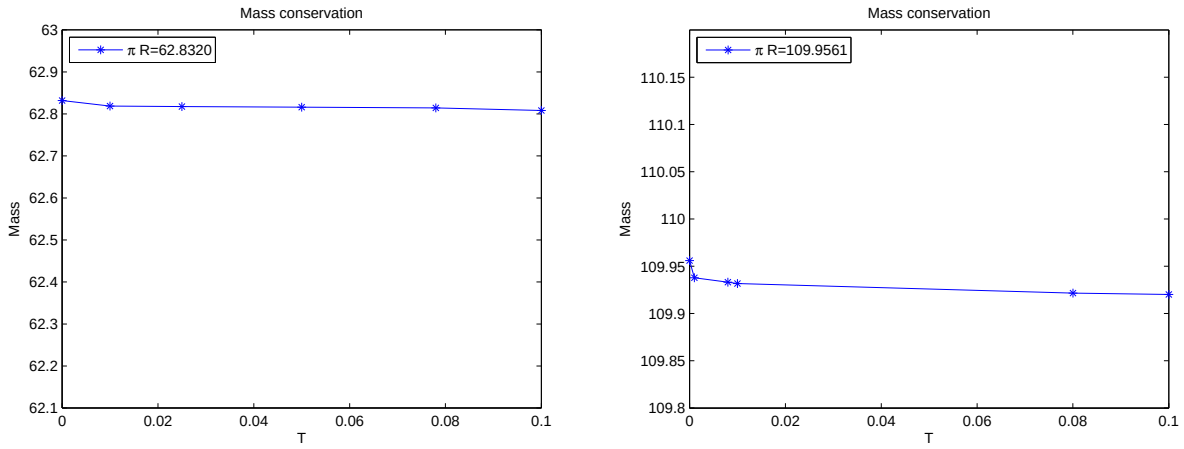

Figure 23 – Mass versus times with R=20 (left), 35 (right) and 1024 mesh grid.

Example 3.5.3. Gaussian data .

Consider the nonlocal transport model problems (3.5.12) with initial condition

$$f(x) = R\exp\left[-\pi \times (x-0.5)^2\right], \tag{3.5.16}$$

for several values of the mass R (R=0.04, 0.5, 1, 20 and 35).

Analysing the Figures 24 - 25, it seems that the problem $u_t + (\mathbb{H}(u)u)_x = 0$ better captures the effect of attenuation and the problem $u_t - (\mathbb{H}(u)u)_x = 0$ captures better the effect of blow-up of concentration type. Qualitative approximations of the nonlocal transport problems show that we have an attenuation for the problem $u_t + (\mathbb{H}(u)u)_x = 0$ with a mass-preserving diffusion mechanism which can be seen in the Figure 24 and a blow up of concentration type for the problem $u_t - (\mathbb{H}(u)u)_x = 0$ with 1024 grid cells at distinct times of simulation which can be seen in the Figure 25. Numerical experiments show that even with thick mesh grid the Lagrangian-Eulerian scheme seems to solve well the problem and the numerical diffusion effect is not very significant.

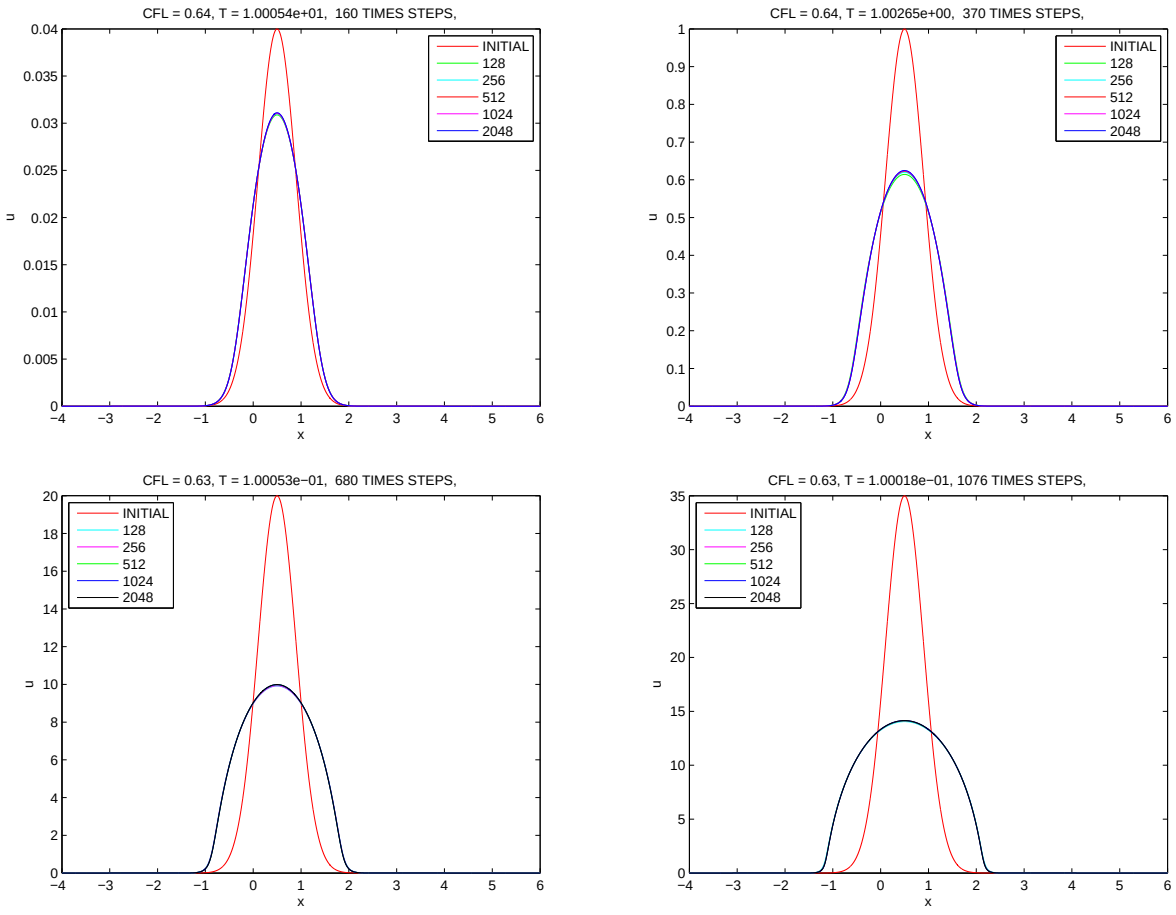

Figure 24 – Numerical solution for $u_t + (\mathbb{H}(u)u)_x = 0$ with f given in (3.5.16) with mass R=0.04, 1 (top) and R=20, 35 (bottom). The solution is shown at several times and with 128, 256, 512, 1024, 2048 grid cells. The computational time is 1 minute.

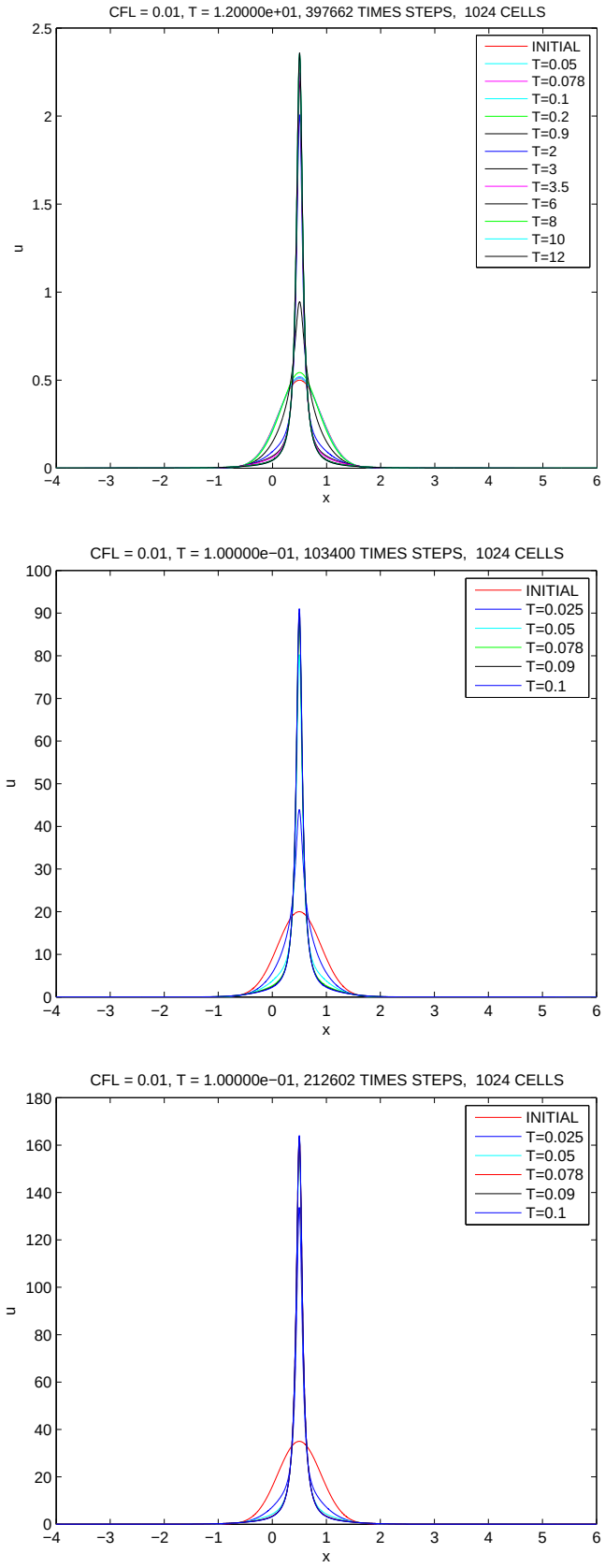

Figure 25 – Numerical solution for $u_t - (\mathbb{H}(u)u)_x = 0$ with f given in (3.5.16) with mass R=0.5 (top), 20 (middle) and 35 (bottom). The solution is shown at several times of simulation with 1024 grid cell. The computational time is 3 days.

True value given by the norms $\|u\|_{L1}$= 20 and $\|u\|_{L1}$= 35 for the Figure 25.

R=20	T=0.025	T=0.05	T=0.1
N	$\|u\|_{L1}$	$\|u\|_{L1}$	$\|u\|_{L1}$
128	20	20	20
256	20	20	20
512	20	20	20
1024	20	20	20

R=35	T=0.025	T=0.01	T=0.1
N	$\|u\|_{L1}$	$\|u\|_{L1}$	$\|u\|_{L1}$
128	35	35	35
256	35	35	35
512	35	35	35
1024	35	35	35

Table 3 – Numerical computation of $\|u\|_{L1}$-norm corresponding to the numerical experiments reported in Figure 25 linked to nonlocal transport equation (3.5.12) at several times of simulation.

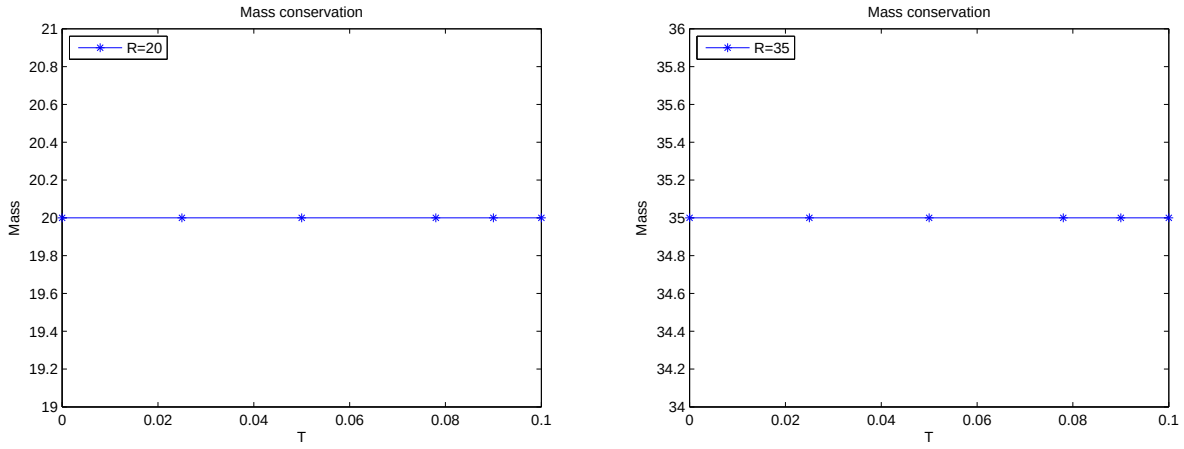

Figure 26 – Mass versus times with R= 20, 35 and with 1024 mesh grid.

Example 3.5.4. Consider the nonlocal transport model problems (3.5.12) with initial condition

$$f(x) = \begin{cases} R \times (1-x^2)^2, & \text{if} \quad -1 \leq x \leq 1 \\ 0, & \text{otherwise,} \end{cases} \tag{3.5.17}$$

for four values of the mass R (R= 1, 20, 35, 100). In Figure 27, the numerical results have been attenuated and we have a mass-preserving diffusion mechanism with mesh grid refinement. The numerical experiments show that even with coarse grid the Lagrangian-Eulerian scheme seems to solve well the problem and as the mass of the initial solution increases, the solution increases in height. The numerical diffusion effect is not very significant. In Figure 28, we have a blow up of concentration type at distinct time of simulations.

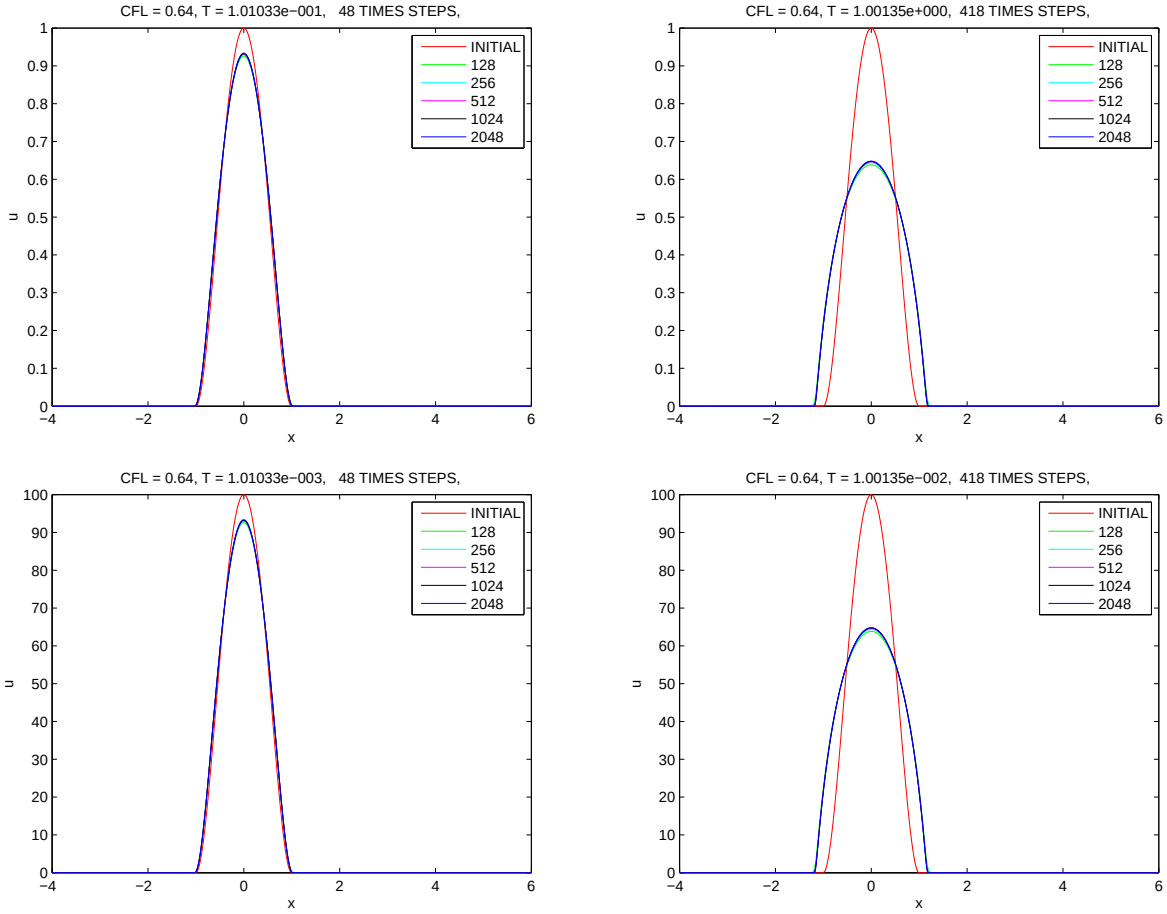

Figure 27 – Numerical solution for $u_t + (\mathbb{H}(u)u)_x = 0$ with f given in (3.5.17) with mass R=1 (top), 100 (bottom). The solution is shown at times $T = 0.1$, 1 (top) amd at time $T = 0.001$, 0.01 (bottom) with 128, 256, 512, 1024, 2048 grid cells. The computational time is 40 seconds.

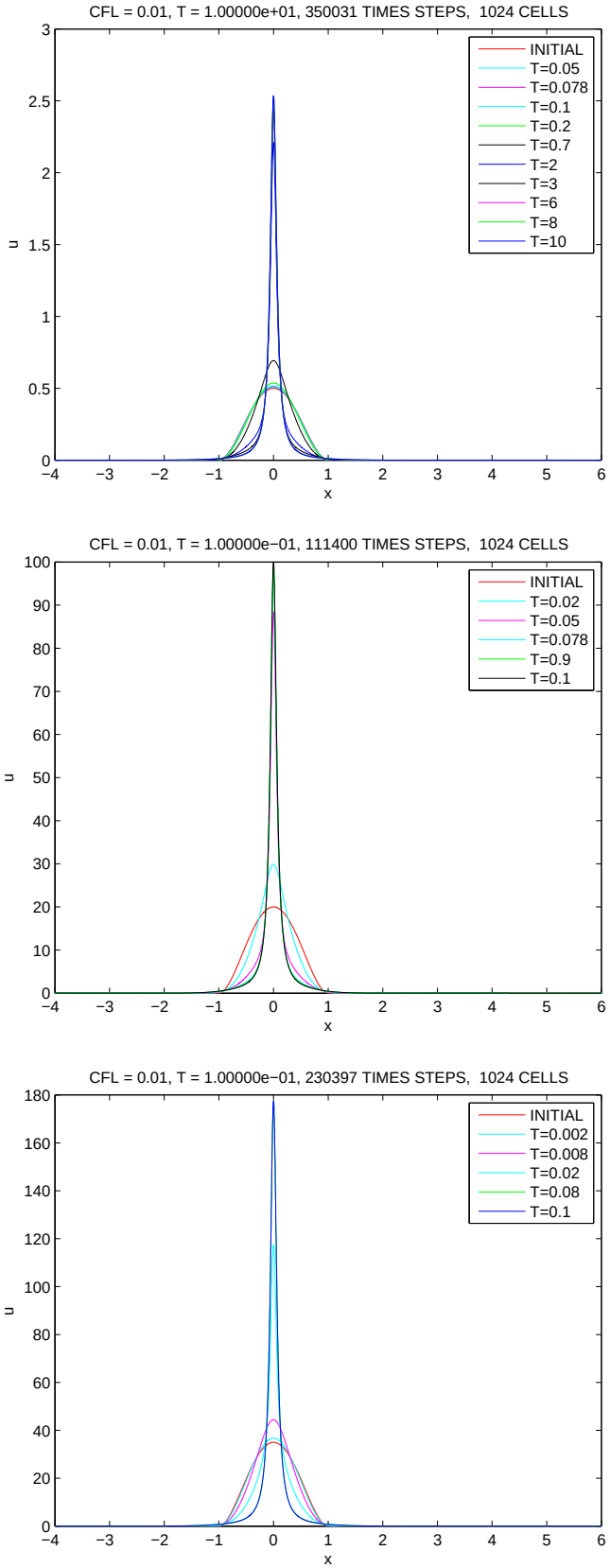

Figure 28 – Numerical solution for $u_t - (\mathbb{H}(u)u)_x = 0$ with f given in (3.5.17) with mass $R = 0.5$ (top), 20 (middle), 35 (bottom). The solution is shown at several time of simulations with 1024 mesh grid. The computational time is 4 days.

True value given by the norms $\|u\|_{L1}$= 20 and $\|u\|_{L1}$= 35 for the Figure 28.

R=20	T=0.02	T=0.078	T=0.1
N	$\|u\|_{L1}$	$\|u\|_{L1}$	$\|u\|_{L1}$
128	21.3333	21.3333	21.3333
256	21.3333	21.3333	21.3333
512	21.3333	21.3333	21.3333
1024	21.3333	21.3333	21.3333

R=35	T=0.002	T=0.02	T=0.1
N	$\|u\|_{L1}$	$\|u\|_{L1}$	$\|u\|_{L1}$
128	37.3333	37.3333	37.3333
256	37.3333	37.3333	37.3333
512	37.3333	37.3333	37.3333
1024	37.3333	37.3333	37.3333

Table 4 – Numerical computation of $\|u\|_{L1}$-norm corresponding to the numerical experiments reported in Figure 28 linked to nonlocal transport equation (3.5.12) at several time of simulations.

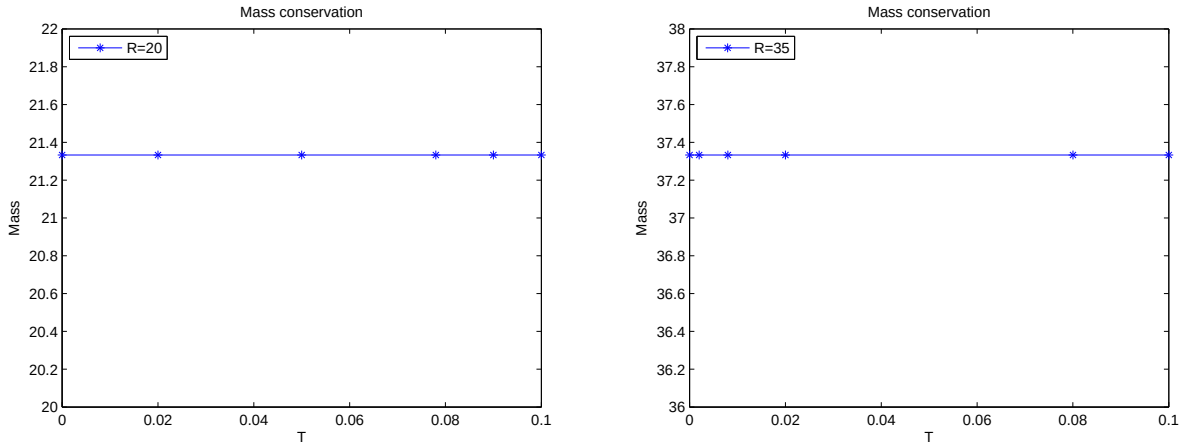

Figure 29 – Mass versus times with R=20 (left), 35 (right) and 1024 mesh grid.

Example 3.5.5. Oscillatory initial data.

In this example, we present and discuss numerical solutions for the nonlocal transport model problems (3.5.12) with oscillatory initial datas. We start our discussion with the positive (above of the x-axis) cases and measure sinusoidal shape like

$$f(x) = \begin{cases} \dfrac{R}{2} + \text{sen}(2\pi n x), & \text{if } \ x \in \left[-\dfrac{1}{2}, \dfrac{3}{2}\right], \\ 0, \qquad \text{otherwise}, \end{cases} \tag{3.5.18}$$

and

$$f(x) = \begin{cases} \dfrac{R}{2}(1 + \dfrac{1}{4}\text{sen}(2\pi n x)), & \text{if } \ x \in \left[-\dfrac{1}{2}, \dfrac{3}{2}\right], \\ 0, \qquad \text{otherwise}, \end{cases} \tag{3.5.19}$$

which numerical solutions are shown in Figures 30 - 31 and 32 - 33 with R=35. Analysing those Figures, it seems that the problem $u_t + (\mathbb{H}(u)u)_x = 0$ better captures the effect of attenuation and the problem $u_t - (\mathbb{H}(u)u)_x = 0$ captures better the effect of blow-up of concentration type. Now, we turn our attention to the symmetric case

$$f(x) = \begin{cases} \dfrac{\pi R}{4}\text{sen}(2\pi n x), & \text{if } \ x \in \left[-\dfrac{1}{2}, \dfrac{3}{2}\right], \\ 0, \qquad \text{otherwise}, \end{cases} \tag{3.5.20}$$

with positive and negative portions with respect to the x-axis. In Figures 34 - 36, numerical approximations are shown for this symmetric case with R=35. Although the Oscillatory is symmetric at the initial time of simulation, we see that the attenuation or the blow up of concentration type are not symmetrics in some sense.

In Figures 34 - 35, it seems that the positive portion of the Oscillatory tends to develop a faster or stronger attenuation with respect to the negative portion and in Figure 36, it seems that the positive portion tends to develop a blow up of concentration type with respect to the negative portion.

In Figures 38 - 40 numerical approximations are shown for the nonlocal problems (3.5.12) with the purely negative portion i.e., along the oscilatory initial data

$$f(x) = \begin{cases} -\dfrac{\pi R}{4}\left|\text{sen}(2\pi n x)\right|, & \text{if } \ x \in \left[-\dfrac{1}{2}, \dfrac{3}{2}\right], \\ 0, \qquad \text{otherwise}. \end{cases} \tag{3.5.21}$$

For several positive – or negative – measure initial datas we can see from our numerical computing that $\|u\|_{L1} \approx$ R as we refine the grid [17]. In Tables 5 , 6 , 7 and 8 it is shown numerical computation of the $\|u\|_{L1}$-norm corresponding to the numerical experiments reported

in Figures 31 , 33 , 36 and 40 linked to the nonlocal transport equation (3.5.12) at simulation time T=0.001 along the oscillatory initial datas. We take R=35, n=1, 2, 4, 8, 32, 64 and 128. In Table 7 Numerical computation of $\|u\|_{L1}$-norm corresponding to the numerical experiments reported in Figure 36 linked to nonlocal transport equation (3.5.12) at simulation time T=0.001 along the symmetric oscillatory initial data. We take R=35, n=1 and 4. As we refine the grid mesh, we may see the sequence of computed norm approaching to the corresponding true value given by the norm $\|u\|_{L1} \to 0$.

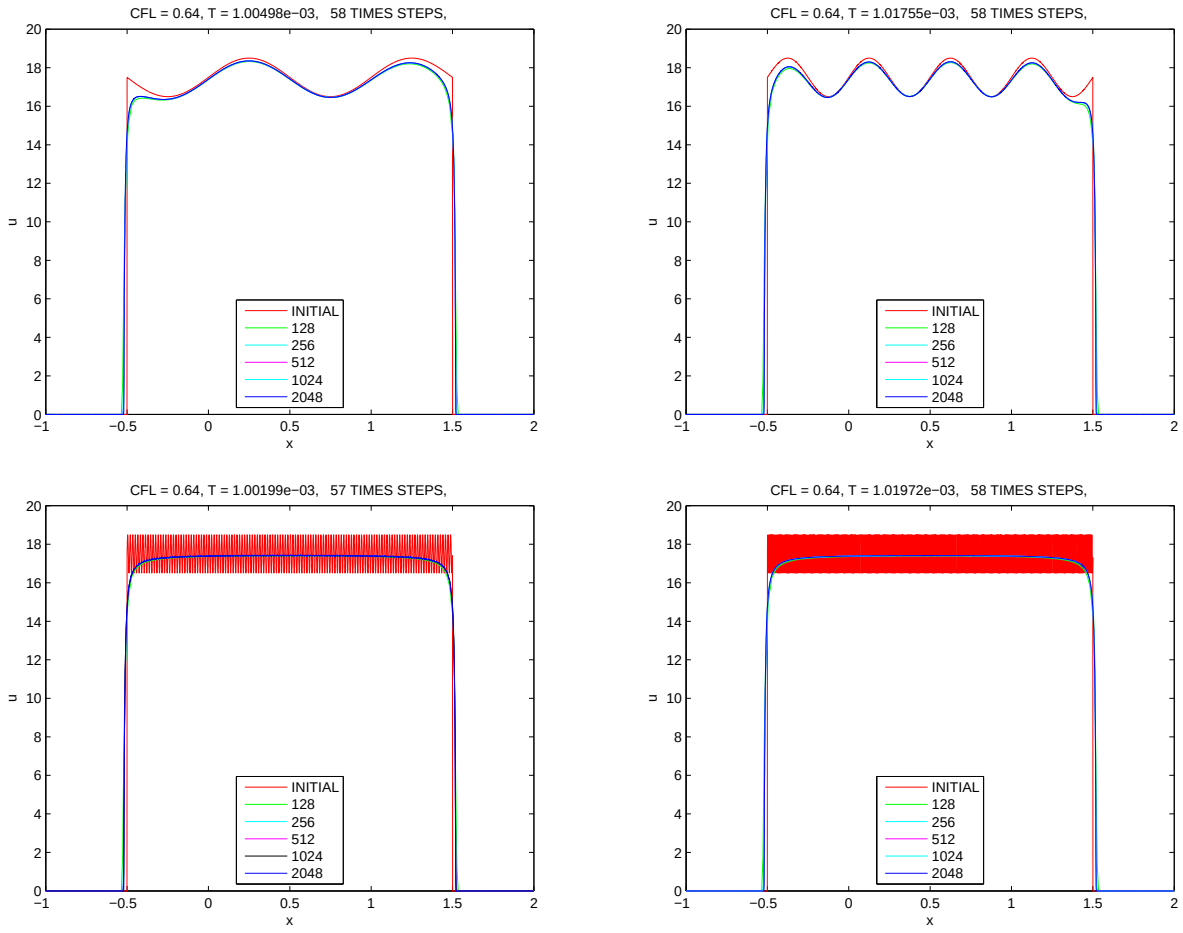

Figure 30 – Numerical solution for $u_t + (\mathbb{H}(u)u)_x = 0$ with mass $R = 35$ and $f(x) = \frac{R}{2} + \text{sen}(2\pi n x)$ if $x \in \left[-\frac{1}{2}, \frac{3}{2}\right]$ and zero otherwise as initial condition. The solution is shown at time $T = 0.001$ with 128, 256, 512, 1024, 2048 grid cells and with n=1, 2, 64,128 respectively.

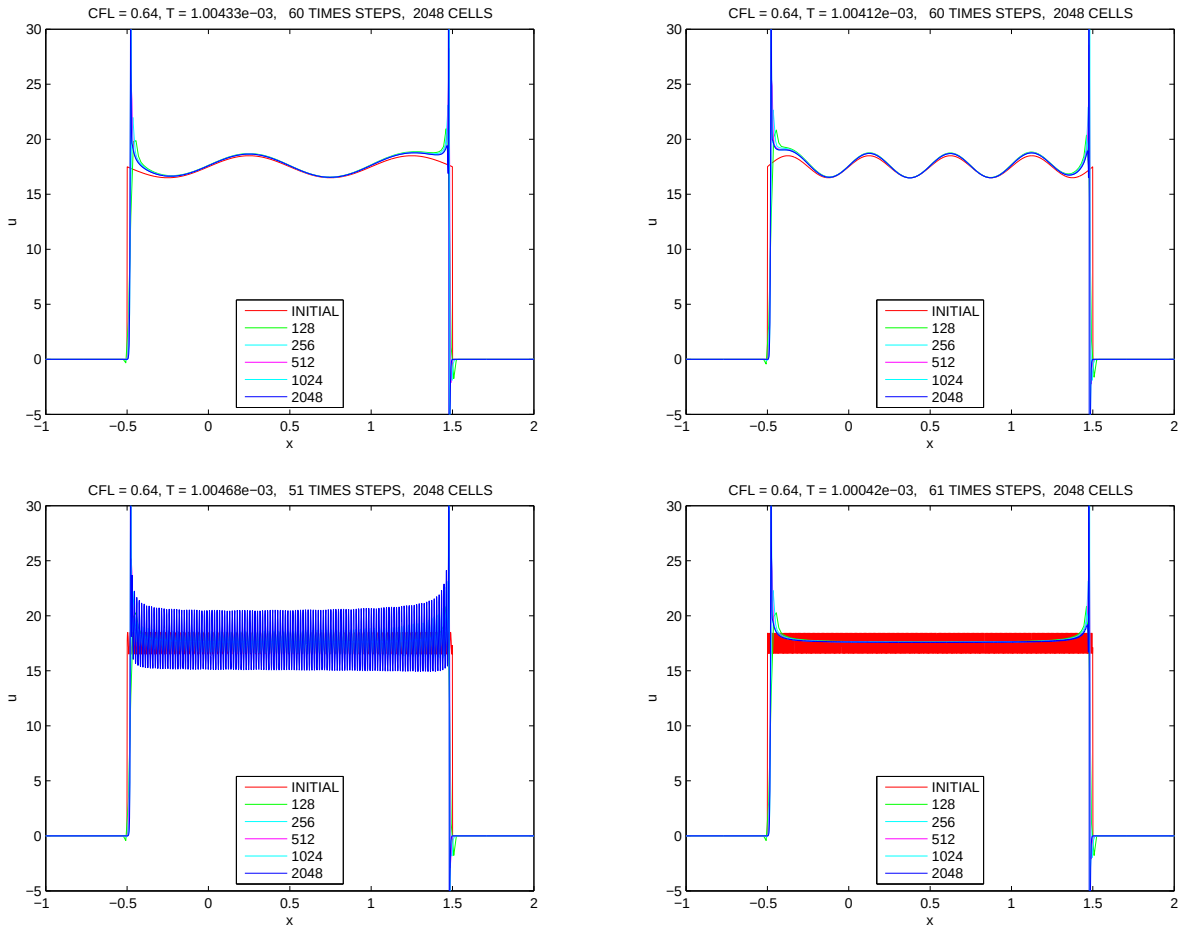

Figure 31 – Numerical solution for $u_t - (\mathbb{H}(u)u)_x = 0$ with mass $R = 35$ and $f(x) = \frac{R}{2} + \text{sen}(2\pi n x)$ if $x \in \left[-\frac{1}{2}, \frac{3}{2}\right]$ and zero otherwise as initial condition. The solution is shown at time $T = 0.001$ with 128, 256, 512, 1024, 2048 grid cells and with n=1, 2, 64, 128 respectively.

True value given by the norms $\|u\|_{L1}$= 35 for the Figure 31.

R=35	$n = 1$	$n = 2$
N	$\|u\|_{L1}$	$\|u\|_{L1}$
128	35	35
256	35	35
512	35	35
1024	35	35
2048	35	35

R=35	$n = 64$	$n = 128$
N	$\|u\|_{L1}$	$\|u\|_{L1}$
128	35	35
256	35	35
512	35	35
1024	35	35
2048	35	35

Table 5 – Numerical computation of $\|u\|_{L1}$-norm corresponding to the numerical experiments reported in Figure 31 linked to the nonlocal transport equation (3.5.12) at simulation time T=0.001 along the oscillatory initial data $f(x) = \frac{R}{2} + \text{sen}(2\pi n x)$ if $x \in \left[-\frac{1}{2}, \frac{3}{2}\right]$ and zero otherwise. We take $R = 35$ and n=1, 2, 64, 128. As we refine the grid mesh, we may see the sequence of computed norm equals to the corresponding true value given by the norm $\|u\|_{L1}$= 35.

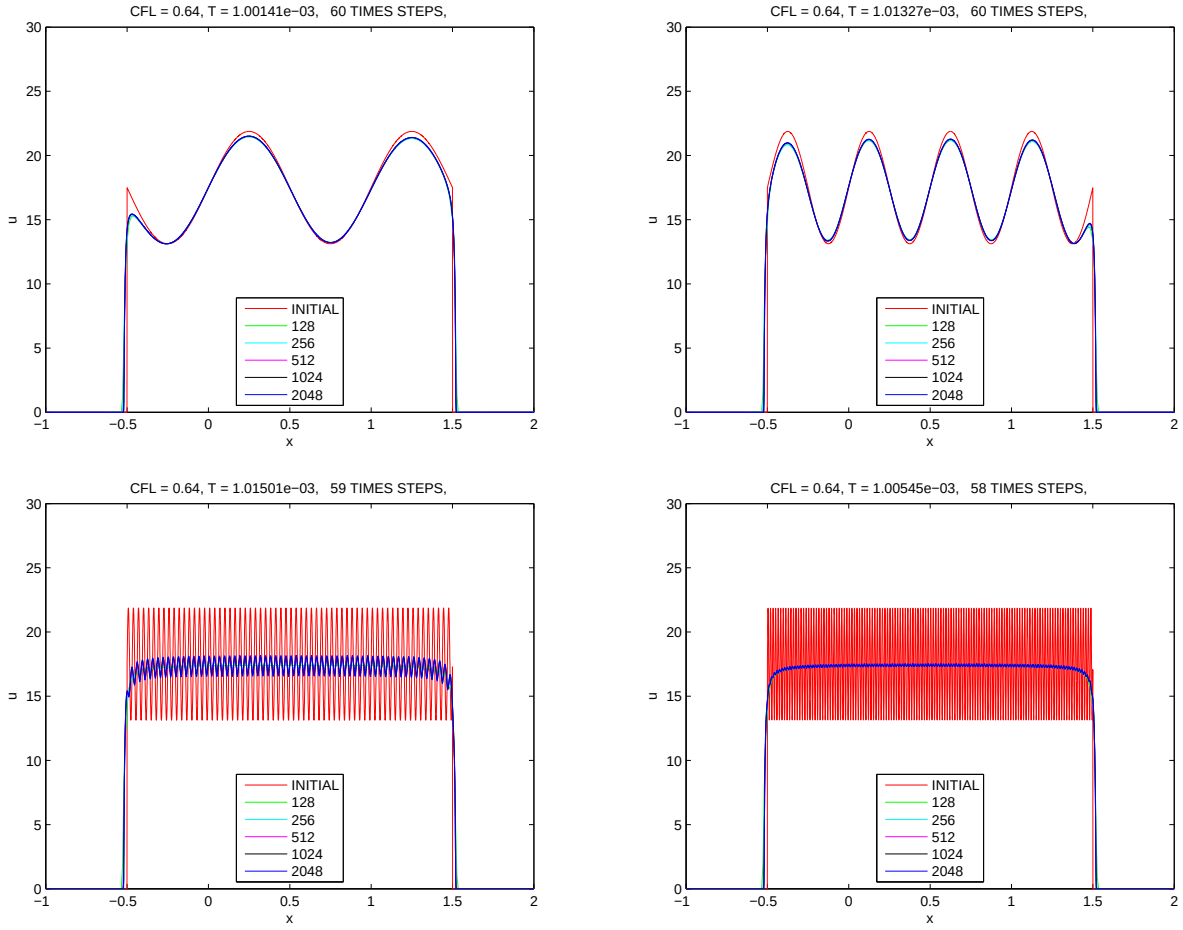

Figure 32 – Numerical solution for $u_t + (\mathbb{H}(u)u)_x = 0$ with mass $R = 35$ and $f(x) = \frac{R}{2}(1 + \frac{1}{4}\text{sen}(2\pi n x))$ if $x \in \left[-\frac{1}{2}, \frac{3}{2}\right]$ and zero otherwise as initial condition. The solution is shown at time $T = 0.001$ with 128, 256, 512, 1024, 2048 grid cells and with n=1, 2, 32, 64 respectively.

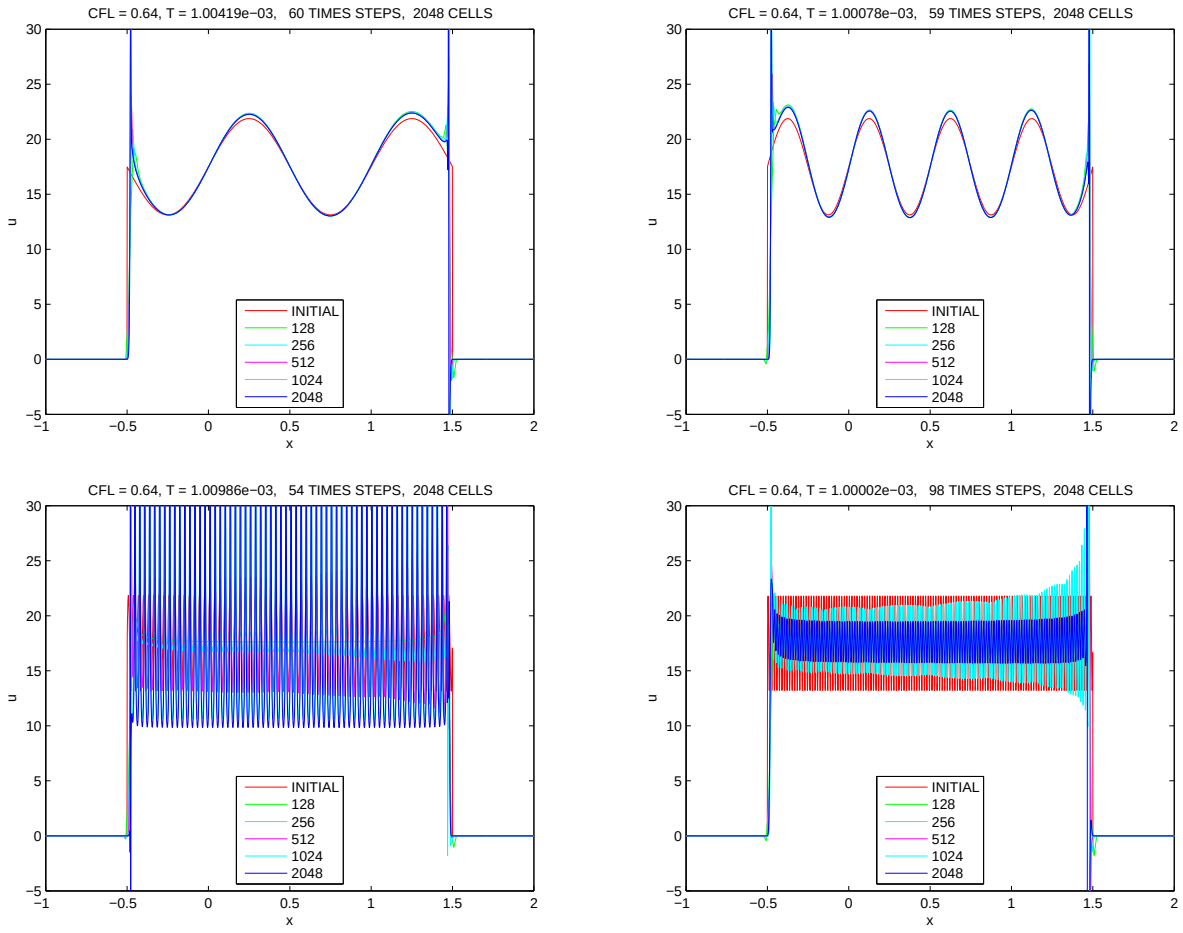

Figure 33 – Numerical solution for $u_t - (\mathbb{H}(u)u)_x = 0$ with mass $R = 35$ and $f(x) = \frac{R}{2}(1 + \frac{1}{4}\text{sen}(2\pi nx))$ if $x \in \left[-\frac{1}{2}, \frac{3}{2}\right]$ and zero otherwise as initial condition. The solution is shown at time T=0.001 with 128, 256, 512, 1024, 2048 grid cells and with n=1, 2, 32 64 respectively.

True value given by the norms $\|u\|_{L1}$= 35 for the Figure 33.

R=35	$n = 1$	$n = 2$
N	$\|u\|_{L1}$	$\|u\|_{L1}$
128	35	35
256	35	35
512	35	35
1024	35	35
2048	35	35

R=35	$n = 32$	$n = 64$
N	$\|u\|_{L1}$	$\|u\|_{L1}$
128	35	35
256	35	35
512	35	35
1024	35	35
2048	35	35

Table 6 – Numerical computation of $\|u\|_{L1}$-norm corresponding to the numerical experiments reported in Figure 33 linked to the nonlocal transport equation (3.5.12) at simulation time T=0.001 along the oscillatory initial data $f(x) = \frac{R}{2}(1 + \frac{1}{4}\text{sen}(2\pi n x))$ if $x \in \left[-\frac{1}{2}, \frac{3}{2}\right]$ and zero otherwise. We take $R = 35$ and n=1, 2, 32,64. As we refine the grid mesh, we may see the sequence of computed norm equals to the corresponding true value given by the norm $\|u\|_{L1}$= 35.

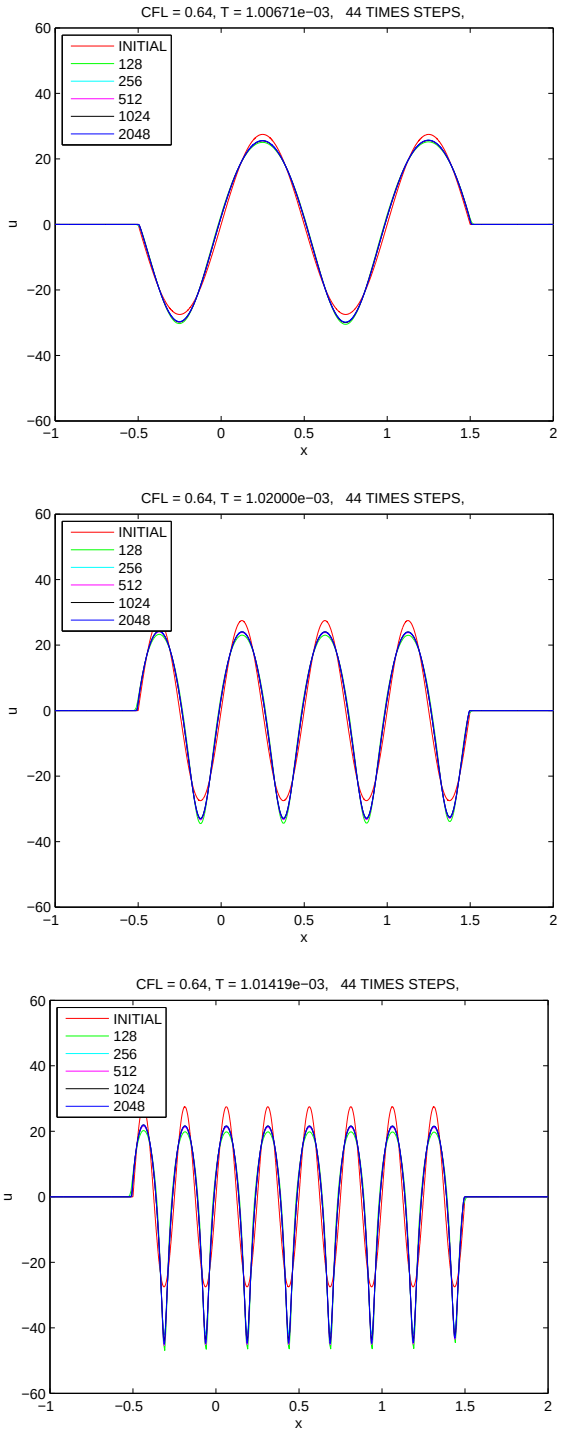

Figure 34 – Numerical solution for $u_t + (\mathbb{H}(u)u)_x = 0$ with mass $R = 35$ and $f(x) = \frac{\pi R}{4}\text{sen}(2\pi n x)$ if $x \in \left[-\frac{1}{2}, \frac{3}{2}\right]$ and zero otherwise as initial condition. The solution is shown at time T=0.001 with 128, 256, 512, 1024, 2048 grid cells and with n=1, 2, 4 respectively.

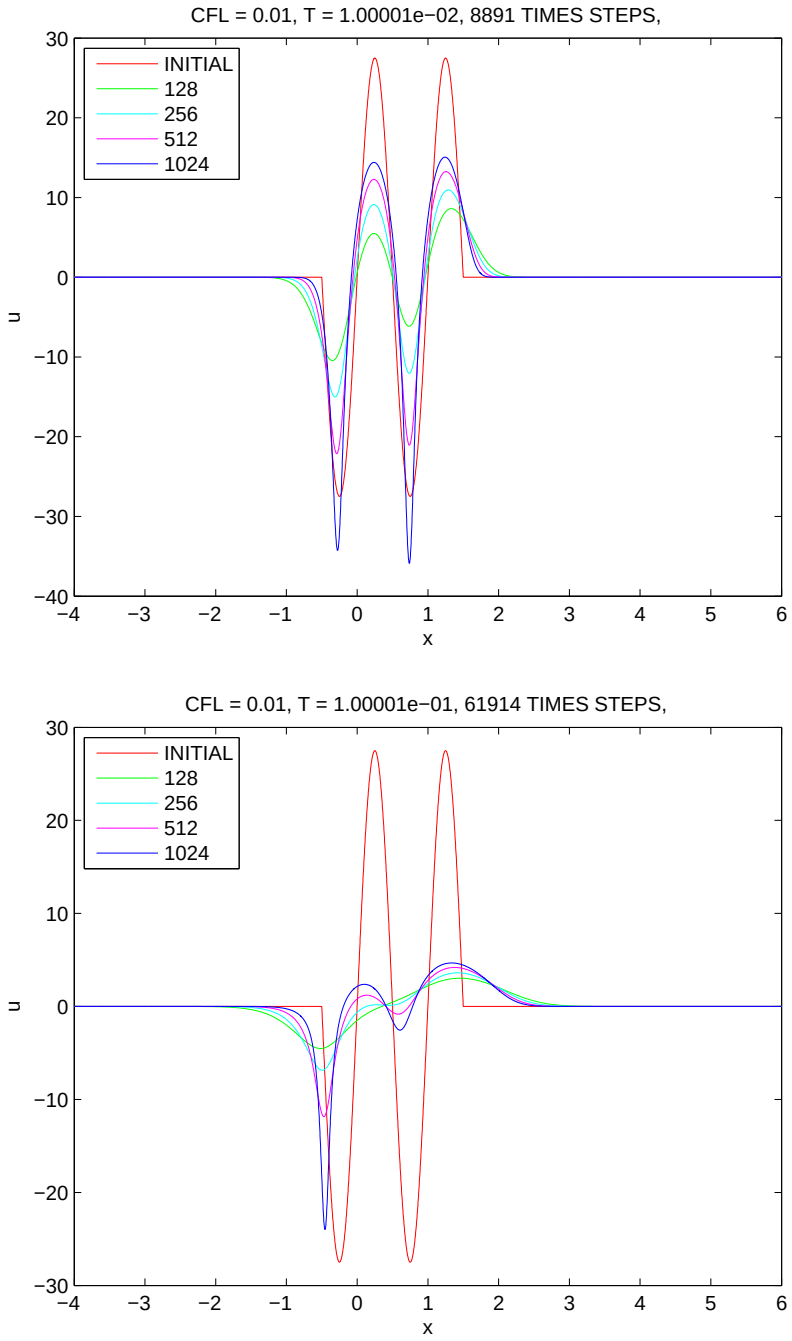

Figure 35 – Numerical solution for $u_t + (\mathbb{H}(u)u)_x = 0$ with mass $R = 35$ and $f(x) = \frac{\pi R}{4}\text{sen}(2\pi n x)$ if $x \in \left[-\frac{1}{2}, \frac{3}{2}\right]$ and zero otherwise as initial condition. The solution is shown at time T=0.01 and 0.1 with 128, 256, 512, 1024 grid cells and with n=1.

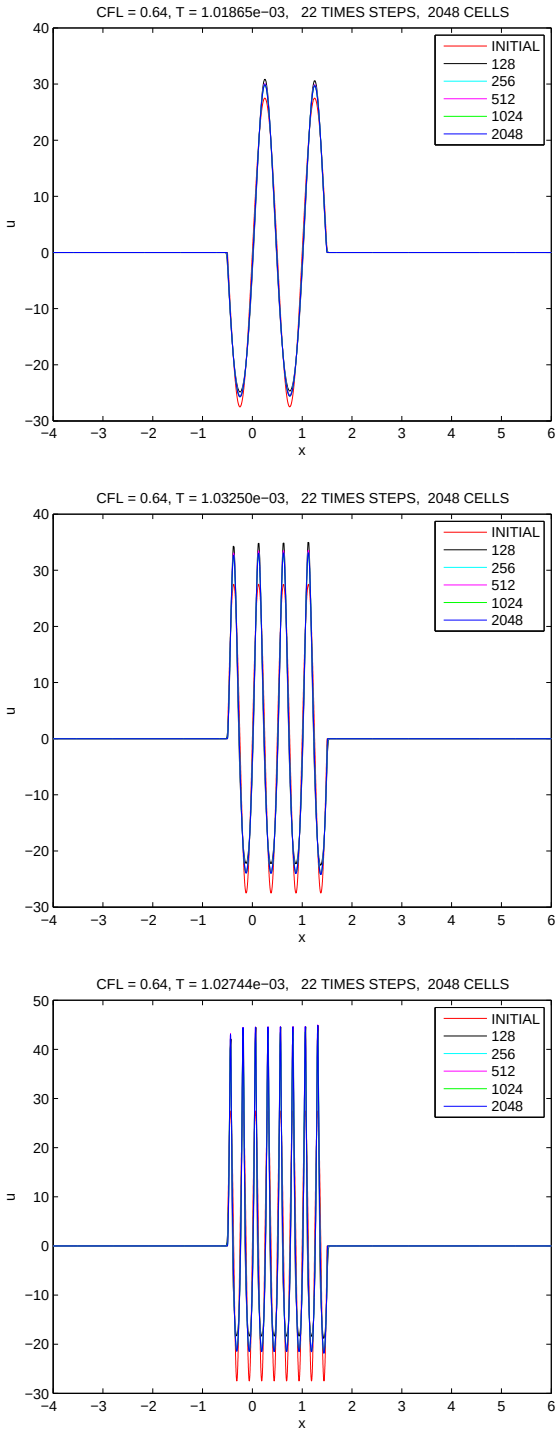

Figure 36 – Numerical solution for $u_t - (\mathbb{H}(u)u)_x = 0$ with mass $R = 35$ and $f(x) = \frac{\pi R}{4}\text{sen}(2\pi n x)$ if $x \in \left[-\frac{1}{2}, \frac{3}{2}\right]$ and zero otherwise as initial condition. The solution is shown at time T=0.001 with 128, 256, 512, 1024, 2048 grid cells and with n=1, 2, 4, respectively.

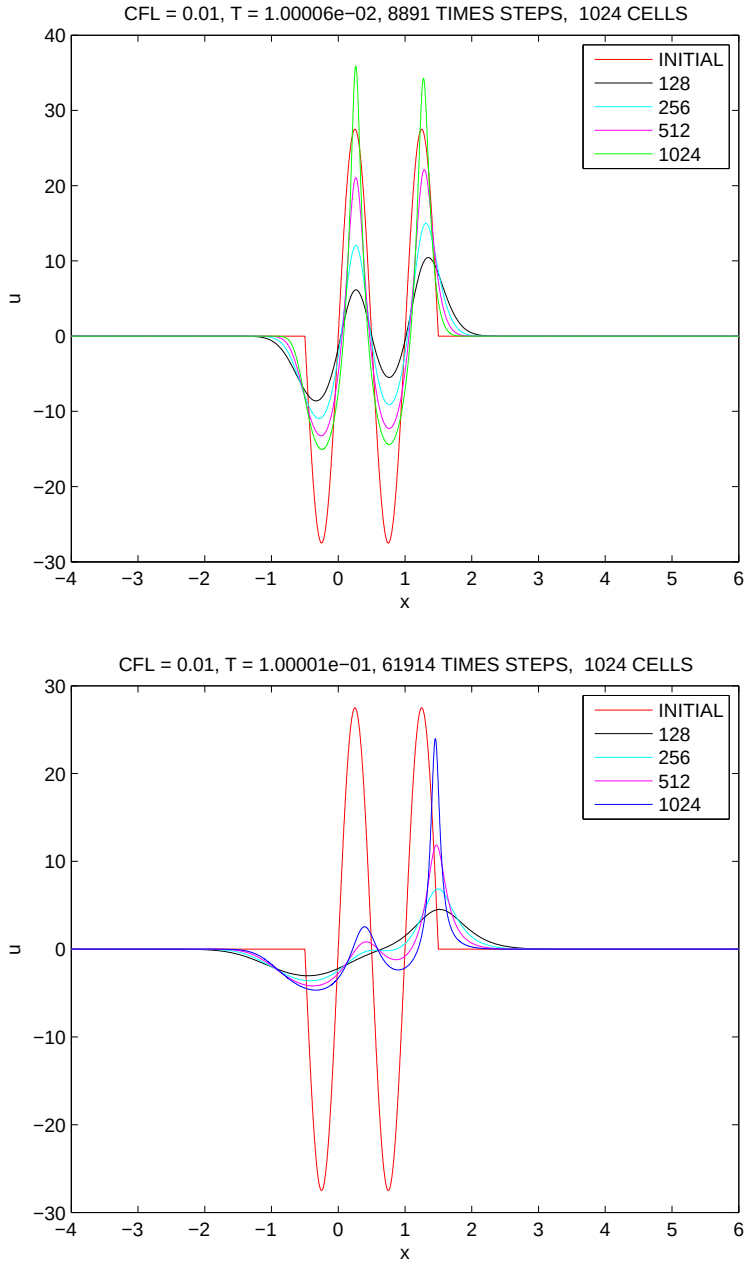

Figure 37 – Numerical solution for $u_t - (\mathbb{H}(u)u)_x = 0$ with mass $R = 35$ and $f(x) = \frac{\pi R}{4}\text{sen}(2\pi n x)$ if $x \in \left[-\frac{1}{2}, \frac{3}{2}\right]$ and zero otherwise as initial condition. The solution is shown at time T=0.01, 0.1 with 128, 256, 512, 1024 grid cells and with n=1 .

True value given by the norms $\|u\|_{L1}= 0$ for the Figure 36.

R=35	$n = 1$	$n = 4$
N	$\|u\|_{L1}$	$\|u\|_{L1}$
128	6.2103e-016	1.2976e-015
256	4.7835e-016	1.3722e-015
512	0	7.9017e-016
1024	0	1.6805e-016

Table 7 – Numerical computation of $\|u\|_{L1}$-norm corresponding to the numerical experiments reported in Figure 36 linked to the nonlocal transport equation (3.5.12) at simulation time T=0.001 along the oscillatory initial data $f(x) = \frac{\pi R}{4}\text{sen}(2\pi n x)$ if $x \in \left[-\frac{1}{2}, \frac{3}{2}\right]$ and zero otherwise. We take $R = 35$, n=1 and 4. As we refine the grid mesh, we may see the sequence of computed norm approaching to the corresponding true value given by the norm $\|u\|_{L1} \to 0$.

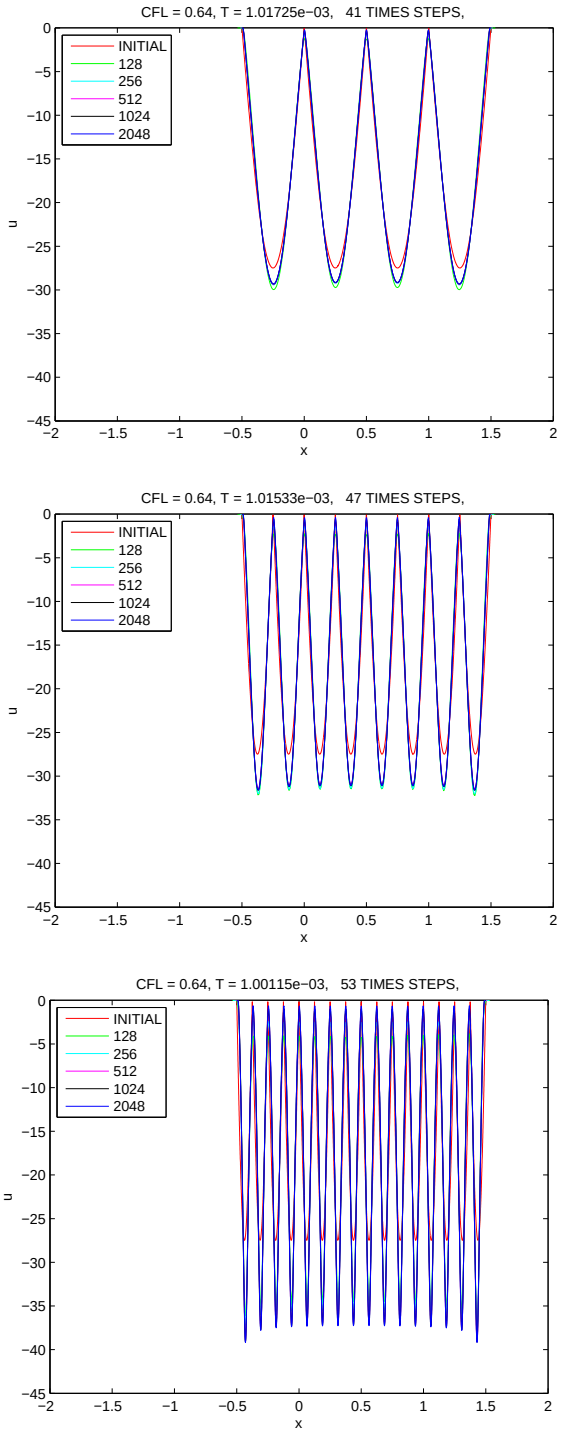

Figure 38 – Numerical solution for $u_t + (\mathbb{H}(u)u)_x = 0$ with mass $R = 35$ and $f(x) = -\dfrac{\pi R}{4}\,|\text{sen}(2\pi n x)|$ if $x \in \left[-\dfrac{1}{2}, \dfrac{3}{2}\right]$ and zero otherwise as initial condition. The solution is shown at time T=0.001 with 128, 256, 512, 1024, 2048 cells and with n=1, 2, 4 respectively.

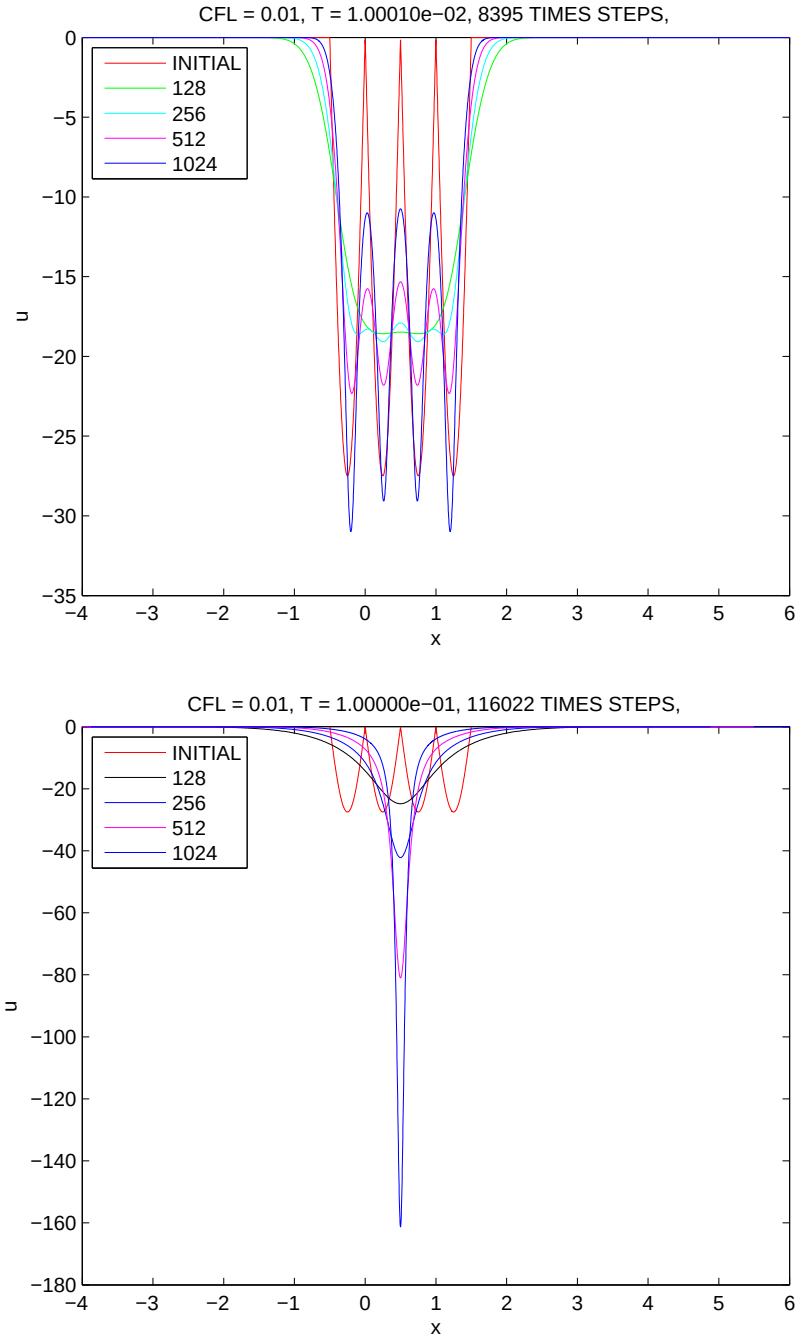

Figure 39 – Numerical solution for $u_t + (\mathbb{H}(u)u)_x = 0$ with mass $R = 35$ and $f(x) = -\frac{\pi R}{4}|\text{sen}(2\pi n x)|$ if $x \in \left[-\frac{1}{2}, \frac{3}{2}\right]$ and zero otherwise as initial condition. The solution is shown at time T=0.01 and 0.1 with 128, 256, 512 and 1024 grid cells with n=1.

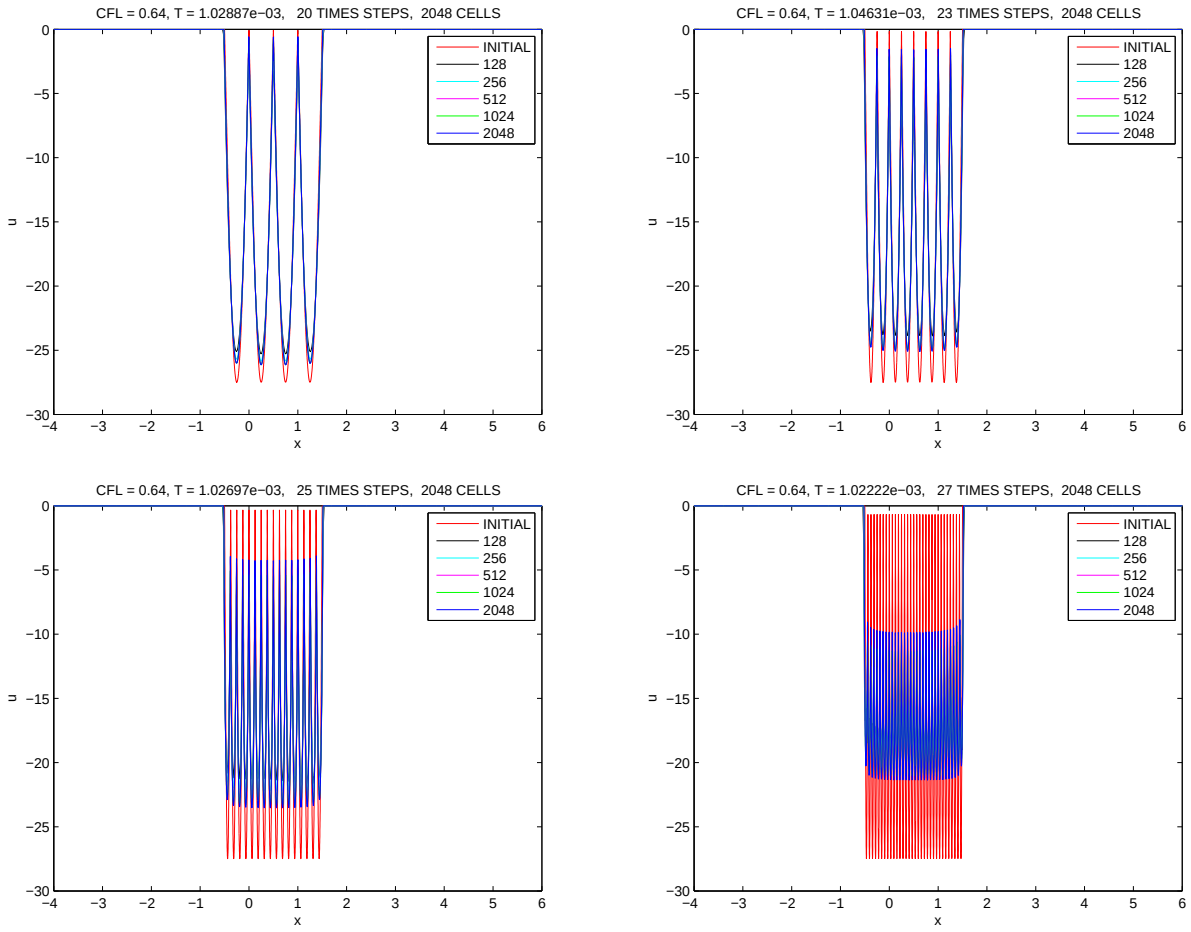

Figure 40 – Numerical solution for $u_t - (\mathbb{H}(u)u)_x = 0$ with mass $R = 35$ and $f(x) = -\dfrac{\pi R}{4}\,|\text{sen}(2\pi n x)|$ if $x \in \left[-\dfrac{1}{2}, \dfrac{3}{2}\right]$ and zero otherwise as initial condition. The solution is shown at time tT=0.001 with 128, 256, 512, 1024, 2048 cells and n=1, 2, 4, 8 respectively.

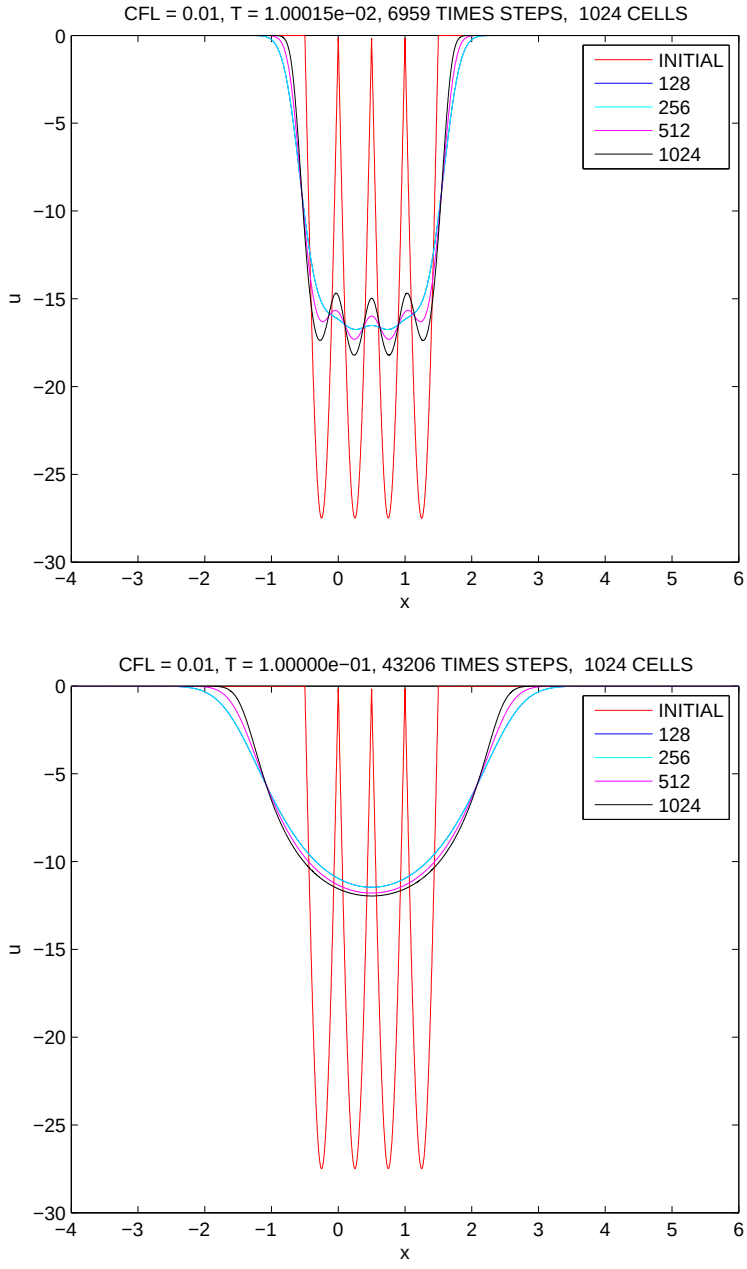

Figure 41 – Numerical solution for $u_t - (\mathbb{H}(u)u)_x = 0$ with mass $R = 35$ and $f(x) = -\frac{\pi R}{4}|\text{sen}(2\pi n x)|$ if $x \in \left[-\frac{1}{2}, \frac{3}{2}\right]$ and zero otherwise as initial condition. The solution is shown at time T=0.01, 0.1 with 128, 256, 512, 1024 cells and n=1.

True value given by the norms $\|u\|_{L1}$= 35 for the Figure 40.

R=35	$n=1$	$n=2$
N	$\|u\|_{L1}$	$\|u\|_{L1}$
128	35.0141	35.0563
256	35.0035	35.0141
512	35.0009	35.0035
1024	35.0002	35.0009
2048	35.0001	35.0002

R=35	$n=4$	$n=8$
N	$\|u\|_{L1}$	$\|u\|_{L1}$
128	35.2259	35.9160
256	35.0562	35.2259
512	35.0140	35.0562
1024	35.0035	35.0140
2048	35.0008	35.0035

Table 8 – Numerical computation of $\|u\|_{L1}$-norm corresponding to the numerical experiments reported in Figure 40 linked to the nonlocal transport equation (3.5.12) at simulation time T=0.001 along the oscillatory initial data $f(x) = -\frac{\pi R}{4}|\text{sen}(2\pi n x)|$ if $x \in \left[-\frac{1}{2}, \frac{3}{2}\right]$ and zero otherwise. We take $R = 35$, n=1, 2, 4 and 8. As we refine the grid mesh, we may see that the sequence of computed norm equals to the corresponding true value given by the norm $\|u\|_{L1}$= 35.

4 The Lagrangian-Eulerian scheme for scalar hyperbolic balance laws

In this Chapter we present the studied Lagrangian-Eulerian framework for scalar hyperbolic balance laws as well as the linear and the nonlinear cases. We study a distinctive aspect of the Lagrangian-Eulerian approach and numerical approximations of scalar balance laws as presented and discussed in [35]. For the numerical approximations of the scalar balance laws problems we use quadrature rules such as the predictor-corrector method, the midpoint method for approximate the source term. In addition, the balance problem is then solved by forward tracking the boundary of grid cells along the so-called integral tubes. This is a distinct feature of the studied Lagrangian-Eulerian approach [35].

4.1 The presentation of the Lagrangian-Eulerian scheme for scalar hyperbolic balance laws

Consider the scalar balance laws problem,

$$\begin{cases} \dfrac{\partial u}{\partial t} + \dfrac{\partial H(u)}{\partial x} = G(u), & t > 0, \quad -\infty < x < \infty, \\ u(x,0) = \eta(x), & -\infty < x < \infty, \end{cases} \tag{4.1.1}$$

under the assumption $\iint_{D_j^n} G(u)\ dx\,dt < \infty$.

Now, write (4.1.1) as follows,

$$\begin{aligned} \nabla_{t,x} \cdot \begin{bmatrix} u \\ H(u) \end{bmatrix} = G(u), \qquad & t > 0, \quad -\infty < x < \infty, \\ u(x,0) = \eta(x), \qquad & -\infty < x < \infty. \end{aligned} \tag{4.1.2}$$

Now, lets us write (4.1.2) over the local space-time "Integral tube" D_j^n (see equation (3.1.6) and the top picture in Figure (8)),

$$\iint_{D_j^n} \nabla_{t,x} \cdot \begin{bmatrix} u \\ H(u) \end{bmatrix} dx\,dt = \iint_{D_j^n} G(u)\ dx\,dt. \tag{4.1.3}$$

Following the same arguments in Chapter 3, it first applies the divergence theorem in (4.1.3) and, by means of the impervious boundaries given by $\sigma_j^n(t)$, reads:

$$\int_{\overline{x}_{j-\frac{1}{2}}^{n+1}}^{\overline{x}_{j+\frac{1}{2}}^{n+1}} u(x,t^{n+1})dx = \int_{x_j^n}^{x_{j+1}^n} u(x,t^n)dx + \iint_{D_j^n} G(u)\ dx\,dt. \tag{4.1.4}$$

This equation can be viewed as *the local space-time Lagrangian-Eulerian conservation relation* for the balance laws (4.1.4). Finally, it is used (4.1.4) to define,

$$\overline{U}_j^{n+1} = \frac{1}{h_j^{n+1}} \int_{\overline{x}_{j-\frac{1}{2}}^{n+1}}^{\overline{x}_{j+\frac{1}{2}}^{n+1}} u(x,t^{n+1})dx = \frac{1}{h_j^{n+1}} \left[\int_{x_j^n}^{x_{j+1}^n} u(x,t^n)dx + \iint_{D_j^n} G(u)dxdt \right], \tag{4.1.5}$$

and its associated projection step over the original mesh grid,

$$U_j^{n+1} = \frac{1}{h} \left[(\frac{h}{2} + f_j^n k)\overline{U}_{j-1}^{n+1} + (\frac{h}{2} - f_j^n k)\overline{U}_j^{n+1} \right]. \tag{4.1.6}$$

The Lagrangian-Eulerian scheme for balance law (LEB1) is fully defined by combining equations (4.1.5) and (4.1.6). Clearly, the key point here is how to design a discretization in a manner which retains an accurate balance between the gradients of the flux function and the source term. Thus, extend the designed proposed scheme for linear hyperbolic conservation laws to the case of balance laws in order to describe the features of the Lagragian-Eulerian procedure.

4.2 Linear case for balance laws

Consider the following balance law problem,

$$\begin{cases} \dfrac{\partial u}{\partial t} + \dfrac{\partial (au)}{\partial x} = G(x,t), \qquad t > 0, \quad -\infty < x < \infty, \\ \\ u(x,0) = \eta(x), \qquad -\infty < x < \infty. \end{cases} \tag{4.2.1}$$

As in Chapter 3 , resulting that $f_j^n = a$, $h_j^{n+1} = h$ and the combination of (4.1.5) and (4.1.6) give The Lagrangian-Eulerian scheme for the scalar linear balance laws:

$$\frac{U_j^{n+1} - \frac{1}{4}\left(U_{j-1}^n + 2U_j^n + U_{j+1}^n\right)}{k} - a\frac{U_{j+1}^n - U_{j-1}^n}{2h} = \frac{1}{k\,h} \left[\begin{array}{l} \dfrac{1}{h}\left(\dfrac{h}{2} + ak\right) \displaystyle\iint_{D_{j-1}^n} G(x,t)\ dx\,dt \\ \\ +\dfrac{1}{h}\left(\dfrac{h}{2} - ak\right) \displaystyle\iint_{D_j^n} G(x,t)dx\,dt \end{array} \right]. \tag{4.2.2}$$

At this point, a distinctive aspect of the new Lagrangian-Eulerian approach can be considered. First, consider the "hyperbolic counterpart" of the balance law (4.2.1), i.e., $G(u) \equiv 0$ and $u_t + au_x = 0$, $u(x,0) = \eta(x)$, along with the well known exact solution $u(x,t) = \eta(x - at)$. If the mesh grid parameters in space h and time k are to obey a CFL condition (e.g.,[1, 35]), then the following mesh grid *representation* of the local approximate solution is given by $u(x_j, t^{n+1}) = u(x_j - ak, t^n) \equiv \eta_j(h - ak)$. By construction, the Lagrangian-Eulerian scheme points (x_j, t^n) and (x_j, t^{n+1}) are inside the space-time local control finite volume D_j^n and away from the parameterized curves $\sigma_j^n(t)$, and $u(x_j, t^{n+1}) = \eta(h - ak)$ is a smooth function in each

D_j^n. Furthermore, it is worth pointing out that in the linear hyperbolic case the integral curves (integral tubes) coincide with the *characteristic curves*. Thus, the source term can be solved by forward tracking the boundary of grid cells from the parameterized curves $\sigma_j^n(t)$ along the so-called integral tubes. Thus, (4.2.2) can be recasted as follows:

$$\frac{U_j^{n+1}-\frac{1}{4}\left(U_{j-1}^n+2U_j^n+U_{j+1}^n\right)}{k}-a\frac{U_{j+1}^n-U_{j-1}^n}{2h}=\frac{1}{kh}\left[\begin{array}{l}\frac{1}{h}[\eta_{j-1}^{-1}\,(h/2+ak)]\iint_{D_{j-1}^n}G(x,t)\;dx\,dt\\ \\ +\frac{1}{h}[\eta_j^{-1}\,(h/2-ak)]\iint_{D_j^n}G(x,t)\;dx\,dt\end{array}\right]. \tag{4.2.3}$$

4.3 Nonlinear case for balance laws

In this section, we turn our attention from the Lagragian-Eulerian procedure developed for linear hyperbolic conservation laws to the case of nonlinear scalar balance laws. From the very beginning of Chapter 4, we design the Lagrangian-Eulerian framework procedure (4.1.5)-(4.1.6) for balance law of type (4.1.1) given by,

$$\overline{U}_j^{n+1}=\frac{1}{h_j^{n+1}}\int_{\overline{x}_{j-\frac{1}{2}}^{n+1}}^{\overline{x}_{j+\frac{1}{2}}^{n+1}}u(x,t^{n+1})dx=\frac{1}{h_j^{n+1}}\left[\int_{x_j^n}^{x_{j+1}^n}u(x,t^n)\,dx+\iint_{D_j^n}G(u)\;dx\,dt\right],$$

$$U_j^{n+1}=\frac{1}{h}\left[(\frac{h}{2}+f_j^nk)\overline{U}_{j-1}^{n+1}+(\frac{h}{2}-f_j^nk)\overline{U}_j^{n+1}\right].$$

The combination of the above equations (see (4.1.5)-(4.1.6)) gives the *Lagrangian-Eulerian scheme 1 (LEB1)* for the scalar nonlinear balance laws:

$$\begin{aligned}U_j^{n+1}\;&=\frac{1}{4}(U_{j-1}^n+2U_j^n+U_j^n)-\frac{k}{4}\left(\mathbb{W}(U_{j+1}^n,U_j^n)-\mathbb{W}(U_{j-1}^n,U_j^n)\right)\\&+\frac{1}{h}\left[\frac{1}{h}\left(\frac{h}{2}+f_j^nk\right)\iint_{D_{j-1}^n}G(u(x,t))\;dx\,dt+\frac{1}{h}\left(\frac{h}{2}-f_j^nk\right)\iint_{D_j^n}G(u(x,t))\;dx\,dt\right],\end{aligned} \tag{4.3.1}$$

along with CFL condition (3.3.2). Where $f_j^n=H(U_j^n)/U_j^n\approx H(U)/U$; see (4.1.1).

In [1, 35] section 3, it is also possible design a *diference finite Lagrangian-Eulerian scheme 2 (LEB2)*:

$$\begin{aligned}U_j^{n+1}\;&=\frac{1}{4}\left(U_{j-1}^n+2U_j^n+U_{j+1}^n\right)-\frac{k}{2h}\left(H(U_{j+1}^n)-H(U_{j-1}^n)\right)\\&+\frac{1}{h}\left[\frac{1}{h}\left(\frac{h}{2}+f_j^nk\right)\iint_{D_{j-1}^n}G(u(x,t))\;dx\,dt+\frac{1}{h}\left(\frac{h}{2}-f_j^nk\right)\iint_{D_j^n}G(u(x,t))\;dx\,dt\right].\end{aligned} \tag{4.3.2}$$

With the CFL condition

$$\frac{\max\{\max_j\{H'(U_j)\}, \max_j\{f_j^n\}\}\, k}{h} \leq \frac{\sqrt{2}}{2}. \tag{4.3.3}$$

Consider $\Phi = \Phi(x,t) \in C^\infty(\mathbb{R})$ (i.e., under a CFL constraint) such that $\Phi_t + f_x(\Phi) = G(\Phi)$ in order to seek the appropriate approximations for grid functions for $\Phi(x,t)$ in the flux and source term for schemes (4.3.1) and (4.3.2).

4.3.1 Predictor-corrector method for the source term approximation

First, suppose $U_j^{n+\frac{1}{2}}$ as a known predictor value for $\Phi(x,t)$ at space-time point (x_j, t^n). It is sufcient to consider the integration just over one "Integral tube" D_j^n the other case D_{j-1}^n is similar. Thus, write the source term approximation as,

$$\iint_{D_j^n} G(\Phi(x,t))\, dx\, dt \approx \iint_{D_j^n} G(U_j^{n+\frac{1}{2}})\, dx\, dt \;=\; G(U_j^{n+\frac{1}{2}}) \iint_{D_j^n} dx\, dt \;=\; G(U_j^{n+\frac{1}{2}})\, \mathcal{A}(D_j^n), \tag{4.3.4}$$

where

$$\mathcal{A}(D_j^n) = \int_{t^n}^{t^{n+1}} \int_{\sigma_j^n(t)}^{\sigma_{j+1}^n(t)} dx\, dt = \int_{t^n}^{t^{n+1}} \left(\sigma_{j+1}^n(t) - \sigma_j^n(t)\right) dt. \tag{4.3.5}$$

Since $\sigma_{j+1}^n(t) - \sigma_j^n(t) = (t-t^n)f_{j+1}^n + x_{j+1}^n - (t-t^n)f_j^n - x_j^n = (t-t^n)(f_{j+1}^n - f_j^n) + h$, we recast (4.3.5) as,

$$\mathcal{A}(D_j^n) = k\left[\frac{k}{2}(f_{j+1}^n - f_j^n) + h\right]. \tag{4.3.6}$$

Now, in view of the balance law $\Phi_t + f_x(\Phi) = G(\Phi)$ we might write $\Phi_t = G(\Phi) - f_x(\Phi)$ and thus reads,

$$G(\Phi_j^{n+\frac{1}{2}}) \approx G(\Phi(x_j^n, t^n) + \frac{k}{2}\Phi_t(x_j^n, t^n)) = G\left[\Phi_j^n + \frac{k}{2}(G(\Phi_j^n) - (f(\Phi))_x)_j^n\right]. \tag{4.3.7}$$

We point out that quantity $f_x(\Phi(x,t))_j^n$ denotes the numerical derivative of function $f(\Phi)$ with respect to space variable x evaluated at point (x_j, t^n). Indeed, a family of slope limiters can be used here, as such the *Mimmod limiter*: $((f(\Phi))_x)_j^n = MM\{\Delta f_{j+\frac{1}{2}}, \Delta f_{j-\frac{1}{2}}\}$ where $MM\{x,y\} \equiv MinMod\{x,y\} = \frac{1}{2}[sgn(x) + sgn(y)] \cdot Min(|x|,|y|)$ [35]. Finally, from equations (4.3.6) and (4.3.7), we might write,

$$\iint_{D_j^n} G(\Phi(x,t))dxdt \approx k\, G\left[U_j^n + \frac{k}{2}(G(U_j^n) - f_x(\Phi)_j^n\right] \left[\frac{k}{2}(f_{j+1}^n - f_j^n) + h\right]. \tag{4.3.8}$$

4.3.2 Midpoint method for the source term approximation

Consider $\Phi = \Phi(x,t) \in C^{\infty}(\mathbb{R})$ such that $\Phi_t + f_x(\Phi) = G(\Phi)$, at time $t = t^{n+\frac{1}{2}}$. It is sufcient to consider the integration just over one "Integral tube" D_j^n the other case D_{j-1}^n is similar. Thus we have,

$$\iint_{D_j^n} G(\Phi(x,t))dx\,dt = \int_{t^n}^{t^{n+1}} \int_{\sigma_j^n(t)}^{\sigma_{j+1}^n(t)} G(\Phi(x,t)\ dx\,dt, \tag{4.3.9}$$

$$\begin{aligned}
&\iint_{D_j^n} G(\Phi(x,t))dx\,dt \approx \int_{t^n}^{t^{n+1}} (\sigma_{j+1}^n(t) - \sigma_j^n(t))G\left(\Phi(\frac{\sigma_{j+1}^n(t)+\sigma_j^n(t)}{2}), t\right)dt \ \approx \\
&\approx \int_{t^n}^{t^{n+1}} (\sigma_{j+1}^n(t^{n+\frac{1}{2}}) - \sigma_j^n(t^{n+\frac{1}{2}}))G\left(\Phi(\frac{\sigma_{j+1}^n(t^{n+\frac{1}{2}})+\sigma_j^n(t^{n+\frac{1}{2}})}{2}), t^{n+\frac{1}{2}}\right)dt \ \approx \\
&\approx\ k\,h\,G\left(\Phi\left(\frac{\sigma_{j+1}^n(t^{n+\frac{1}{2}})+\sigma_j^n(t^{n+\frac{1}{2}})}{2}, t^{n+\frac{1}{2}}\right)\right) \ \approx\ k\,h\,G\left(\Phi(x_j^n + \frac{1}{2}(f_j^n k + h), t^n + \frac{k}{2})\right) \approx \\
&\approx k\,h\,G\left(\Phi(x_j,t^n) + \frac{1}{2}(f_j^n k + h)(\Phi_x)_j^n + \frac{k}{2}(G(\Phi_j^n) - f_x(\Phi)_j^n)\right).
\end{aligned} \tag{4.3.10}$$

Finally, the approximation for the source term by means of the midpoint rule gives:

$$\iint_{D_j^n} G(u(x,t))dx\,dt \approx khG\left(U_j^n + \frac{1}{2}(f_j^n k + h)(u_x)_j^n + \frac{k}{2}(G(U_j^n) - f_x(\Phi)_j^n)\right) \tag{4.3.11}$$

where $(u_x)_j^n = MM(\Delta u_{j+\frac{1}{2}}, \Delta u_{j-\frac{1}{2}})$ and $f_x(\Phi)_j^n = MM(\Delta f_{j+\frac{1}{2}}, \Delta f_{j-\frac{1}{2}})$, $MM\{x,y\} \equiv MinMod\{x,y\} = \frac{1}{2}[sgn(x) + sgn(y)] \cdot Min(|x|,|y|)$ [35].

For the scalar linear balance laws we consider the same quadrature rules to approximate the source term with $f_j^n = a$, $h_j^{n+1} = h$.

4.4 Numerical experiments for scalar balance laws

We are interested in designing well-balanced conceptually simple schemes, which have a well balanced property for static and moving equilibrium, applicable to a wide class of systems with source. One may find, in a variety of physical problems, source terms that are balanced by internal forces and this balance supports multiple steady-state solutions that are stable. The well-balance property can be formally enunciated as follows. Consider the system of balance laws as such,

$$\frac{\partial u}{\partial t} + \frac{\partial (H(u))}{\partial x} = g(u), \qquad t > 0, \qquad x \in \mathbb{R}, \tag{4.4.1}$$

we denote u^e the stationary solution, which satisfies the equation,

$$\frac{\partial (H(u^e))}{\partial x} = g(u^e), \qquad x \in \mathbb{R}. \tag{4.4.2}$$

A numerical scheme is said to be **well-balanced** (in the sense that it must exactly preserve physically relevant steady states), if it fully satisfies a discrete version of the equilibrium equation (4.4.2). If a method is not well-balanced, the truncation error of solutions near of equilibrium state may be larger than $u(x,t) - u^e(x)$ [35].

Here, numerical approximations with grid refinement are presented and discussed for scalar balance laws in order to show the well-balance of the Lagrangian-Eulerian scheme in the sense that the method captures the correct steady states entropy-solution and to give evidence of the convergence of the scheme.

Example 4.4.1. Langseth, Tveito, and Winther (SINUM)

In [27], we consider the problem

$$u_t + (f(u))_x = g(u), \tag{4.4.3}$$

with initial condition

$$u(x,0) = \begin{cases} 0.1 + 0.1\text{sen}(2\pi x), & 0 \leq x \leq 1, \\ 0.1, & \text{Otherwise}, \end{cases} \tag{4.4.4}$$

where the flux function is $f(u) = \frac{1}{2}u^2$ and the source term is $g(u) = u(1-u)$.

In Figure 42 it is shown numerical approximations of the problem (4.4.3) - (4.4.4) by means of the Lagrangian-Eulerian scheme for balance laws 4.1.5 - 4.1.6 (LgBL or LEB1) along the midpoint rule (see Section 4.3.2) for approximating the source term at time t=1.5 [35]. In the case of no availability of an analytic solution (see [27]), an approximation to the expected "exact solution" is computed using a very fine mesh (2048 cells) numerical solution as the reference solution (solid line in Figure 42), for comparison purpose with numerical approximations with 128 cells (top), 256 cells (middle) and 512 cells (bottom). Such solutions are in a very good agreement with that reported in [27], where the initial data give rise into a shock. But due to the balance between flux function and source term, the left and right state of the shock will increase and asymptotically reach the steady-state equilibrium $u = 1$. Comparing the computed solution with the Lagrangian-Eulerian scheme for balance laws (4.3.2) and that one reported in [27], it is found that our solution is quite accurate and capturing all qualitative details, even in a coarse grid (left picture in Figure 42). The Lagrangian-Eulerian scheme seems to be well-balanced in the sense that the method captured the correct steady states entropy-solution as reported in [27].

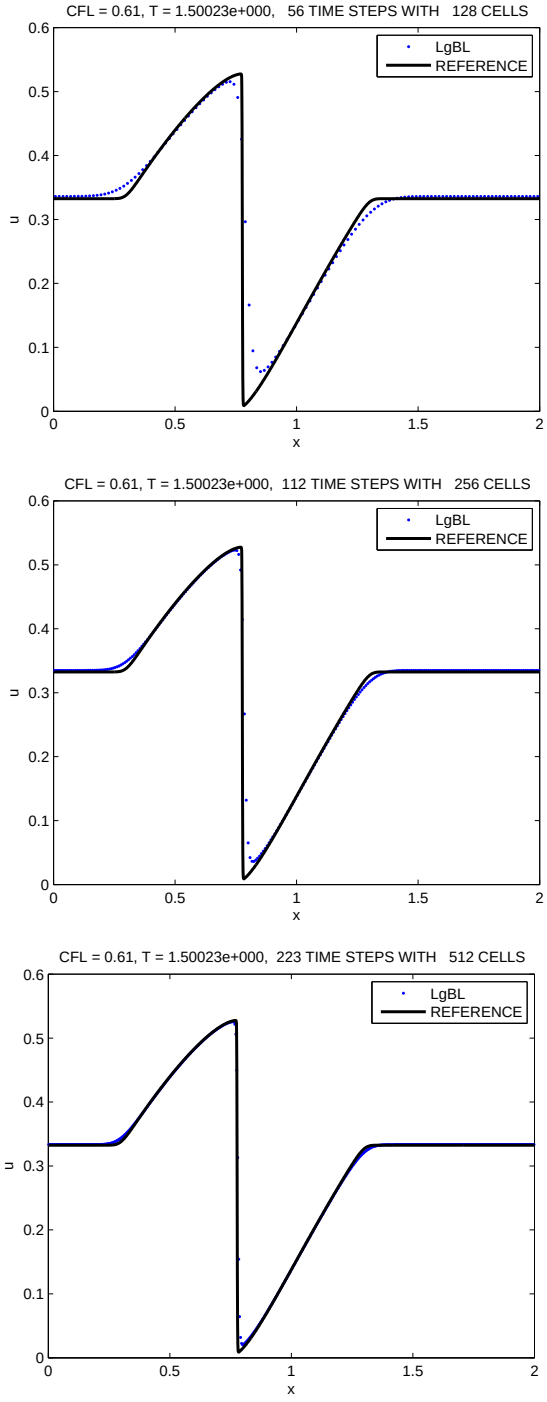

Figure 42 – Approximated solutions with a smooth source function with multiple equilibria at time T=1.5 and CFL condition equals 0.61. The computational time is 30 seconds.

Example 4.4.2. A Puzzling Numerical Example

Consider the balance law problem

$$\begin{cases} u_t + f(u)_x = k(x)g(u), & 0 < k \in L^1_{loc} \cap C^0(\mathbb{R}), \\ u_0(x) = Y(x), & x \in \mathbb{R}, \end{cases} \tag{4.4.5}$$

where $f(u) = \dfrac{u^2}{2}$, $k(x) = 0.2$, $g(u) = u$ and Y the Heaviside function.

The main goal of this example is, as in [19], to emphasize the qualitative difference between time-splitting, (or fractional step methods) and well-balanced numerical schemes when it comes to computing the entropy solution of a simple scalar, yet non-resonant, balance law (4.4.5), f is genuinely non-linear, which means that it is strictly convex in u and $g \in C^1(\mathbb{R})$, see [19] for more details. This results in the classical "one-half" order of convergence in L^1, which is known to be optimal for Godunov type [36, 42], denoting the entropy solution u and its numerical approximation by $u^{\Delta t}$; see [42] that states: $\forall t \in [0, T]$, $\|u^{\Delta t}(t, .) - u(t, .)\|_{L^1}(\mathbb{R}) \leq C\sqrt{\Delta t}$. The analysis discussed in [43] reveals that the "constant C" is actually an exponential in time, which results in the more rigorous statement: $\forall t \in [0, T]$, $\|u^{\Delta t}(t, .) - u(t, .)\|_{L^1}(\mathbb{R}) \leq C\exp(\max[g'(u)]t)\sqrt{\Delta t}$. This estimate is disastrous from a computational standpoint, because in order to keep the absolute error below a given tolerance, the computational grid's parameters are meant to decrease exponentially with time (except if $g' \leq 0$, for which $TV(u)(t, .)$ decays exponentially too). Figure 43 shows numerical approximations with 128, 256 and 512 cells with the Lagrangian-Eulerian scheme for balance law (4.1.5)-(4.1.6) (LgBL1 or LEB1) along with the Predictor-corrector method (see Section 4.3.1) for approximating the source term at time $t = 10$ [35]. And an approximation to the expected "exact solution" is computed using a very fine mesh (2048 cells) as the reference solution (solid line in Figure 43), for comparison purpose with numerical approximations with 128 cells, 256 cells and 512 cells. As expected, the method converges with refinement.

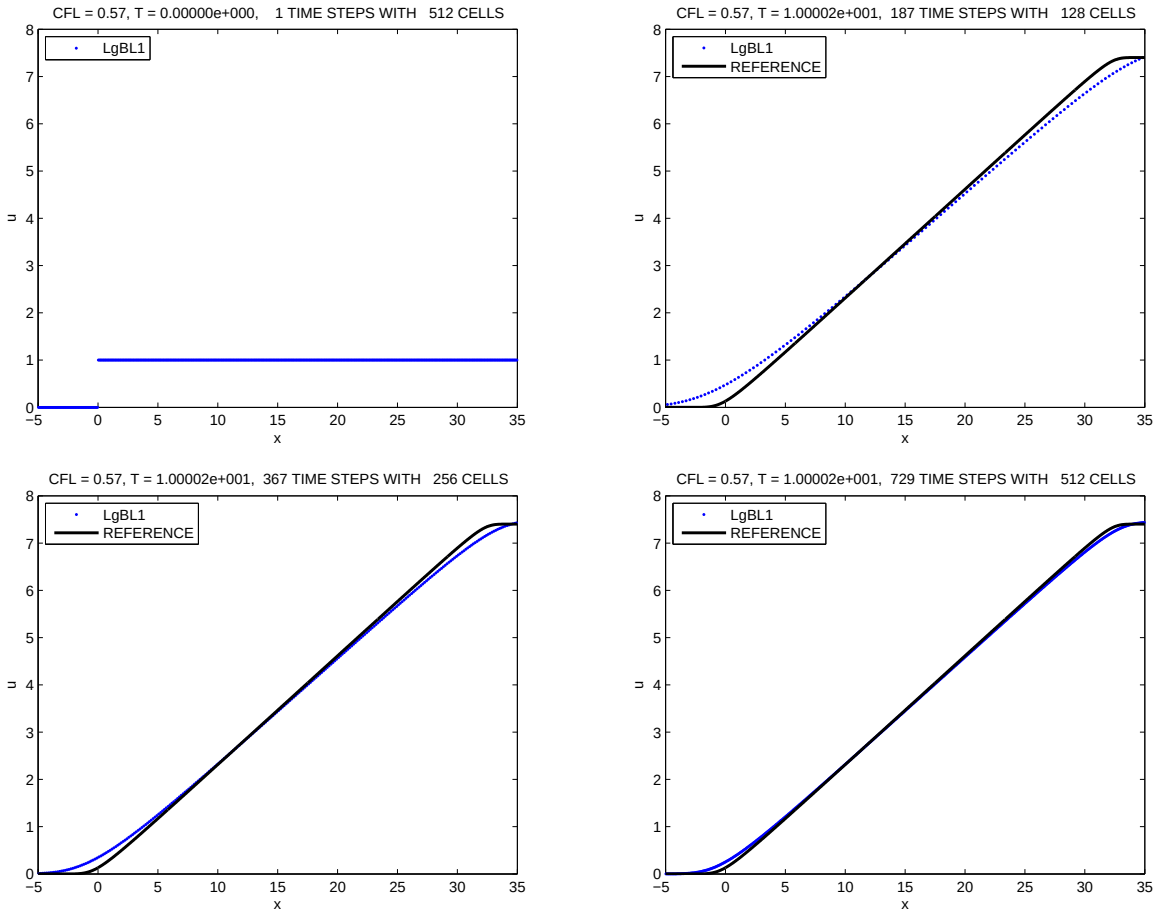

Figure 43 – Numerical approximations for the scalar balance laws. The solution is shown first at time T=0 with 512 cells, and with 128, 256, 512 cells with time T=10 from top to the bottom and CFL condition equals 0.57. The computational time is 1 minute.

5 The Lagrangian-Eulerian scheme for systems of hyperbolic conservation laws and balance laws

In this Chapter, we study how to extend the scalar Lagrangian-Eulerian procedure to the one-dimensional system of balance laws $u_t + f_x(u) = g(u)$, where now $u(x,t)$ can be viewed as the unknown $n-$vector of the form $u = (u^1(x,t), u^2(x,t), \cdots, u^n(x,t))^\top$, and $f(u)$ is the flux vector function such that $f(u) = (f^1(u), f^2(u), \cdots, f^n(u))^\top$. Essentially, the analogue Lagrangian-Eulerian scheme for system of balance laws retain all the simplicities of the one single equation case, which in turn is carried out by a straightforward componentwise application of the scalar framework. Thus, for simplicity of presentation, let us consider the following prototype 2×2 system of balance laws (see Section 2.4) and present numerical experiments for systems of hyperbolic conservation laws and balance laws such as the shallow water equations and the immiscible three-phase flow.

5.1 Systems of balance laws

Consider the system of balance laws

$$u_t + [f(u)]_x = g(u), \tag{5.1.1}$$

where $f(u) = [f^1(u), f^2(u)]$, $u = [u^1, u^2]$, $u^1 = u^1(x,t)$, and $u^2 = u^2(x,t)$, with $g(u) = [g^1(u), g^2(u)]$. System (5.1.1) can be written in open form as,

$$\begin{cases} u^1_t + [f^1(u^1, u^2)]_x = g^1(u^1, u^2), \\ u^2_t + [f^2(u^1, u^2)]_x = g^2(u^1, u^2), \end{cases} \tag{5.1.2}$$

As before, we consider the space-time control finite volumes for each variable u^1, u^2 as follows,

$$\begin{cases} D^n_{u^1,j} = \{(t,x) \ / \ t^n \le t \le t^{n+1}, \quad \sigma^n_{u^1,j}(t) \le x \le \sigma^n_{u^1,j+1}(t)\}, \\ D^n_{u^2,j} = \{(t,x) \ / \ t^n \le t \le t^{n+1}, \quad \sigma^n_{u^2,j}(t) \le x \le \sigma^n_{u^2,j+1}(t)\}, \end{cases} \tag{5.1.3}$$

where $\sigma^n_{u^1,j}(t)$ and $\sigma^n_{u^2,j}(t)$ are parametrized curves such that $\sigma^n_{u^1,j}(t^n) = x^n_j$ and $\sigma^n_{u^2,j}(t^n) = x^n_j$. These curves $\sigma^n_{u^1,j}(t)$ and $\sigma^n_{u^2,j}(t)$, define the "lateral boundaries" of integral tubes for each primitive variable u^1, u^2, which in turn will be used to desgin a balancing *unbiased* upwinding Riemann-solver-free discretization between the numerical flux functions and the source terms by

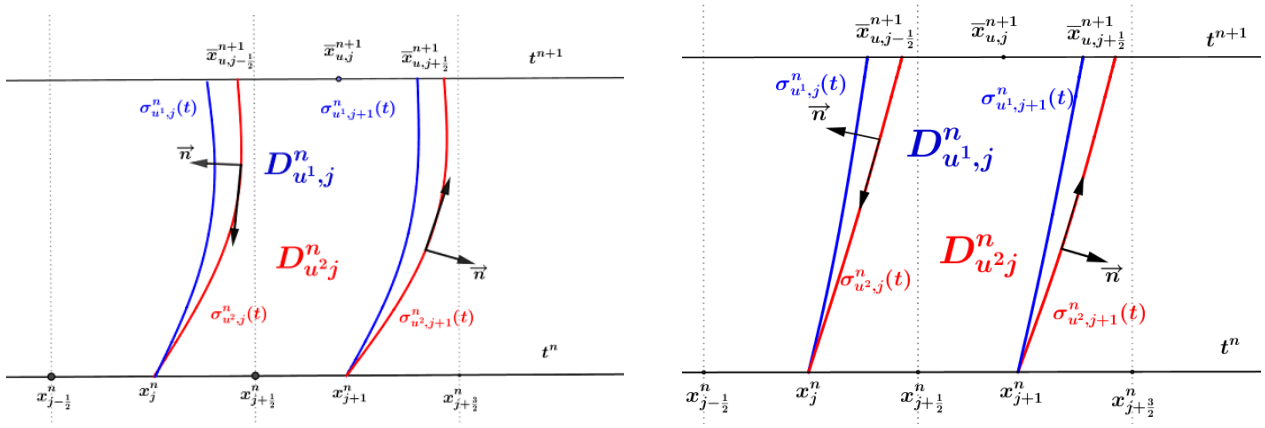

Figure 44 – On the left (resp. right) is shown an illustration of the continuous (resp. discrete) local space-time domain $D^n_{s,j}$, for each $s = u^1, u^2$.

forward tracking the boundaries along the so-called integral tubes (see left picutre in the Figure 44). Formally, the divergence theorem can be used in the (5.1.3), the space-time finite volumes $D^n_{u^1,j}$ $D^n_{u^2,j}$. By construction of the algorithm, as before, this implies that curves $\sigma^n_{s,j}(t)$ and $\sigma^n_{s,j+1}(t)$, for $s = u^1, u^2$ are naturally zero-flux boundaries. Similarly, from this fact the space-time $D^n_{s,j}$, $s = u^1, u^2$ are then called as "Integral tubes" for $t^n \leq t \leq t^{n+1}$. As a consequence we get $\left[1, \dfrac{d\sigma^n_{s,j}(t)}{dt}\right] \perp n_s$ and $\left[1, \dfrac{d\sigma^n_{s,j+1}(t)}{dt}\right] \perp n_s$ since the slopes $\dfrac{d\sigma^n_{s,j}(t)}{dt}$ are one-to-one equal to the slope of the vector $[s, f^\alpha(u)]$, $s = u^1, u^2$; $\alpha = 1, 2$, respectively, over the parametrized curves $\sigma^n_{s,j}(t)$ and $\sigma^n_{s,j+1}(t)$, $s = u^1, u^2$, $j \in \mathbb{Z}$. Therefore $\sigma^n_{s,j}(t)$, $s = u^1, u^2$ are solutions of the set of ODEs,

$$\frac{d\sigma^n_{u^1,j}(t)}{dt} = \frac{f^1(u^1, u^2)}{u^1}, \quad \sigma^n_{u^1,j}(t^n) = x^n_j, \quad t^n < t \leq t^{n+1}, \tag{5.1.4}$$

$$\frac{d\sigma^n_{u^2,j}(t)}{dt} = \frac{f^2(u^1, u^2)}{u^2}, \quad \sigma^n_{u^2,j}(t^n) = x^n_j, \quad t^n < t \leq t^{n+1}, \tag{5.1.5}$$

where $\lim\limits_{u^1 \to 0} \dfrac{f^1(u^1, u^2)}{u^1}$ and $\lim\limits_{u^2 \to 0} \dfrac{f^2(u^1, u^2)}{u^2}$ are well defined. As a consequence of the divergence theorem and the above equations (5.1.3)-(5.1.5), the integrals over curves $\sigma^n_{s,j}(t)$, $s = u^1, u^2$ vanish and the line integral over the boundary of the region $\partial D^n_{s,j}$ leads to,

$$\int_{\overline{x}^{n+1}_{j-\frac{1}{2}}}^{\overline{x}^{n+1}_{j+\frac{1}{2}}} u^1(x, t^{n+1})dx = \int_{x^n_j}^{x^n_{j+1}} u^1(x, t^n)dx + \iint_{D^n_{u^1,j}} g^1(u^1, u^2)dt\,dx, \tag{5.1.6}$$

$$\int_{\overline{x}^{n+1}_{j-\frac{1}{2}}}^{\overline{x}^{n+1}_{j+\frac{1}{2}}} u^2(x, t^{n+1})dx = \int_{x^n_j}^{x^n_{j+1}} u^2(x, t^n)dx + \iint_{D^n_{u^2,j}} g^2(u^1, u^2)dt\,dx, \tag{5.1.7}$$

we can define as before $\overline{x}^{n+1}_{s,j-\frac{1}{2}} = \sigma^n_{s,j}(t^{n+1})$ and $\overline{x}^{n+1}_{s,j+\frac{1}{2}} = \sigma^n_{s,j+1}(t^{n+1})$ for $s = u^1, u^2$. Equations (5.1.6)-(5.1.7) are called "locally conservative relation" to the system of balance laws

(5.1.2). Thus, the approximations of the variables u^1, u^2 for system are a rather component-wise extension of the scalar framework given by,

$$\begin{aligned} U_j^{1,n} &= \frac{1}{h}\int_{x_{j-\frac{1}{2}}^n}^{x_{j+\frac{1}{2}}^n} u^1(x,t^n)\,dx, \quad \text{and} \quad \overline{U}_j^{1,n+1} = \frac{1}{h_{u^1,j}^{n+1}}\int_{\overline{x}_{j-\frac{1}{2}}^{n+1}}^{\overline{x}_{j+\frac{1}{2}}^{n+1}} u^1(x,t^{n+1})\,dx \quad j\in\mathbb{Z}, \\ U_j^{2,n} &= \frac{1}{h}\int_{x_{j-\frac{1}{2}}^n}^{x_{j+\frac{1}{2}}^n} u^2(x,t^n)\,dx, \quad \text{and} \quad \overline{U}_j^{2,n+1} = \frac{1}{h_{u^2,j}^{n+1}}\int_{\overline{x}_{j-\frac{1}{2}}^{n+1}}^{\overline{x}_{j+\frac{1}{2}}^{n+1}} u^2(x,t^{n+1})\,dx \quad j\in\mathbb{Z}, \end{aligned} \tag{5.1.8}$$

respectively, and the initial condition is $U^1(x_j^0,t^0) = U_j^{1,0}$ and $U^2(x_j^0,t^0) = U_j^{2,0}$ over the local space-time cells $[x_{j-\frac{1}{2}}^0, x_{j+\frac{1}{2}}^0]$, $j\in\mathbb{Z}$. Next, we use (5.1.8) into the "locally conservative relation" to get,

$$\overline{S}_j^{n+1} = \frac{1}{h_{s,j}^{n+1}}\int_{\overline{x}_{j-\frac{1}{2}}^{n+1}}^{\overline{x}_{j+\frac{1}{2}}^{n+1}} s(x,t^{n+1})\,dx = \frac{1}{h_{s,j}^{n+1}}\left[\int_{x_j^n}^{x_{j+1}^n} s(x,t^n)\,dx. + \iint_{D_{s,j}^n} g^\alpha(u^1,u^2)\;dx\,dt\right]. \tag{5.1.9}$$

In (5.1.9) $S = U^1, U^2$ and $s = u^1, u^2$ denotes a representation of a component-wise extension of the scalar case to systems of balance law in compact form (5.1.1). Next, the local approximations $\overline{S}_j^{n+1}$, $j\in\mathbb{Z}$ are projected over the original grid and reads,

$$S_j^{n+1} = \frac{1}{h}\left[c_{s,0j}\overline{S}_{j-1}^{n+1} + c_{s,1j}\overline{S}_j^{n+1}\right]. \tag{5.1.10}$$

Here $c_{s,0j} = (\frac{h}{2} + f_{s,j}^n k^n)$, $c_{s,1j} = h - c_{s,0j} = (\frac{h}{2} - f_{s,j}^n k^n)$ and we use the approximations

$$\begin{aligned} f_{u^1,j}^n &\equiv \frac{f^1(U_j^{1,n}, U_j^{2,n})}{U_j^{1,n}} \approx \frac{f^1(u^1,u^2)}{u^1}, \\ f_{u^2,j}^n &\equiv \frac{f^2(U_j^{1,n}, U_j^{2,n})}{U_j^{2,n}} \approx \frac{f^2(u^1,u^2)}{u^2}. \end{aligned}$$

Notice that now the curve $\sigma_{s,j}^n(t)$ is a simple straight line for $f_{s,j}^n$ (see right picture in Figure 44), along with $k^n = \Delta t^n = t^{n+1} - t^n$. Finally, combination of equations (5.1.9) and (5.1.10) form the building-block for the Lagrangian-Eulerian scheme. Thus, for each discrete variable $S = U^1, U^2$ and for $s = u^1, u^2$ we define $\mathbb{W}_s(S_j^n, S_{j+1}^n) \equiv \dfrac{f_{s,j}^n + f_{s,j+1}^n}{h_{s,j}^{n+1}}(S_j^n + S_{j+1}^n)$, and we get,

$$\begin{aligned} U_j^{1,n+1} =& \frac{1}{4}(U_{j-1}^{1,n} + 2U_j^{1,n} + U_{j+1}^{1,n}) - \frac{k^n}{4}\left(\mathbb{W}_{u^1}(U_j^{1,n}, U_{j+1}^{1,n}) - \mathbb{W}_{u^1}(U_{j-1}^{1,n}, U_j^{1,n})\right) \\ &+ \frac{1}{h}\left[\frac{1}{h}\left(\frac{h}{2} + f_{u^1,j}^n k\right)\iint_{D_{u^1,j-1}^n} g^1(u^1,u^2)\;dx\,dt + \frac{1}{h}\left(\frac{h}{2} - f_{u^1,j}^n k\right)\iint_{D_{u^1,j}^n} g^1(u^1,u^2)\;dx\,dt\right], \end{aligned} \tag{5.1.11}$$

$$U_j^{2,n+1} = \frac{1}{4}(U_{j-1}^{2,n} + 2U_j^{2,n} + U_{j+1}^{2,n}) - \frac{k^n}{4}\left(\mathbb{W}_{u^2}(U_j^{2,n}, U_{j+1}^{2,n}) - \mathbb{W}_{u^2}(U_{j-1}^{2,n}, U_j^{2,n})\right)$$
$$+\frac{1}{h}\left[\frac{1}{h}\left(\frac{h}{2} + f_{u^2,j}^{2,n}k\right)\iint_{D^n_{u^2,j-1}} g^2(u^1,u^2)\,dx\,dt + \frac{1}{h}\left(\frac{h}{2} - f_{u^2,j}^{n}k\right)\iint_{D^n_{u^2,j}} g^2(u^1,u^2)\,dx\,dt\right], \tag{5.1.12}$$

along the CFL condition $\max_j\{f_{u^1,j}^n, f_{u^2,j}^n\}(k/h) \leq \sqrt{(2)}/2$ and with initials conditions $U_j^{1,0} = u^1(x_j^0, 0)$, $U_j^{2,0} = u^2(x_j^0, 0)$.

The extension of the Lagrangian-Eulerian scheme finite difference (4.3.2) to system of hyperbolic balance law can be write as

$$U_j^{1,n+1} = \frac{1}{4}(U_{j-1}^{1,n} + 2U_j^{1,n} + U_{j+1}^{1,n}) - \frac{k}{2h}\left[f^1(U_{j+1}^{1,n}, U_{j+1}^{2,n}) - f^1(U_{j-1}^{1,n}, U_{j-1}^{2,n})\right]$$
$$+\frac{1}{h}\left[\frac{1}{h}\left(\frac{h}{2} + f_{u^1,j}^{n}k\right)\iint_{D^n_{u^1,j-1}} g1(u^1,u^2)\,dx\,dt + \frac{1}{h}\left(\frac{h}{2} - f_{u^1,j}^{n}k\right)\iint_{D^n_{u^1,j}} g^1(u^1,u^2)\,dx\,dt\right], \tag{5.1.13}$$

$$U_j^{2,n+1} = \frac{1}{4}(U_{j-1}^{2,n} + 2U_j^{2,n} + U_{j+1}^{2,n}) - \frac{k}{2h}\left[f^2(U_{j+1}^{1,n}, U_{j+1}^{2,n}) - f^2(U_{j-1}^{1,n}, U_{j-1}^{2,n})\right]$$
$$+\frac{1}{h}\left[\frac{1}{h}\left(\frac{h}{2} + f_{u^2,j}^{n}k\right)\iint_{D^n_{u^2,j-1}} g^2(u^1,u^2)\,dx\,dt + \frac{1}{h}\left(\frac{h}{2} - f_{u^2,j}^{n}k\right)\iint_{D^n_{u^2,j}} g^2(u^1,u^2)\,dx\,dt\right], \tag{5.1.14}$$

along the CFL condition $\max_j\{\|F'(U_j^{1,n}, U_j^{2,n})\|_2, f_{u^1,j}^n, f_{u^2,j}^n, \}(k/h) \leq \sqrt{2}/2$, where F is the vector function $f = [f^1, f^2]$. Note that the CFL condition to the Lagragian-Eulerian scheme (5.1.13), (5.1.14) is a extension of the scalar case (4.3.2), in which is considered the eigenvalues of jacobian matrix of f [35].

5.2 Numerical experiments

In this section we perform numerical tests using the Lagrangian-Eulerian method with mesh refinement for systems of hyperbolic conservation laws (see, Section 2.4) – the purely hyperbolic shallow water equations and the immiscible three-phase flow in porous media – in order to give some numerical evidence of the convergence of the Lagrangian-Eulerian scheme. For the purely hyperbolic shallow water equations, the numerical solutions for the height, the

velocity and height versus velocity are presented at various times with mesh refinement. For the immiscible three-phase flow problem, we present the numerical solution for water saturation, gas saturation and oil saturation of two Riemann problems with mesh refinement. Then, we present numerical approximations of the well known system of balance laws modeling the shallow-water problem and present three test cases (transcritical flow without shock, transcritical flow with shock, and subcritical flow) with numerical and analytical solutions for water height (h) and discharge (M) with three level of refinement. Then, we also present the reproductions of test cases for the modified system for shallow water equations-small perturbation of steady flow over a slanted surface. For shallow water equations, the numerical solution is shown for the height, the velocity and height versus velocity, and for the modified system for shallow water equations we present the evolution of the numerical solution in the supercritical case, the subcritical case and with large bottom slope.

5.2.1 Hyperbolic system of conservation laws

If we set the source term of the system (5.1.1) equal to zero ($g(u) \equiv 0$), we get the prototype for systems of hyperbolic conservation laws in the form $u_t + [f(u)]_x = 0$, keeping in mind that the meaning of the variable must be understood in the new framework. From (5.1.9)-(5.1.10) or (5.1.11)-(5.1.12), we can see that the Lagrangian-Eulerian scheme can be used for systems of conservation laws.

Example 5.2.1. The shallow water equations:

It is well-known that solutions of hyperbolic conservation laws can develop shock discontinuities in a finite time, independent of whether the initial data is smooth or not (as we consider here). Hence, the solutions of hyperbolic conservation laws, must be viewed in the weak sense.

In [1, 27], it was considered a 2×2 nonlinear system of balance laws in the form of (in dimensionless and scaled variables),

$$\begin{bmatrix} h \\ hv \end{bmatrix}_t + \begin{bmatrix} hv \\ v^2h + \frac{1}{2}h^2 \end{bmatrix}_x = \begin{bmatrix} 0 \\ h - C\frac{1+h}{\mathrm{tg}\theta}v^2 \end{bmatrix}, \tag{5.2.1}$$

where h is the height of the free surface and v is the averaged horizontal velocity, modeling the flow of water downing in a channel having a rectangular cross section and inclined at a constant angle θ to the horizontal. This is a prototype model for shallow-water flow in an inclined channel with friction. Precisely, as in [27], the friction coefficient C is taken to be 0.1, while the inclination angle $\theta = \frac{\pi}{6}$. In our current implementation, we will consider first the equation of hyperbolic system (5.2.1), then the balance laws system (5.2.1) with the initial velocity $v_0 =$

1.699, while the initial height of the free surface consists of a triangular perturbation of the uniform flow level, $h_0(x) = x + 1.5$, $-0.5 \leq x \leq 0$, $h_0(x) = -x + 1.5$, $0 \leq x \leq 0.5$, and 1 elsewhere [1].

In Figures 45, 46, 47, 48 are shown numerical approximations by means of the scheme (5.1.9)-(5.1.10) with zero source term along the initial value problem described just above, and computed solutions for v, (the averaged horizontal velocity) h, the height and hv with initial times $t = 0$, $t = 0.5$, $t = 1.0$ and $t = 1.5$, from top to bottom. The purely hyperbolic shallow water solutions (with 512, 256, 128, 64 grid cells) were compute with the scheme introduced in this work in Section 3.3 . As expected from the analysis in [27], we have two waves moving in opposite directions. For the purely hyperbolic shallow water solutions, we are able to capture this correct qualitative behavior with a very good accuracy [1]. The model (5.2.1) correspond to uniform flow (v_0=constant and h_0=constant) with the frictional and gravitational forces in perfect balance. In order to study the balance between convective/source in the model (5.2.1), it is considered as initial conditions a perturbation of an uniform flow, in which the gravitational and frictional forces balance as expected from the model problem.

In Figure 49 numerical approximations are shown by means of the Lagrangian-Eulerian scheme (5.1.9)-(5.1.10) for the initial value problem described above and computed solutions for v, (the averaged horizontal velocity) h, (the height) and hv with 128, 256 and 512 cells from top to bottom at time $t = 1.5$. As in [27] with no friction ($C = 0$), two symmetrical waves will arise from the initial data. On the other hand, the introduction of friction not only downs the velocity of these waves, but also changes the shape. For instance, if $C = 0.1$ is considered, one can still observe two waves, but the symmetry is now lost. The numerical solutions are in a very good agreement to that reported in [1, 27], corresponding to the balance between the frictional and gravitational forces at time evolves. The approximation of the source terms in this example of system of balance laws was performed by means of the predictor-corrector method [35].

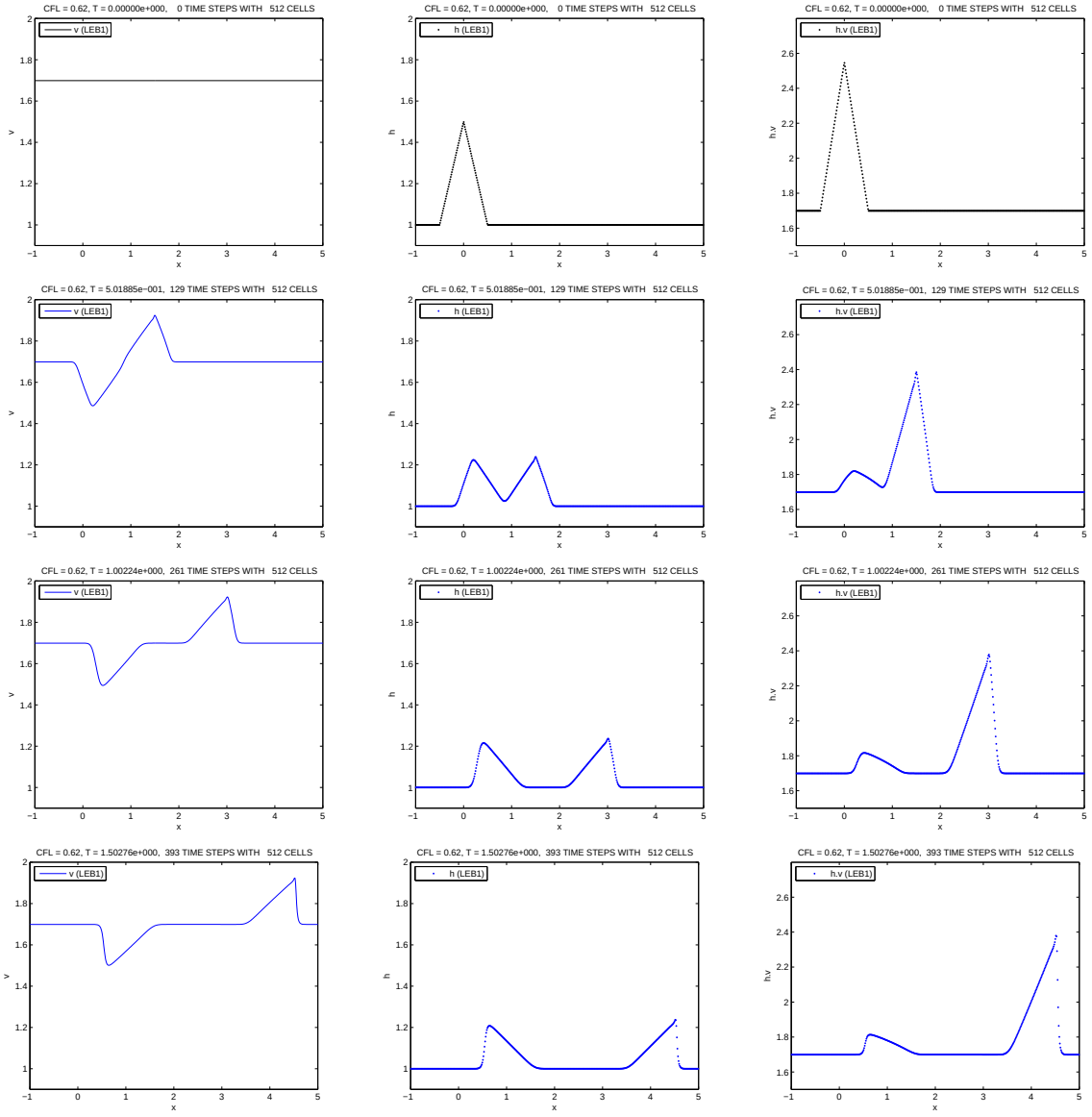

Figure 45 – Numerical approximations to the shallow water equations (2.4.17) . The numerical solutions to the height topography, the velocity and height versus velocity are shown from top to bottom at simulation times $T = 0$, $T = 0.5$, $T = 1.0$ and $T = 1.5$ with 512 mesh grid cells, CFL condition equals 0.62 and one minute as computational time.

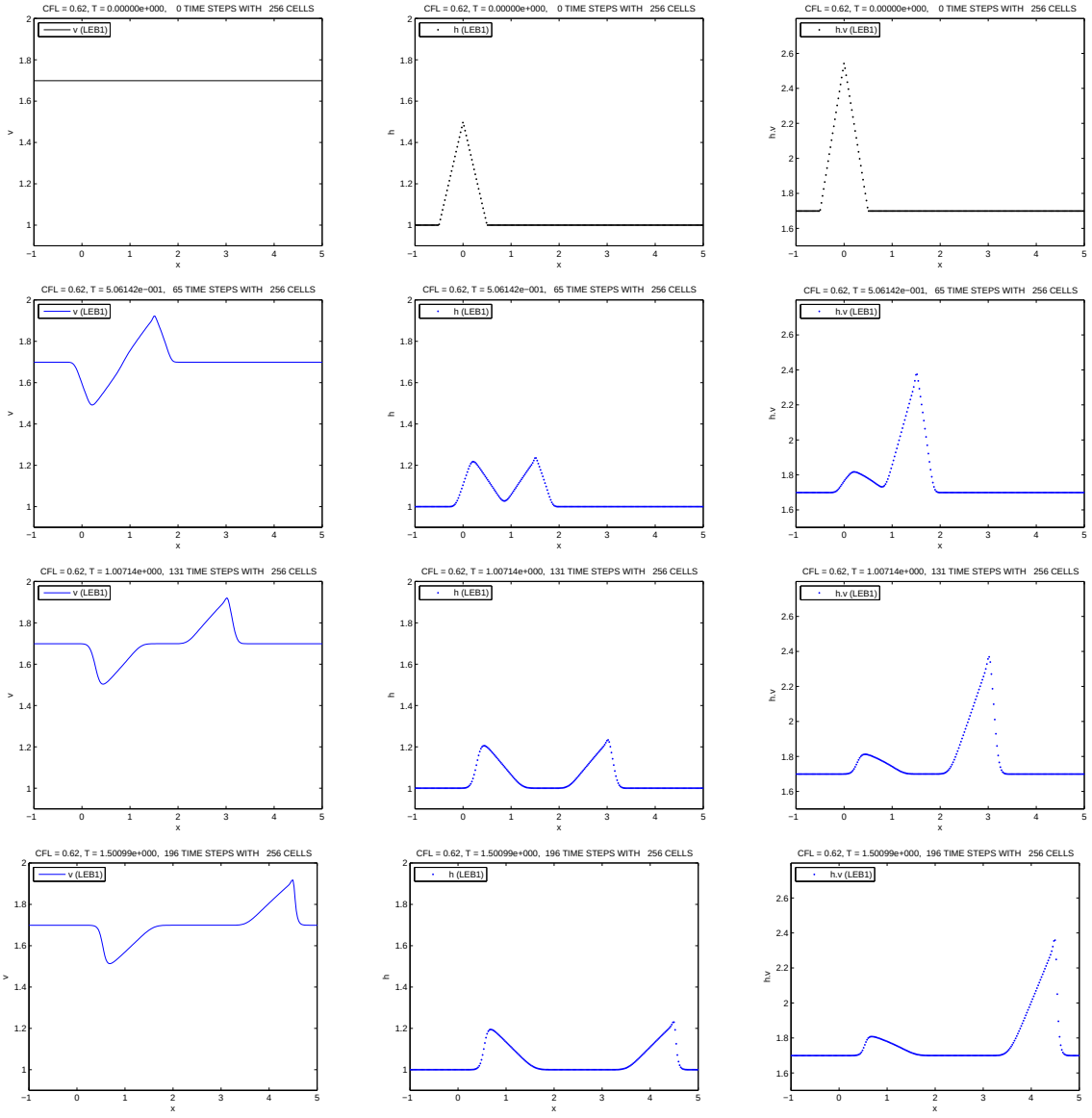

Figure 46 – Numerical approximations to the shallow water equations (2.4.17) . The numerical solutions to the height topography, the velocity and height versus velocity are shown from top to bottom at simulation times $T = 0$, $T = 0.5$, $T = 1.0$ and $T = 1.5$ with 256 mesh grid cells, CFL condition equals 0.62 and one minute as computational time

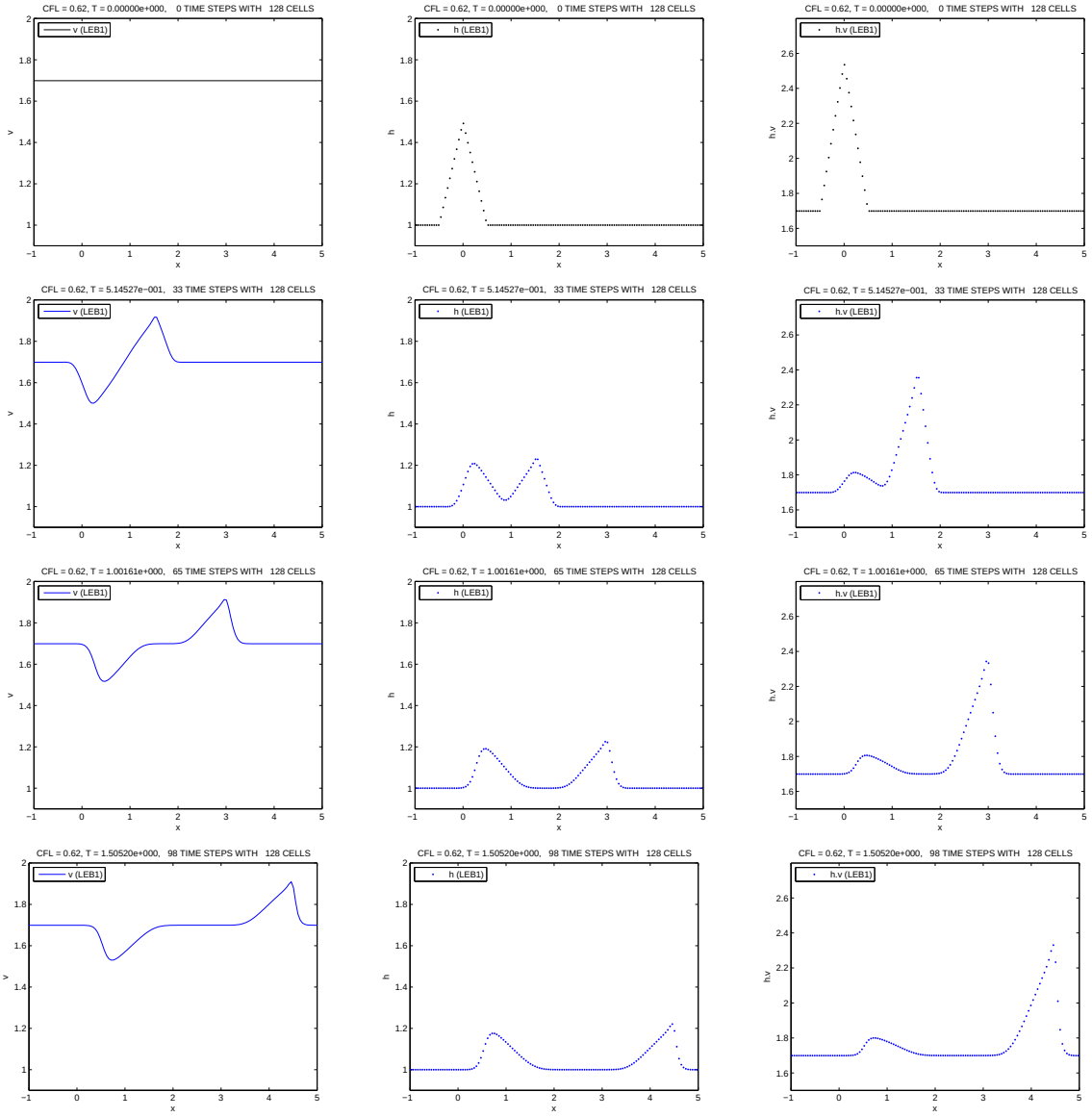

Figure 47 – Numerical approximations to the shallow water equations (2.4.17) . The numerical solutions to the height topography, the velocity and height versus velocity are shown from top to bottom at simulation times $T = 0$, $T = 0.5$, $T = 1.0$ and $T = 1.5$ with 128 mesh grid cells, CFL condition equals 0.62 and one minute as computational time.

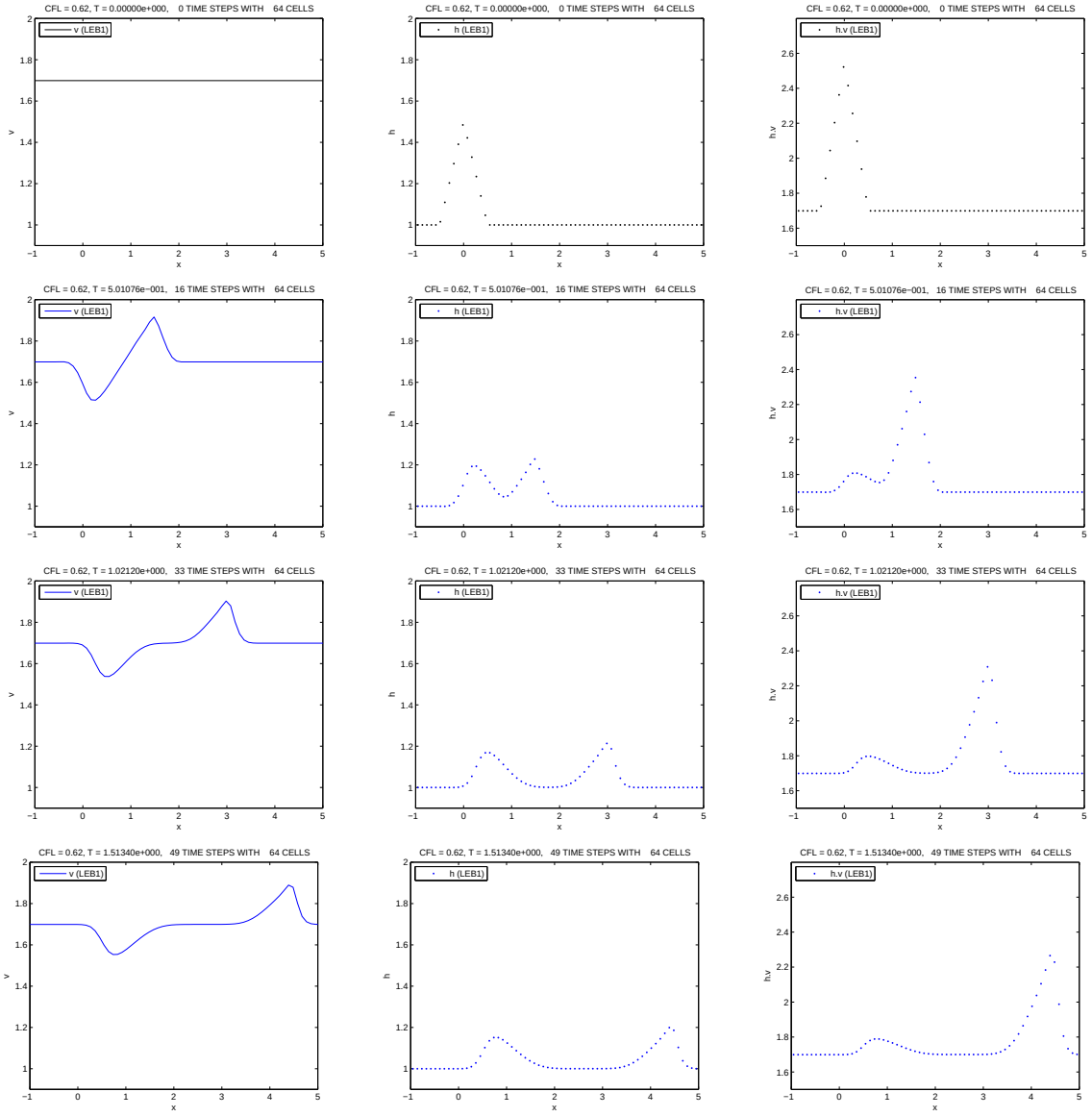

Figure 48 – Numerical approximations to the shallow water equations (2.4.17) . The numerical solutions to the height topography, the velocity and height versus velocity are shown from top to bottom at simulation times $T = 0$, $T = 0.5$, $T = 1.0$ and $T = 1.5$ with 64 mesh grid cells, CFL condition equals 0.62 and one minute as computational time.

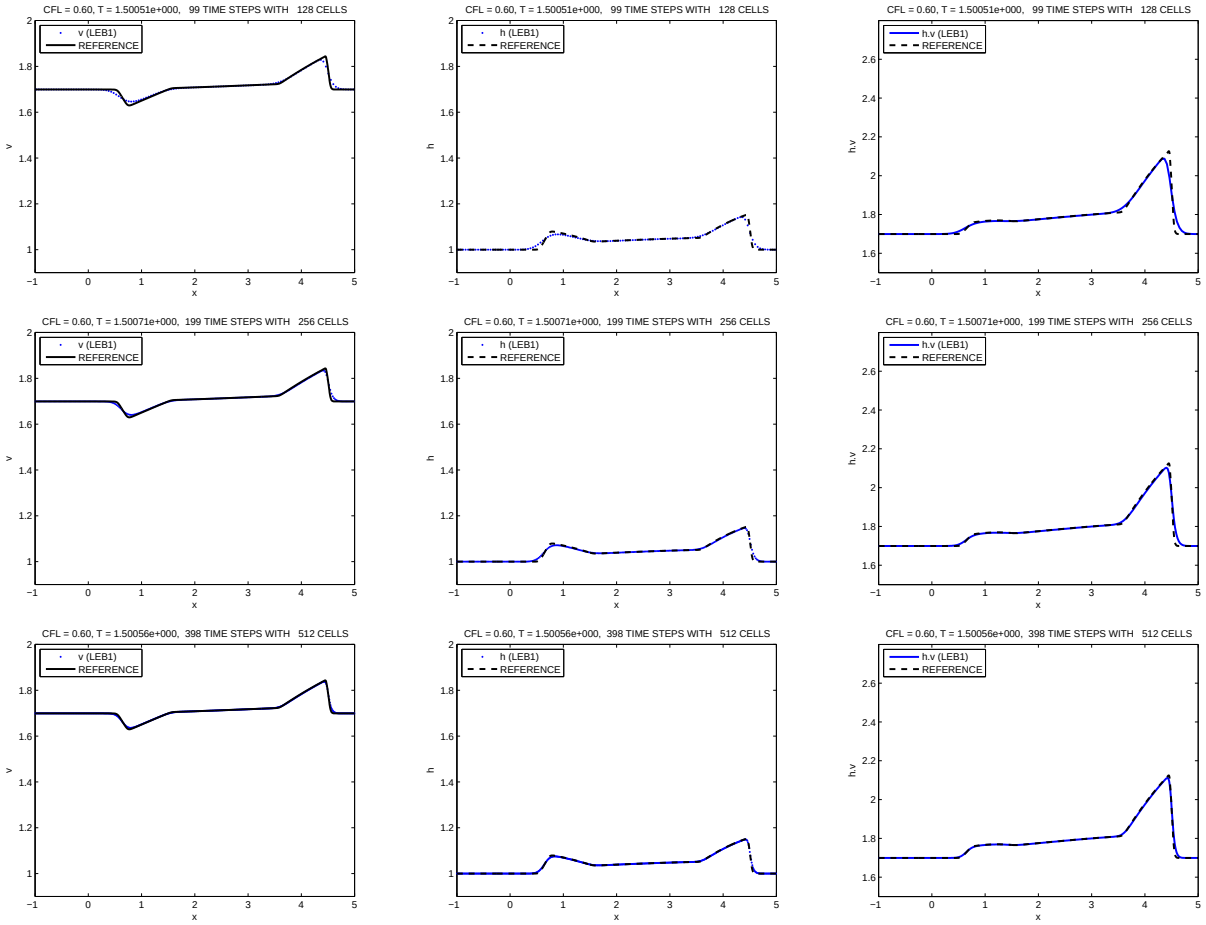

Figure 49 – Numerical approximations to the shallow water equations (5.2.1). The numerical solutions to the height topography, the velocity and height versus velocity are shown from top to bottom at simulation time $T = 1.5$ with 128, 256 and 512 mesh grid cells with computational times, 2 minutes, 4 minutes, 9 minutes respectively. In each frame we compare numerical solutions obtained on grids having 128, 256 and 512 cells against a reference numerical solution of 2048 cells.

Example 5.2.2. Immiscible three-phase flow:

We present the result of numerical solution of the non-strictly hyperbolic three-phase system of conservation laws in porous media applications (2.4.26)-(2.4.32) by means of the scheme (5.1.9)-(5.1.10) with zero source term, for two Riemann problems, namely RP1 and RP2, given by:

$$RP1 = \begin{cases} s_w^L = 0.613 & \text{and} \quad s_w^R = 0.05, \\ s_g^L = 0.387 & \text{and} \quad s_g^R = 0.15, \end{cases} \tag{5.2.2}$$

and

$$RP2 = \begin{cases} s_w^L = 0.721 & \text{and} \quad s_w^R = 0.05, \\ s_g^L = 0.279 & \text{and} \quad s_g^R = 0.15, \end{cases} \tag{5.2.3}$$

for each variable. We use the quadratic model by Corey-Pope [1], which has been used extensively for phase relative permeabilities,

$$k_w = s_w^2, \quad k_o = s_o^2 \quad \text{and} \quad k_g = s_g^2. \tag{5.2.4}$$

We consider the following viscosity values $\mu_o = 1.0$, $\mu_w = 0.5$, and $\mu_g = 0.3$ [1]. From the analysis discussed in [31], we remark that for the choice of parameters described above, a transitional shock wave is present in the solution of (5.2.3), which in turn is not present in the solution of (5.2.2). Since the oil phase saturation can be directly obtained from the other two phase saturations (i.e., $s_o = 1 - s_w - s_g$), we display the water saturation, the gas saturation and the oil saturation profile in Figures 50, 51 and 52 respectively, showing the effect of a grid refinement in the numerical solution of (2.4.26)-(2.4.27) with $D_w = 0$ and $D_g = 0$ - with Riemann data (5.2.2) on the left and (5.2.3) on the right and we take the CFL condition $\max\{\|\partial(f_w, f_g)/\partial(s_w, s_g)\|_2, f_{w,j}^n, f_{g,j}^n, \}(k/h) \leq \sqrt{2}/2$ in the the saturation triangle [31, 35].

In the studied model, has been chosen for convenience, the saturations of water and gas. The diffusive term is represented by the righthand side of the system (2.4.26)-(2.4.27) and it incorporates the capillary pressure effects. We neglect the diffusive effect, by just taking $D_w = 0$ and $D_g = 0$ in (2.4.26)-(2.4.32). We point out that for a wave to be truly defined as a "shock wave", a discontinuity must be the zero-diffusion limit of traveling wave solutions. For such solutions, diffusion balances the convergence of waves caused by hyperbolic nonlinearity. Moreover, the set of non-classical wave solutions obtained in the zero-diffusion (zero-capillarity) limit might depends sensitively on the form of the diffusion matrix and not only on the hyperbolic structure of the equations [1]. In each frame we compare numerical solutions obtained on grids having 32, 64, 128 and 256 cells against a reference numerical solution of 2048 cells. It is clear from the pictures in Figures 50, 51, and 52, that as the grid is refined we have some good evidence of numerical convergence of the scheme. We remark that the numerical solutions pre-

sented here are in very good agreement with the semi-analytic results reported in [31], yielding a numerical verification of our computations [1].

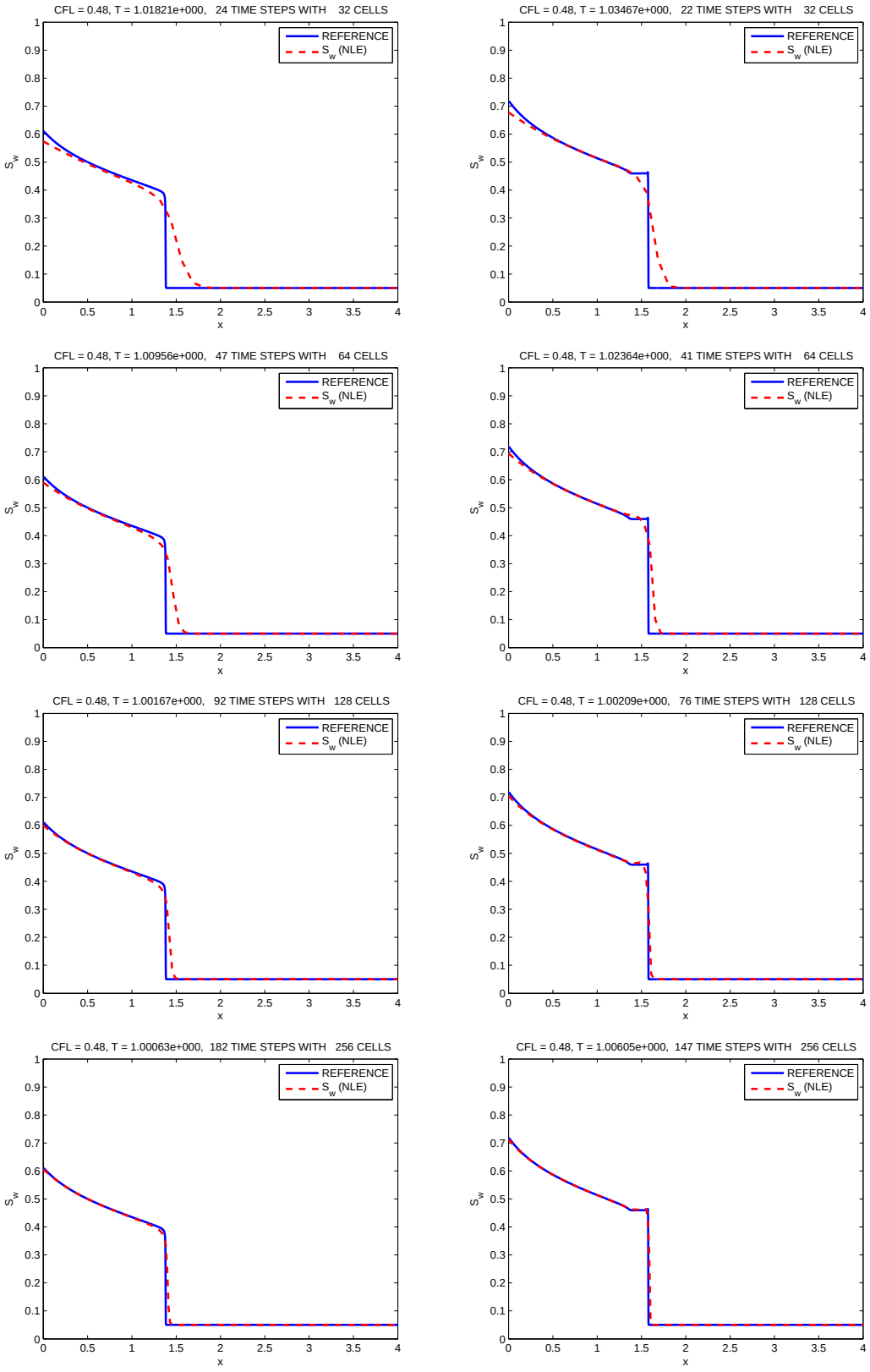

Figure 50 – Grid refinement study. Water saturation profiles are shown as a function of distance. RP1 on the left and RP2 on the right. We compare numerical solutions obtained on grids having 32, 64, 128 and 256 cells against a reference numerical solution of 2048 cells at time T=1, CFL condition equals 0.48 and with computational times equal 5 minutes for RP1 Riemann problem and 4 minutes for RP2 Riemann problem.

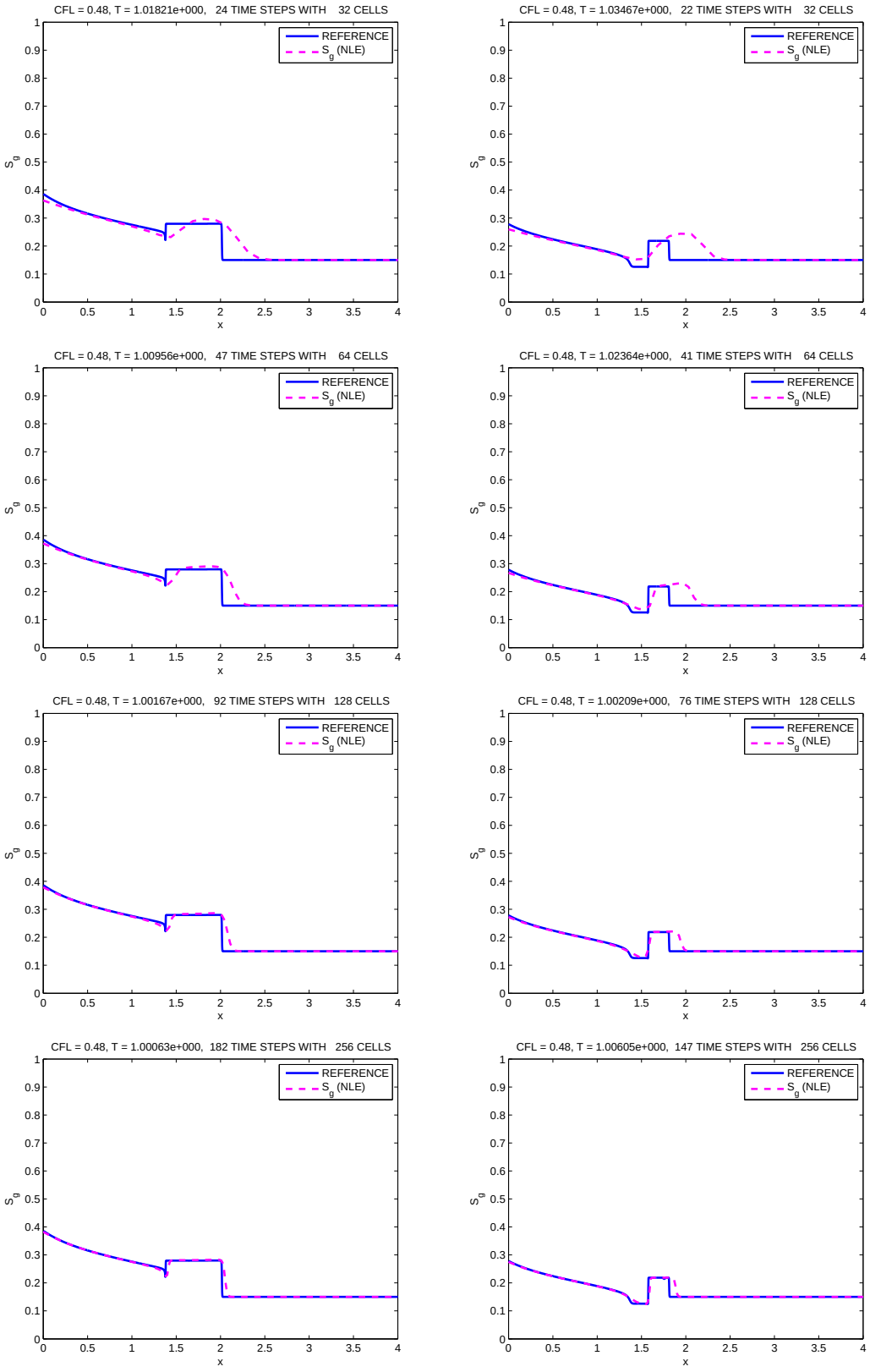

Figure 51 – Grid refinement study. Gas saturation profiles are shown as a function of distance. RP1 on the left and RP2 on the right. We compare numerical solutions obtained on grids having 32, 64, 128 and 256 cells against a reference numerical solution of 2048 cells at time T=1,CFL condition equals 0.48 and with computational times equal 5 minutes for RP1 Riemann problem and 4 minutes for RP2 Riemann problem.

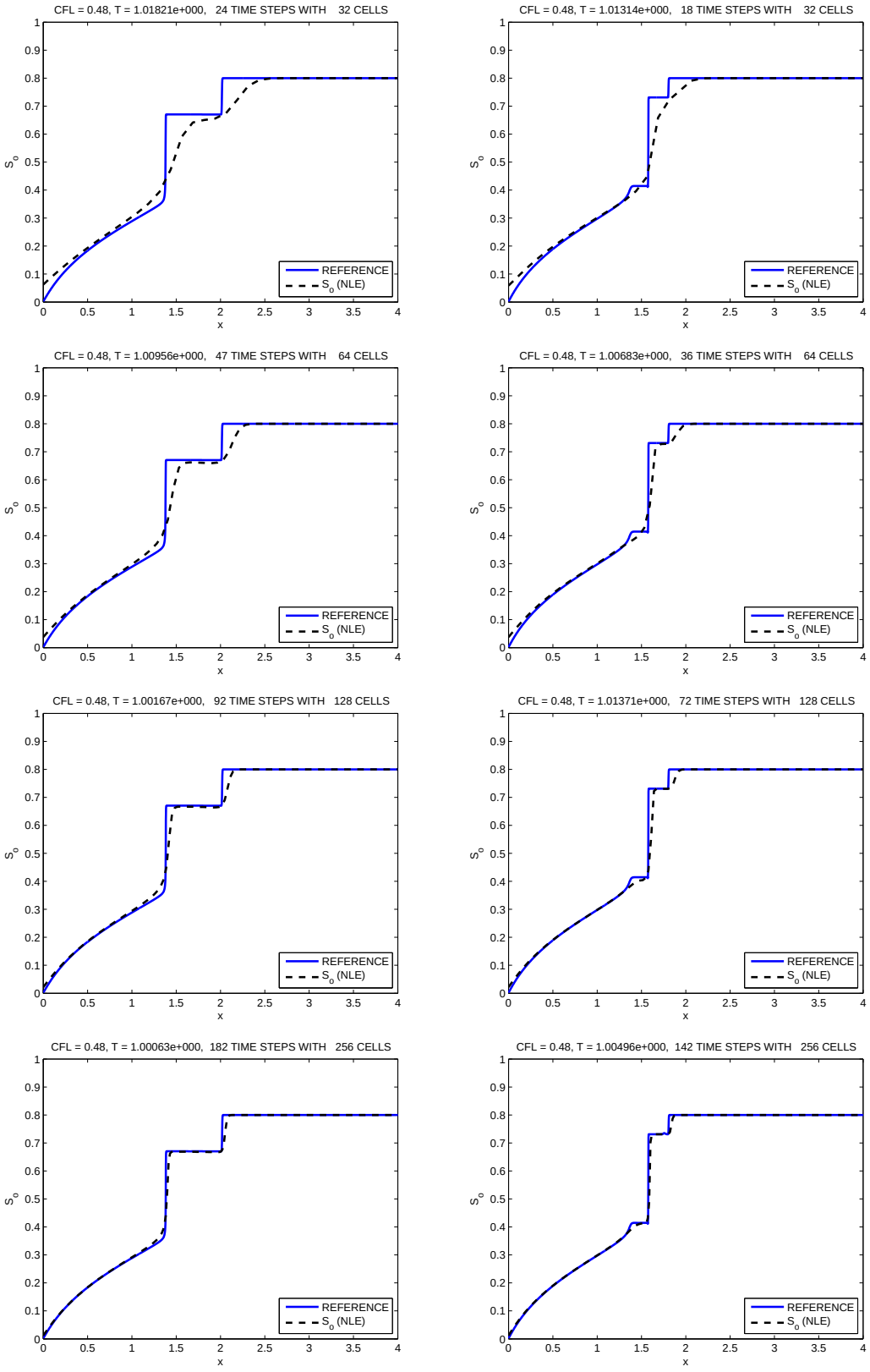

Figure 52 – Grid refinement study. Oil saturation profiles are shown as a function of distance. RP1 on the left and RP2 on the right. We compare numerical solutions obtained on grids having 32, 64, 128 and 256 cells against a reference numerical solution of 2048 cells at time T=1, CFL condition equals 0.48 and with computational times equal 5 minutes for RP1 Riemann problem and 4 minutes for RP2 Riemann problem.

Example 5.2.3. The shallow water problem

During the last decades there has been an enormous amount of activity related to approximate solutions for the shallow water equation written in conservative form as

$$\begin{cases} \dfrac{\partial h}{\partial t} + \dfrac{\partial (hv)}{\partial x} = 0, \\ \dfrac{\partial (hv)}{\partial t} + \dfrac{\partial \left(hv^2 + \frac{g}{2}h^2\right)}{\partial x} = -ghZ_x. \end{cases} \tag{5.2.5}$$

where $Z(x)$ is the function characterizing the bottom topography, $h(t,x)$ is the height of the water above the bottom, g is the acceleration due to gravity and $v(t,x)$ is the flow velocity. Computing their numerical solutions is not trivial due to nonlinearity, the presence of the convective term and the coupling of the equations through the source term. It is well known that the solutions of (5.2.5) present steep fronts and even shock discontinuities, which need to be resolved accurately in applications and often cause severe numerical difficulties. Balance laws often admit steady state solutions in which the source term is exactly balanced by the flux gradients. Such cases, along with their perturbations, are very difficult to capture numerically. A straightforward treatment of the source terms will fail to preserve this balance (4.4.2) (see, [10, 16, 40]). For this purpose we rewrite (5.2.5) as

$$\begin{cases} \dfrac{\partial h}{\partial t} + \dfrac{\partial (hv)}{\partial x} = 0, \\ \dfrac{\partial (hv)}{\partial t} + \dfrac{\partial (hv^2)}{\partial x} = -\dfrac{\partial}{\partial x}\left(\dfrac{g}{2}h^2\right) - gh\dfrac{\partial Z}{\partial x}. \end{cases} \tag{5.2.6}$$

Applying the Lagrangian-Eulerian method to each equation, we get

$$\begin{cases} \displaystyle\int_{D^n_{h,j}} \left(\frac{\partial h}{\partial t} + \frac{\partial (hv)}{\partial x}\right) dA = 0, \\ \displaystyle\int_{D^n_{m,j}} \left(\frac{\partial (hv)}{\partial t} + \frac{\partial (hv^2)}{\partial x}\right) dA = -g \int_{D^n_{m,j}} h \left(\frac{\partial h}{\partial x} + \frac{\partial Z}{\partial x}\right) dA. \end{cases} \tag{5.2.7}$$

The integrals on the left side in (5.2.7) is discussed in [2]. We will focus on how to approximate the integral on the right side. We have

$$I^n_{m,j} = \int_{D^n_{m,j}} h \left(\frac{\partial h}{\partial x} + \frac{\partial Z}{\partial x}\right) dA = \int_{t^{n+1}}^{t^n} \int_{\sigma^n_j(t)}^{\sigma^n_{j+1}(t)} h \frac{\partial (h+Z)}{\partial x}\, dx\, dt. \tag{5.2.8}$$

Therefore from (5.2.8) we get,

$$I^n_{m,j} \approx H^n_j \int_{t^{n+1}}^{t^n} \left[h(\sigma^n_{j+1}(t),t) + Z(\sigma^n_{j+1}(t)) - (h(\sigma^n_j(t),t) + Z(\sigma^n_j(t)))\right]. \tag{5.2.9}$$

The last integral can be approximated using Taylor series expansion of order one, where we use a slope limiter to approximate the derivatives $(H_x)_j$ and $(Z_x)_j$, and the trapezoidal rule for the integral in time [2]. The final approximation gives

$$I^n_{m,j} \approx H^n_j(H^n_{j+1}+Z_{j+1}-(H^n_j+Z_j))+0.5H^n_j(\Delta t)^2(f^n_{h,j+1}(H_x)^n_{j+1}+f^n_{h,j}(Z_x)_{j+1}-(f^n_{h,j}(H_x)^n_j-f^n_{h,j+1}(Z_x)_{j+1})). \tag{5.2.10}$$

The topography is flat with a bump for $x \in [8, 12]$, as follows: $Z(x) = 0.2 - 0.05(x - 10)^2$.

Transcritical flow without shock: This test case is performed according to the initial and boundary conditions given by [16, 40]. The initial water height is $0.33\,m$. A unit discharge of $1.53\,m^2/s$ is imposed at the upstream boundary, and open boundary conditions $(dh/dx = 0, dv/dx = 0)$ are applied at the downstream side. The numerical solutions for water height and discharge can be seen in Figure 53 after the steady state has been reached (which happens at time 41.5 sec). We show in Figure 53 the numerically evaluated water height and discharge with the corresponding analytical solutions, with three levels of refinement (200, 600 and 1000 mesh points). At the end of the bump a constant level is again reached. Discharge shows an underestimation near the bump, reduced on refinement [2, 16, 40].

Transcritical flow with shock: The initial water height is also 0.33 m. A unit discharge of $0.18\,m^2/s$ is imposed on the upstream boundary and a depth of $0.33\,m$ is imposed on the downstream boundary. The steady state here is reached at 175.5 sec. We show in Figure 54 the analytical and numerical solution for water surface profile and discharge, with three levels of refinement (200, 600 and 1000 mesh points). A local peak in numerical solution for discharge is observed on the jump after the bump [2, 16, 40].

Subcritical flow over a bump without a shock: A unit discharge of $4.42\,m^2/s$ is imposed on the upstream boundary and a depth of $2.0\,m$ is imposed on the downstream boundary. The steady state is reached at time 85.5 sec. Figure 55 shows the solutions for this case after reaching the steady state, with three levels of refinement (200, 600 and 1000 mesh points).

For all the three cases, the Lagrangian-Eulerian scheme produced qualitatively correct results compared to analytical solutions with 200 mesh grid cells.

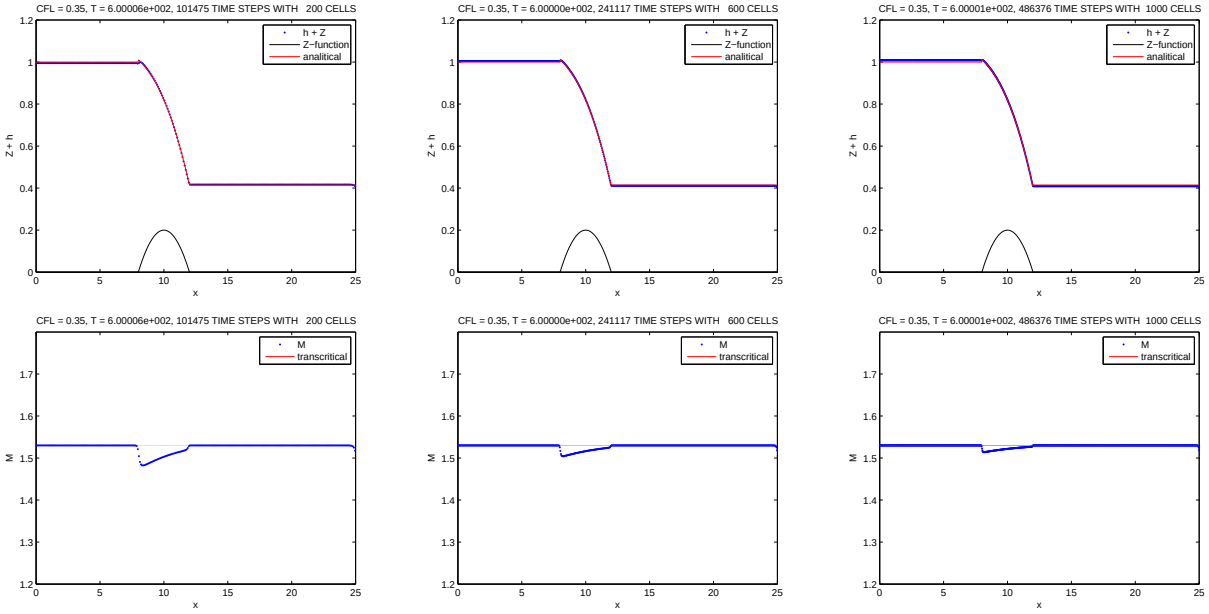

Figure 53 – Transcritical flow without shock test case: Numerical and analytic solutions for water height (h) and discharge (M) with three level of refinement. Top: Numerical solution of $h + Z$ with 200, 600 and 1000 mesh grid points at time T=600 sec. Bottom: discharge M with 200, 600 and 1000 mesh grid points.

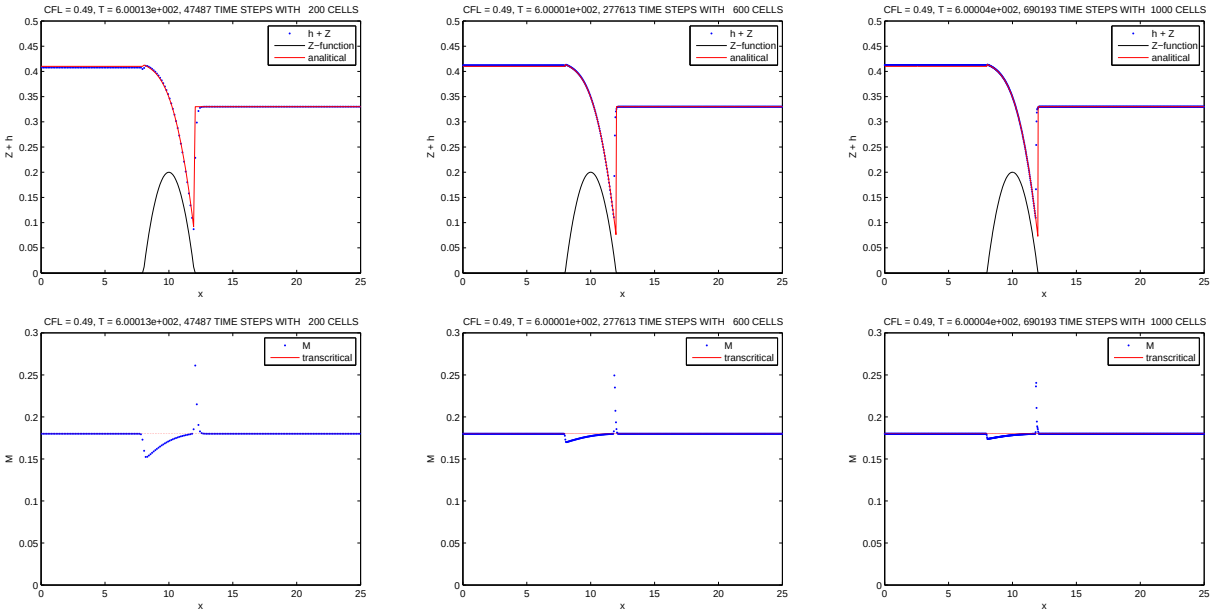

Figure 54 – Transcritical flow with shock: Numerical and analytic solutions for water height (h) and discharge (M) with three level of refinement. The steady-state has been already reached (exhibited time is T= 600 sec). Top: $h + Z$ solutions with 200, 600 and 1000 mesh grid points. Bottom: discharge M with 200, 600 and 1000 mesh grid points.

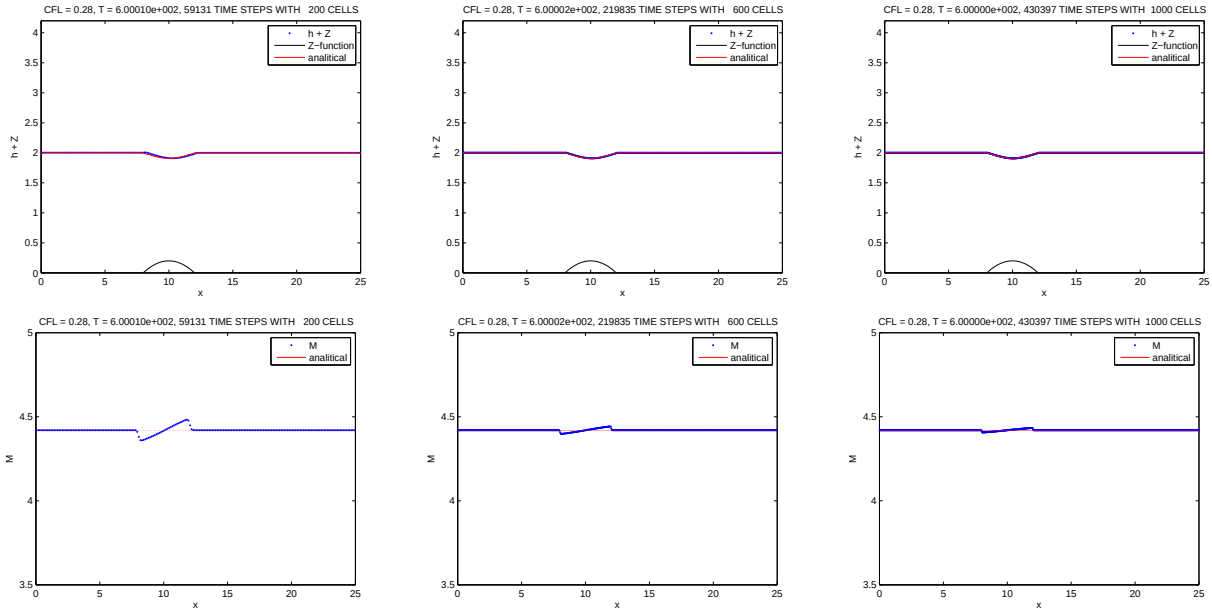

Figure 55 – Subcritical test case: Numerical and analytic solutions for water height (h) and discharge (M) with three level of refinement. The steady-state has been already reached (exhibited time is $T = 600$ sec). Top: $h + Z$ solutions with 200, 600 and 1000 mesh grid points. Bottom: discharge M with 200, 600 and 1000 mesh grid points.

Example 5.2.4. The modified system for shallow water equations

Here we consider the modified system for shallow water equations (5.2.11) presented in [12] with water source term $R(x,t)$ and a bottom friction term with the classical Manning formulation and the reproductions of test cases presented in the cited paper– small perturbation of steady flow over a slanted surface. In these test cases we will consider $R(x,t)$ identically zero. As in (5.2.1), we use the same approximation for the source term. In one spatial dimension the equation is reduced to:

$$\begin{cases} \dfrac{\partial h}{\partial t} + \dfrac{\partial (hv)}{\partial x} = R(x,t), \\ \dfrac{\partial (hv)}{\partial t} + \dfrac{\partial \left(hv^2 + \frac{g}{2}h^2\right)}{\partial x} = -ghZ_x - g\dfrac{n^2}{h^{\frac{1}{3}}} v\,|v|\,, \end{cases} \tag{5.2.11}$$

with the initial data

$$h(x,0) = h_0 + \begin{cases} 0.2h_0, & 1 \le x \le 1.25 \\ 0, & \text{otherwise} \end{cases}, \qquad q(x,0) = q_0. \tag{5.2.12}$$

The first test is a supercritical case (top), with $h_0 = 0.09564$, $q_0 = 0.1$, $n = 0.02$ and the (*constant*) slope of topography $Z_x = -0.01$. We show on Figure 56 (top) the initial state, a snapshot at time $t = 1.0$ sec, where the perturbation propagates to the right and the steady state at time $t = 100$ sec.

Next, the subcritical case (middle) is presented with $h_0 = 0.02402$, $q_0 = 0.002$, $n = 0.1$ and the slope of topography again as $Z_x = -0.01$. Here, the shape of the propagated solution is different from the previous case. We show on Figure 56 (middle) the initial state, a snapshot at time $t = 0.5$ sec and the steady state solution at time $t = 100$ sec.

Then, the last test case on Figure 56 (bottom) with $h_0 = 0.44894$, $q_0 = 2$ and $n = 0.1$ shows a magnitude of topography slope larger than the other cases, $Z_x = -\dfrac{1}{\sqrt{13}}$. In this case, the perturbation propagates faster than in previous tests, but the numerical steady state is achieved at large times. These tests are evaluated with 200 grid cells.

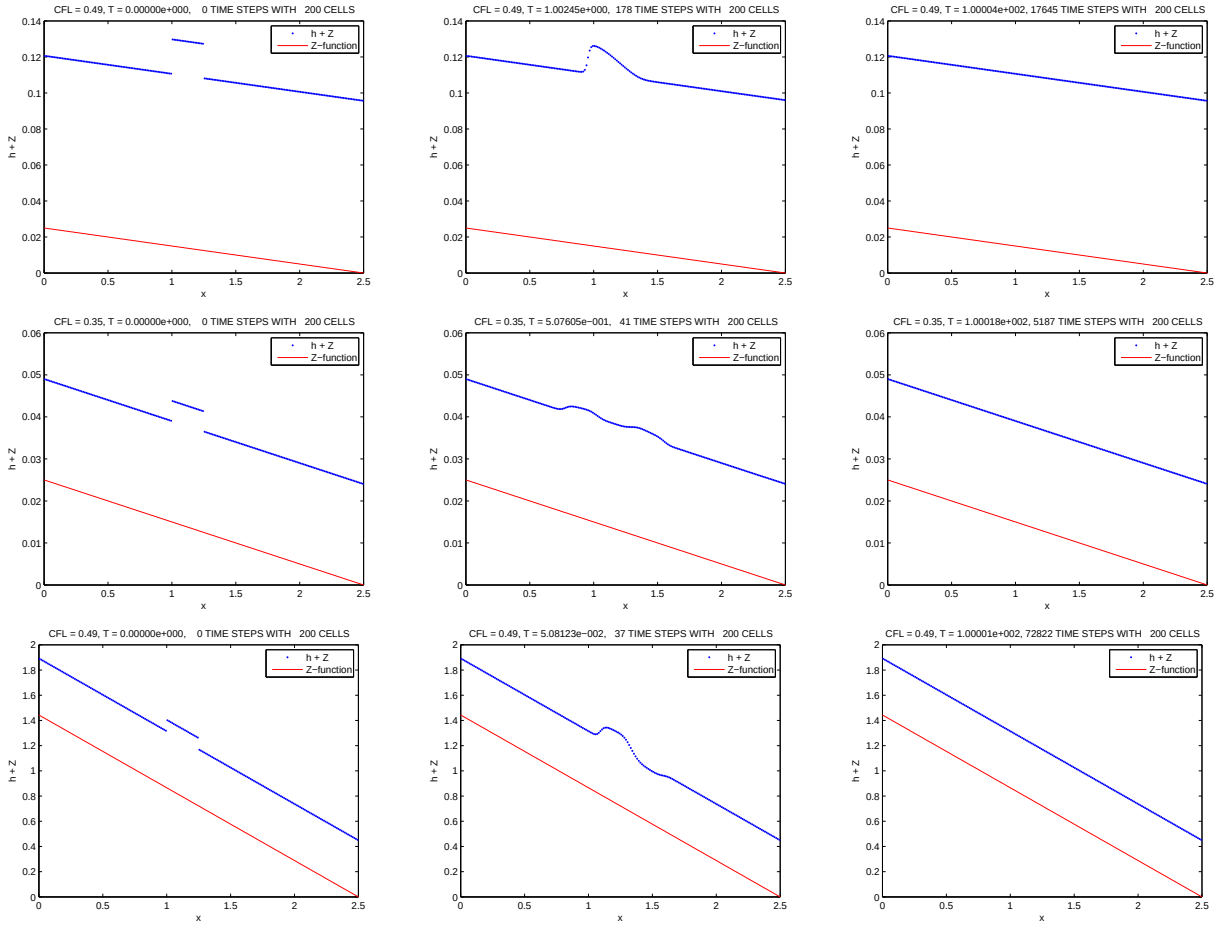

Figure 56 – **Top**: Supercritical test case at initial time (left), T= 1.0 sec (middle), and steady state at T= 100sec (right). **Middle**: Subcritical test case at initial time (left), T= 0.5 sec (middle), and steady state at t = 100 sec (right). **Bottom**: Larger slope topography test case at initial time (left), T= 0.05 sec (middle), and steady state at T= 100 sec (right).

6 Conclusion and perspectives

The aim of this dissertation is to study numerical approximations for – scalar and system – of hyperbolic conservation laws and balance laws, using a Lagrangian-Eulerian approach based on locally conservative finite volume method. Specifically, we concerned with non classical model in the state of the art, namely, a hyperbolic conservation law with nonlocal flux.

6.1 Conclusion

In this work we studied a locally conservative and divergence space-time finite control volume in a Lagrangian-Eulerian framework, first developed in the context of purely hyperbolic conservation laws, in order to design a locally conservative scheme to account the balance between numerical approximations of the hyperbolic flux function and the source term linked to steady solutions. We learned that the Lagragian-Eulerian scheme is a conservative and consistent numerical method for conservation laws. In addition, this scheme is independent on a particular form of the flux function and is aimed to be not dependent on a particular structure of the source term [1, 35].

In chapter 2, we presented some definitions of concepts studied through the study.

In Chapter 3, we discussed the construction of the Lagrangian-Eulerian scheme, and its conservative form applied for solving – linear and nonlinear – hyperbolic conservation law problems and hyperbolic conservation law problems with nonlocal flux. For the construction of this scheme, we write the conservation law in space-time in divergence form. Next we define a control volume, called integral-tube, where we impose local conservation. For this, the divergence theorem plays a role. We use the modified equation to the Lagrangian-Eulerian scheme for linear sclacar hyperbolic conservation laws to discuss the numerical nature of the scheme. Then we discussed numerical experiments of the linear and nonlinear scalar hyperbolic conservation laws, specifically the Burgers' equation and Buckley-Leverett's equation. We observe that the Lagrangian-Eulerian approach is able to capture qualitative correct solutions for linear and nonlinear scalar problems. The first experiment has a test for the linear case and study the nature of the scheme in the sense of the modified equation, there we find that according to the CFL condition that the scheme has a diffusive property (when $v < \frac{1}{2}$) or dispersive property (when $\frac{1}{2} < v < \frac{\sqrt{2}}{2}$). An accurate algorithm for the approximation of the Hilbert transform on the real line and qualitative numerical solutions to the hyperbolic conservation laws with nonlocal flux, were presented and discussed with distinct initial measure data such

as Gaussian measure initial data and Oscillatory initial data. Based on the qualitative numerical experiments, we conclude that the studied Lagrangian-Eulerian scheme is able to compute qualitatively correct approximations by showing strong evidence of blow-up of concentration type with mass-preserving of the initial data with respect to the hyperbolic conservation law with nonlocal flux. As we reproduce numerical experiments of [11, 17], it seems that for some initial data the nonlocal tansport model problem can be better interpreted as $u_t = -(\mathbb{H}(u)u)_x$. In this case the term $-(\mathbb{H}(u)u)_x$ is decreased with large grandient and the solution is faster as the height of the initial data decreased and numerical experiments show that we have evidence of attenuation for any $R > 0$ with an insignificant diffusion effect as we refine the grid. Otherwise when analysing the case $u_t = (\mathbb{H}(u)u)_x$, the term $(\mathbb{H}(u)u)_x$ increased with a large gradient. In this case, numerical results show that we have evidence of blow up of concentration type for any $R > 0$ with mass-preserving as time evolves. Then we can speculate that for the problem $u_t - (\mathbb{H}(u)u)_x = 0$ the mass R serves as a trigger for the concentration effect and the mass-preserving. Otherwise for the problem $u_t + (\mathbb{H}(u)u)_x = 0$ the mass R stops the trigger which leads to an evidence of a diffusion attenuation effect. These results are quite distinct from those reported in Juan's thesis [17]. In this relevant work are presented fairly robust numerical evidences that the term viscous provides a limear $R_l > R > 0$ for the blow-up mechanism trigger.

In Chapter 4, we used the same framework for numerically approximate the linear and nonlinear scalar problems for balance laws. For balance law, we need to integrate the source term on the integral-tube defined by the associated conservation laws. Then we presented and discussed numerical approximations with grid refinement for scalar balance laws in order to show the well-balancing of the Lagrangian-Eulerian scheme in the sense that the method captured the correct steady states entropy-solution and to give evidence of the convergence of the scheme.

In Chapter 5, we used the Lagrangian-Eulerian framework for systems of hyperbolic conservation laws and balance laws, and we presented and discussed numerical experiments of hyperbolic conservation law and balance law problems, specifically the shallow water equations, the immiscible three-phase flow problem with mesh refinement. All numerical experiments were performed with the most simple first order version of the Lagrangian-Eulerian scheme, and comparison is made between the numerical results and accurate approximate solutions or exact solutions whenever possible. We observe that the studied Lagrangian-Eulerian approach is able to capture qualitative correct solutions for linear and nonlinear problems as well as for systems in one-dimensional space.

6.2 Perspectives

Based on the good results reported in numerical experiments, we expect to apply the Lagrangian-Eulerian scheme to the non conservative Baer-Nunziato model [13]. The isentropic Baer-Nunziato model is a two-phase flow model formulated in Eulerian coordinates where balance equations account for the evolution of mass and momentum of each phase. The velocities of each phase are denoted u_i, $i \in \{1,2\}$, while the densities are denoted by ρ_i, $i \in \{1,2\}$. Each phase has a statistical phase fraction α_i, $i \in \{1,2\}$, with the saturation constraint $\alpha_1 + \alpha_2 = 1$. The model reads:

$$\partial_t \mathbb{U} + \partial_x f(\mathbb{U}) + c(\mathbb{U})\partial_x \mathbb{U} = 0, \quad x \in \mathbb{R}, \quad t > 0,$$

with

$$\mathbb{U} = \begin{bmatrix} \alpha_1 \\ \alpha_1\rho_1 \\ \alpha_1\rho_1 u_1 \\ \alpha_2\rho_2 \\ \alpha_2\rho_2 u_2 \end{bmatrix}, \quad f(\mathbb{U}) = \begin{bmatrix} 0 \\ \alpha_1\rho_1 u_1 \\ \alpha_1\rho_1 u_1^2 + \alpha_1 p_1(\rho_1) \\ \alpha_2\rho_2 u_2 \\ \alpha_2\rho_2 u_2^2 + \alpha_2 p_2(\rho_2) \end{bmatrix}, \quad c(\mathbb{U})\partial_x \mathbb{U} = \begin{bmatrix} u_2 \\ 0 \\ -p_1(\rho_1) \\ 0 \\ +p_1(\rho_1) \end{bmatrix} \partial_x \alpha_1.$$

The state vector $\mathbb{U}$ is expected to belong to the natural physical space

$$\Omega = \left\{ \mathbb{U} \in \mathbb{R}^5, 0 < \alpha_1 < 1 \quad \text{and} \quad \alpha_i\rho_i > 0 \quad for \quad i \in \{1,2\} \right\}.$$

As an other perspective, we also intend to formulate a semidiscrete scheme by using the same Lagrangian-Eulerian framework studied in this master dissertation.

In general, based on the numerical results reported in this master's work together with the important theoretical and numerical results of Juan's thesis [17], we can conjecture the existence of a limear value for nonlocal hyperbolic flow models that preserve the mass. It is worth emphasizing that a complete and mathematically rigorous understanding of this model constitute an open problem.

Analising the approach to nonlocal flux, perhaps the hyperbolic problem with nonlocal flux supports self-similar solutions. The advantages from a theoretical standpoint are generally well understood [14]. However an other interest from a computational point of view can be very useful to save computational time. Numerical experiments provide preliminary evidence of blow-up of concentration type and attenuation, in that sense we can argue self-similarity to study The mass R for which the effect of blow-up of concentration type and attenuation effect are quickly obtained from the conclusion that we have blow-up or attenuation for any $R > 0$.

Bibliography

[1] E. Abreu, W. Lambert, J. Perez, and A. Santo. "A lagrangian-eulerian algorithm for solving hyperbolic conservation laws with applications." In: *Proceedings of the 6th International Conference on Approximation Methods and Numerical Modelling in Environment and Natural Resources (MAMERN VI)* (2015), pp. 599–617.

[2] E. Abreu, W. Lambert, J. Perez, and A. Santo. "A new finite volume approach for transport models and related applications with balancing source terms". In: *Mathematics and Computers in Simulation* 137 (2017), pp. 2–28.

[3] D. Amadori, S. Y. Ha, and J. Park. "On the global well-posedness of BV weak solutions to the Kuramoto–Sakaguchi equation". In: *Journal of Differential Equations* (2016).

[4] D. Amadori and W. Shen. "An integro-differential conservation law arising in a model of granular flow". In: *Journal of Hyperbolic Differential Equations* 9.01 (2012), pp. 105–131.

[5] N. Andrianov and G. Warnecke. "The Riemann problem for the Baer–Nunziato two-phase flow model". In: *Journal of Computational Physics* 195.2 (2004), pp. 434–464.

[6] J. Aquino, A. S. Francisco, F. Pereira, T. J. Pereira, and H. A. Souto. "A Lagrangian strategy for the numerical simulation of radionuclide transport problems". In: *Progress in Nuclear Energy* 52.3 (2010), pp. 282–291.

[7] J. Aquino, A. S. Francisco, F. Pereira, and H. A. Souto. "An overview of Eulerian–Lagrangian schemes applied to radionuclide transport in unsaturated porous media". In: *Progress in Nuclear Energy* 50.7 (2008), pp. 774–787.

[8] J. Aquino, F. Pereira, H. A. Souto, and A. S. Francisco. "A forward tracking scheme for solving radionuclide advective problems in unsaturated porous media". In: *International Journal of Nuclear Energy Science and Technology* 3.2 (2007), pp. 196–205.

[9] H. Bae and R. Granero-Belinchón. "Global existence for some transport equations with nonlocal velocity". In: *Advances in Mathematics* 269 (2015), pp. 197–219.

[10] F. Benkhaldoun and M. Seaïd. "A simple finite volume method for the shallow water equations". In: *Journal of computational and applied mathematics* 234.1 (2010), pp. 58–72.

[11] R. Bilato, O. Maj, and M. Brambilla. "An algorithm for fast Hilbert transform of real functions". In: *Advances in Computational Mathematics* 40.5-6 (2014), pp. 1159–1168.

[12] A. Chertock, S. Cui, A. Kurganov, and T. Wu. "Well-balanced positivity preserving central-upwind scheme for the shallow water system with friction terms". In: *International Journal for numerical methods in fluids* 78.6 (2015), pp. 355–383.

[13] F. Coquel, J. M. Hérard, K. Saleh, and N. Seguin. "A robust entropy- satisfying finite volume scheme for the isentropic Baer- Nunziato model". In: *ESAIM: Mathematical Modelling and Numerical Analysis* 48.1 (2014), pp. 165–206.

[14] C. M. Dafermos. "Hyperbolic conservation laws in continuum physics". In: *Meccanica* 325 (2016).

[15] V. Deledicque and M. V. Papalexandris. "A conservative approximation to compressible two-phase flow models in the stiff mechanical relaxation limit". In: *Journal of Computational Physics* 227.21 (2008), pp. 9241–9270.

[16] O. Delestre, C. Lucas, P. A. Ksinant, F. Darboux, C. Laguerre, T. N. Vo, F. James, and S. Cordier. "SWASHES: a compilation of shallow water analytic solutions for hydraulic and environmental studies". In: *International Journal for Numerical Methods in Fluids* 72.3 (2013), pp. 269–300.

[17] J. G. G. Delgado. "Well-posedness and blow-up of global solutions for a nonlinear transport equation with nonlocal flux and measure data: theory and numerics". PhD thesis. Universidade Estadual de Campinas, 2016.

[18] L. C. Evans. "Partial differential equations". In: *American Mathematical Society.* (2010).

[19] L. Gosse. "Computing qualitatively correct approximations of balance laws". In: *SIMAI Springer Series* 2 (2013).

[20] C. H. Huang, T. Arbogast, and J. Qiu. "An Eulerian–Lagrangian WENO finite volume scheme for advection problems". In: *Journal of Computational Physics* 231.11 (2012), pp. 4028–4052.

[21] G. S. Jiang and C. W. Shu. *Efficient implementation of weighted ENO schemes.* Tech. rep. DTIC Document, 1995.

[22] F. John. "Partial differential equations". In: *Applied mathematical sciences* 1 (1978).

[23] J. Douglas Jr, F. Pereira, and L. M. Yeh. "A locally conservative Eulerian–Lagrangian numerical method and its application to nonlinear transport in porous media". In: *Computational Geosciences* 4.1 (2000), pp. 1–40.

[24] J. Douglas Jr, F. Pereira, and L.M. Yeh. "A locally conservative Eulerian-Lagrangian method for flow in a porous medium of a mixture of two components having different densities". In: *Numerical Treatment of Multiphase Flows in Porous Media.* Springer, 2000, pp. 138–155.

[25] B. L. Keyfitz and H. C. Kranzer. "A system of non-strictly hyperbolic conservation laws arising in elasticity theory". In: *Archive for Rational Mechanics and Analysis* 72.3 (1980), pp. 219–241.

[26] A. Kiselev, F. Nazarov, and A. Volberg. "Global well-posedness for the critical 2D dissipative quasi-geostrophic equation". In: *Inventiones mathematicae* 167.3 (2007), pp. 445–453.

[27] J. O. Langseth, A. Tveito, and R. Winther. "On the convergence of operator splitting applied to conservation laws with source terms". In: *SIAM journal on numerical analysis* 33.3 (1996), pp. 843–863.

[28] R. J. LeVeque. *Finite volume methods for hyperbolic problems*. Vol. 31. Cambridge university press, 2002.

[29] R. J. LeVeque. *Finite difference methods for ordinary and partial differential equations: steady-state and time-dependent problems*. Vol. 98. Siam, 2007.

[30] T. P. Liu and C. H. Wang. "On a nonstrictly hyperbolic system of conservation laws". In: *Journal of differential equations* 57.1 (1985), pp. 1–14.

[31] D. Marchesin and J. B. Plohr. "Wave structure in WAG recovery". In: *SPE Journal* 6.02 (2001), pp. 209–219.

[32] C. A. Micchelli, Y. Xu, and B. Yu. "On computing with the Hilbert spline transform". In: *Advances in Computational Mathematics* (2013), pp. 1–24.

[33] S. Mishra. "Numerical Methods for Conservation Laws and Related Equations". In: *Lecture Notes, ETH Zurich* (2010).

[34] O. A. Oleinik. "Discontinuous solutions of non-linear differential equations". In: *Uspekhi Matematicheskikh Nauk* 12.3 (1957), pp. 3–73.

[35] J. Perez. "Lagrangian-Eulerian approximation methods for balance laws and hyperbolic conservation laws". PhD thesis. Universidade Estadual de Campinas, 2015.

[36] F. Sabac. "The optimal convergence rate of monotone finite difference methods for hyperbolic conservation laws". In: *SIAM journal on numerical analysis* 34.6 (1997), pp. 2306–2318.

[37] D. G. Schaeffer and M. Shearer. "The classification of 2× 2 systems of non-strictly hyperbolic conservation laws, with application to oil recovery". In: *Communications on pure and applied mathematics* 40.2 (1987), pp. 141–178.

[38] D. W. Schwendeman, C.W. Wahle, and A. K. Kapila. "The Riemann problem and a high-resolution Godunov method for a model of compressible two-phase flow". In: *Journal of Computational Physics* 212.2 (2006), pp. 490–526.

[39] V. D. Sharma. *Quasilinear hyperbolic systems, compressible flows, and waves*. CRC Press, 2010.

[40] J. Singh, M. S. Altinakar, and Y. Ding. "Two-dimensional numerical modeling of dam-break flows over natural terrain using a central explicit scheme". In: *Advances in Water Resources* 34.10 (2011), pp. 1366–1375.

[41] J. Smoller. *Shock waves and reaction—diffusion equations*. Vol. 258. Springer Science & Business Media, 2012.

[42] T. Tang and Z. H. Teng. "Error bounds for fractional step methods for conservation laws with source terms". In: *SIAM journal on numerical analysis* 32.1 (1995), pp. 110–127.

[43] T. Tang and Z. H. Teng. "The sharpness of Kuznetsov's O ($\sqrt{\Delta}x$) L^1 -error estimate for monotone difference schemes". In: *mathematics of computation* 64.210 (1995), pp. 581–589.

[44] J. W. Thomas. *Numerical partial differential equations: conservation laws and elliptic equations*. Vol. 33. Springer Science & Business Media, 2013.